



Montanuniversität Leoben

Lehrstuhl für Gießereikunde

Department für Metallurgie



Vorstand Univ.Prof.Dipl.-Ing.Dr. Peter Schumacher

Thermal physical and mechanical properties of raw sands and sand cores for aluminum casting

Submitted by

Xin Wang

Supervised by

Univ.-Prof. Dipl.-Ing. Dr.phil. Peter Schumacher,
Dipl.-Ing. Bernhard Stauder

Leoben, December 2014



Acknowledgements

My first deepest gratitude goes to Professor Peter Schumacher and Dipl.-Ing Bernhard Stauder, my supervisors, for their constant encouragement and guidance during all the stages of this thesis. Without this, the thesis could not be in its present form.

Secondly, I would like to express my gratitude to Dr. Jiehua Li, who help me improve the writing of this thesis. I am also greatly indebted to the colleagues from Nematik Linz GmbH, who have instructed and helped me a lot during the eight months.

Last but not least, my great thanks would go to my beloved family and friends for their love and great confidence to me.

Statutory Declaration

I declare that I have authored this thesis independently, that I have not used other than the declared sources / resources and that I have explicitly marked all material which has been quoted either literally or by content from the used sources.

Date

signature

.....

.....

Outline

Outline	4
Abstract	6
1 Introduction	10
2 Theory of sand cores	12
2.1 Raw sands.....	12
2.1.1 Natural sands.....	12
2.1.2 Synthetic sands	14
2.2 Raw sands properties.....	14
2.2.1 Physical properties	14
2.2.2 Chemical property.....	21
2.3 Binders	21
2.3.1 Chemical composition of binders and promoters	22
2.3.2 Organic binders	22
2.3.3 Inorganic binders	25
2.3.4 Dehydration	28
2.4 Thermal properties	28
2.5 Mechanical properties of sand cores.....	29
3 Experimental Methods	31
3.1 Properties of raw sands.....	31
3.1.1 Grain size distribution	31
3.1.2 Grain morphology 2D-shape factor	33
3.1.3 Optical microscopy	33
3.1.4 Scanning electron microscopy.....	34
3.2 Technological investigation of thermal physical properties	34
3.2.1 Core making process.....	35
3.2.2 Dipping trials	38

3.2.3	Ring mould trials	39
3.3	Mechanical properties	40
3.3.1	Semi-sealed mould test – casting box.....	41
3.3.2	Shake out trials	42
3.4	Simulation of dipping trial	43
4	Results.....	45
4.1	Raw sands.....	45
4.1.1	Grain size distribution	45
4.1.2	Grain morphology 2D-Shape factor.....	49
4.1.3	Optical microscopy	51
4.1.4	Scanning electron microscopy.....	52
4.2	Thermal properties	69
4.2.1	Dipping trials	69
4.2.2	Ring mould test.....	73
4.3	Decoring behaviour	81
4.4	Simulation of dipping trial	91
5	Conclusion	95
	References.....	98
	FIGURE CAPTIONS	103
	TABLE CAPTIONS.....	108
	Appendixes.....	A-1

Abstract

A better understanding of the thermal physical and mechanical properties of raw sands and sand cores is of great importance to optimize and improve the quality of the casting productions in casting industry. By adjusting the properties of sand cores, higher efficiency and lower cost of casting productions can be achieved. However, there is still a lack of the detailed investigation on the thermo-physical and mechanical properties of raw sands and sand cores.

This thesis is aimed to investigate the thermo-physical and mechanical properties of different raw sands (natural and synthetic sands) bonded in cores with different binders. Furthermore, the tested and optimized sand cores were used for experimental Al alloys casting. Simulation was also employed to obtain thermal conductivity λ value of the sand cores, with an aim to use accurate parameters for the real Al alloy castings and also to improve the experimental accuracy of the simulation.

Five different raw sands, (MIN sand / Cerabreads sand / Zircon sand / H32 silica sand / Kerphalite sand) were investigated. Their grain size distributions, microscopic surface, roughness and morphology were obtained using sieve Analysis, granulometry, Scanning Electron Microscopy (SEM) and optical microscopy.

The mechanical properties of sand cores were investigated with a special focus on the de-coring ability of sand cores. Five different sand cores composed of the same silica sand but with different binders and process parameters were tested. Silica sand cores were found to be consistent with the observation using SEM. However, binder systems were found to have different effects on decoring and the binder bridges between sand grains.

Thermal physical properties were determined indirectly using a 'Dipping trial' and a 'Ring mould' with defined process parameters. Such types of instrumented experimental casting can be indirectly related to the thermal behaviour in the inner core moulds, which are surrounded by the molten Al alloy. Simulations were also performed to obtain a technological thermal conductivity of the sand cores relative to SiO_2 sand. A good agreement was obtained between simulations and experiments is the 'dipping trials'. The temperature transfer was compared for different sand cores of various raw sands, which were bonded by organic binders or inorganic binders. Especially, sand cores dried by microwave were also investigated to elucidate the origin of the water peak during the experimental casting process.

In summary, this thesis provides a comprehensive experimental investigation on thermal physical and mechanical properties of sand cores with different binders and raw sands. The obtained results can be used to optimize the production of sand cores and the selection of raw sands.

Key words: thermal physical properties, mechanical properties, raw sand, sand cores.

Ein besseres Verständnis der thermischen, physikalischen und mechanischen Eigenschaften von Rohsanden und Sandkernen ist unabdingbar für die Verbesserung und Optimierung der Produktionsqualität in der Gussindustrie. Die Anpassung der Sandkerne ermöglicht eine effizientere Gussproduktion und eine Senkung der Kosten. Bisher wurden die physikalischen und mechanischen Eigenschaften von Rohsanden und Sandkernen jedoch noch nicht ausreichend untersucht.

Diese Arbeit analysiert die thermischen, physikalischen und mechanischen Eigenschaften von verschiedenen (natürlichen und synthetischen) Rohsande gebundenen Sandkernen. Außerdem wurden die geprüften und optimierten Sandkerne für den realen Guss von Al-Legierungen eingesetzt zur Bestimmung der Temperaturleitfähigkeit λ der Sandkerne wurden verschiedene Sande eingesetzt, um die genauen Parameter für den realen Al-Guss zu ermitteln und auch die experimentelle Simulationsgenauigkeit zu verbessern.

Bei den Rohsanden wurden aufgrund ihrer unterschiedlichen Größe und Morphologie fünf verschiedene Sande – MIN-Sand / Cerabeads Sand / Zirkonsand / H32 Quarzsand / Kerphalite-Sand – untersucht. Korngrößenverteilungen, mikroskopische Rauheit, Morphologie und andere Parameter dieser Rohsande wurden mithilfe von Siebanalysen-Granulometrie und Untersuchungen mit Rasterelektronen- (SEM/EDX) und Lichtmikroskopen analysiert. Die verwendeten Quarzsandkerne wurden mit SEM/EDX im Hinblick auf Binderbrücken untersucht.

Die thermophysikalischen Eigenschaften der Sandkerne wurden unter Verwendung definierter Parameter durch Tauchversuche sowie durch die Verwendung von Ringgussformen gemessen. Diese Messungen können mit dem thermischen Verhalten der inneren Kerne in Beziehung gesetzt werden, die von der Al-Schmelze umgeben sind. Zwischen den Simulationen und dem in den "Tauchverfahren" mit denselben Parametern durchgeführten Experiment wurde eine gute Übereinstimmung erzielt. Insbesondere wurden auch mit Mikrowellen getrocknete Sandkerne untersucht, um den Ursprung der Wasserspitze während des experimentellen Gießverfahrens zu klären.

Die mechanischen Eigenschaften der Sandkerne wurden im Hinblick auf die Entkernungsfähigkeit von Sandkernen untersucht. Geprüft wurden fünf verschiedene Sandkerne aus demselben Quarzsand, aber mit verschiedenen Bindern und Verfahrensparametern, die in einer speziellen Entkernungsform abgegossen wurden. Die Ergebnisse der Entkernung der Bindersysteme haben verschiedene Auswirkungen auf das Entkernungsergebnis und die Bruchflächen zwischen den Sandkörnern. Die erzielten

Ergebnisse dienen der Optimierung der Produktion von Sandkernen und der Auswahl von Rohsanden.

Schlagwörter: Thermophysikalische Eigenschaften von Sanden; mechanische Eigenschaften von Sanden; Rohsande.

1 Introduction

During the production of complex castings, such as cylinder heads, (see in **Figure 1-1**). It is necessary to shape the inner cavities of the castings using sand cores. High demands on surface quality and dimensional precision of sand cores are necessary to obtain a good casting quality.



Figure 1-1: Complex casting parts.

During casting, sand cores play a decisive role of improving the performance of the casting production. The control and optimization of sand core properties are of great importance to the casting and subsequent de-coring process.

A better understanding of thermal and mechanical properties of sand cores is important because thermal and mechanical properties of sand cores affect deformation, flowability, shape retention, gas permeability, disintegration, high temperature resistance, etc. Therefore, elucidating their properties is necessary to provide a theoretical basis for further production development.

The physical and chemical properties of sand cores are significant parameters. Rao and Bawa ^{[1][2]} have proposed that grain size distributions, shapes and the surface morphology of raw sands influence the flowability, permeability, adhesiveness, surface fineness and strength of sand cores. These parameters of the sand cores affect the quality of aluminum casting. Therefore, the investigation on sand grain size distributions, shapes and the surface characterizations is necessary.

Furthermore, thermal properties of the sand cores significantly affect the thermal response of the casting ^[3]. For a thorough understanding of the behaviour of foundry sand cores mixtures, Solenicki G., Budic I., Ciglar D. ^[4] designed novel types of moulds which make it possible to study the heat transfer coefficient over temperature.

Mechanical properties of sand cores have been discussed by Klaushish ^[5], Beeley ^[6] with a special focus on the yield strength and tensile strength. However, thermal shock strength and effects of molten Al alloy on the casting process still remain to be explored. In the 'shake out' after casting, Elanchezhian C. and Vijaya Ramnath B. ^[7] have discussed the retained strength, which can exhibit the abilities of sand cores to disintegrate during shake out operation.

In this thesis, the investigation of mechanical properties will be focused on the influences of retained strength of different sand cores after casting. In order to determine thermal transfer, five different sands and binders were investigated with newly developed moulds.

2 Theory of sand cores

2.1 Raw sands

Two types of raw sands, i.e. natural sand and blended sand, are mainly used in the foundry industry. Natural sand consists of silica sand with organic and inorganic waste material. Blended sand can also be called compounded formulated or synthetic sand. Blended sand is made by adding a bond to a 'washed and dried' or unbonded base sand. This unbonded sand is sometimes called 'sharp sand', however, the name has nothing about the actual grain shape. The unbonded base sand may be silica, olivine, zircon and others. Each sand has properties that make its use desirable in certain situations ^[8].

2.1.1 Natural sands

H32 Silica sand

Silica is one of the most widely used sands. It is refractory, cheap and plentiful, however, it exhibits a large volume change with increasing temperature, quartz crystals exhibit phase changes at defined temperatures ^[9].

Foundry silica sands are composed almost entirely of quartz, SiO_2 . Some impurities may be present, such as ilmenite FeO-TiO_2 , magnetite, FeO_3O_4 , or the ferrous orthosilicate, $(\text{Mg, Fe}_2) \text{SiO}_4$, known as olivine. Silica sand is widely used because it is inexpensive and readily available, although the crystallographic reactions that quartz undergoes on heating have been proposed to be related to defects on the casting surface ^[11].

Because it has a higher thermal expansion rate, silica sand cores are believed to cause expansion defects in casting, such as a finning or veining and scabbing. It has a relatively low refractory stability which can cause sand burn-on, particularly with steel or heavy section iron castings. It is chemically reactive to certain alloys; for example, ferrous alloys containing manganese. The oxides of Mn and Fe react with silica to form low melting point silicates, leading to a serious sand burn on defects ^[10]. This property directly affects the thermal expansion of silica sand because the silica sand contains high percentage of silica.

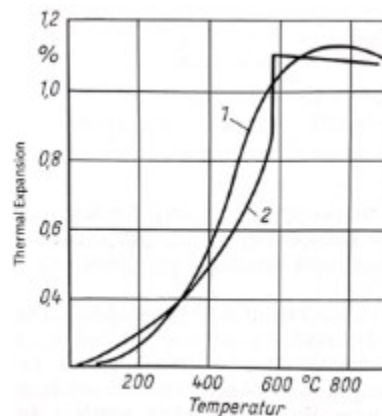


Figure 2-1: Thermal expansion of silica and silica sand, 1. Silica sand, 2. Silica^[11].

The SiO₂ modification results in a volume change, and a change of the thermal expansion behaviour of silica sand and the binder situation in the sand mould systems^[11], as shown in **Figure 2-1**, the thermal expansion of silica sand has higher values than silica from about 300 °C to 573 °C, even silica sand has no 'jump' with increasing temperature, while silica has obvious 'jump' at 573 °C.

Zirconium Sand

Zirconium sand has a lowest linear thermal expansion and a high temperature resistance. However, its high bulk density of about 2.7 g / cm³ has led to granular segregation defects, especially for the resin coated sands which are often used in mixtures of silica and zirconium (for cost reasons). Due to the big differences of the bulk densities between silica and zirconium sand granular segregation effects and other defects during the core manufacturing process are possible that lead to a rework and waste^[12].

The castings are preferable to be of smooth surface finish and sound in metallurgical properties. Therefore, the moulds are required to resist metal penetration and "burn in". A low thermal expansion and thereby a high dimensional accuracy and reduced cleaning is preferable^[13].

Kerphalite KF (Andalusit)

Kerphalite is characterized by its high temperature resistance and low linear thermal expansion. Kerphalite KF is, therefore, used as a substitute for zirconium and chromite sand in mixtures with silica sand from 30 % up to the pure mineral in the Cold Box, Warm Box and Croning process, respectively. However, its biggest disadvantage is that Kerphalite KF is a crushed grain and only one typical grain size is available. Due to the relative high dust

loading and the large specific surface, a higher amount of binder (up to 25 %) is required to obtain similar strengths compared with silica sand ^[14].

2.1.2 Synthetic sands

Cerabeads

Cerabeads is synthetically manufactured sand and consists of Mullite sintered above 1500 °C, resulting in a very high temperature resistance. Due to the round grains, the Cerabeads has the highest flowability during core shooting. The very low thermal expansion (similar to zirconium sand) makes their application fields comparable. Veining defects and other sand expansion defects can be avoided. Mixtures of at least 30 % Cerabeads with silica sand show good results and allow core sand mixtures at reasonable costs. Such mixtures remain uniform during manufacturing. A reproducible gas permeability of the sand material can be obtained when the grain size distribution is controlled, according to reproducible sieve analyses. Additionally, the round grain helps to reduce the wear of the core shooting machine ^[15].

Min sand

Minsand is synthetic sand produced via an alumina oxide rich mineral basis. Because of its almost perfectly spherical particle shape, Minsand is widely used in the foundry industry as mould and core sand. In the core production, binder savings of up to 50 % compared to other sands are achievable without a loss in the core strength. At the same time, Minsand cores show excellent surfaces and thus produce excellent casting surfaces ^[16].

2.2 Raw sands properties

The physical properties of raw sands are affected by grain shape, grain size distribution, grain fineness, permeability, density, and coefficient of thermal expansion. The chemical composition of raw sands has been reported to affect pH value and fusion point ^[17].

2.2.1 Physical properties

As noted above, the physical properties of raw sands are a vital factor in bonding raw sands into sand mould in the core makings. The shape of sand particle, particle density, bulk

density, grain size distribution and flowability of sands are the important parameters during the core making process. Linear thermal expansion and phase transformation also affect the quality of cores.

The particle density (also called specific density) of dense aggregates such as a core is a particular property in the concrete mixture design. The bulk density of an aggregate, or its unit mass, represents in part its void content at a given degree of compaction and it's, therefore, an indirect measurement of the grading and shape characteristics [18].

Table 2-1. Comparison of physic properties of raw sands [19].

Properties	Al ₂ O ₃	Kerphalite	Cerabeads	MIN sand	Zircon sand	Silica sand H32
Specific density						
(g / cm ³)	3.97	3,13	2,86	3,11	4,7	2,65
Bulk density						
(g / cm ³)	1.5	1,55	1,56	1,58	1,83	1,4

The weight per unit volume of the solid portion of a granular mixture is called particle density. The oven-dry weight of a unit volume of base sand without binders inclusive of pore spaces is called bulk density, the values are shown in **Table 2-1**.

2.2.1.1 Shape

Figure 2-2 shows four typical morphologies of sands, as described in the concrete industry. Compounded, angular, subangular and rounded shapes are often observed and used.

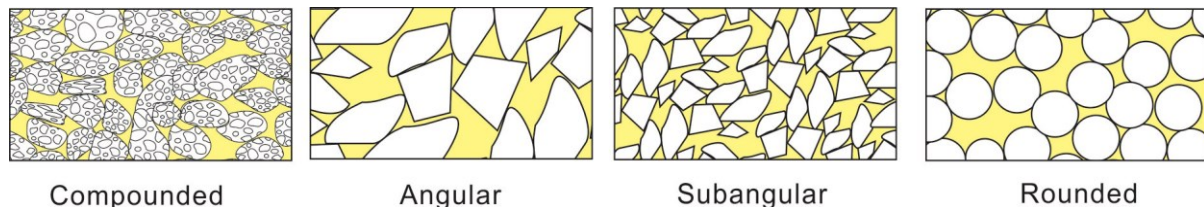


Figure 2-2: Types of sand grains [20].

Rounded Grains The rounded grains have the least contact with each other in a compacted structure, thereby making the sand highly permeable to gases. Sand having rounded grains, however, lacks strength and does not pack up to the optimum extent. The binder requirement is reduced.

Angular Grain The angular grains have defined edges, and their surfaces are nearly faceted. They produce a higher strength and a lower permeability in the mould than subangular grains. The binder consumption is likely to be higher.

Compounded Grains In some cases, the grains are cemented together so that they fail to be separated when screened. They may be consisted of rounded, subangular, angular grains or a combination of these three different types of grains. Such types of grains are called compounded grains and are undesirable to most casting application due to their tendency to breakdown at high temperatures.

Subangular Grains The subangular grains have a comparatively lower permeability and greater strength than the rounded grains, because the contacting surfaces are flat and a stronger bond respectively larger bond surface is possible.

In practice, a sand grain contains a mixture of grain shapes, depending on the origin of the sand. A subangular-to-rounded grain mixture would be the best combination for sand cores [21].

2.2.1.2 Grain size

The grain size of sand is defined by a grain fineness number, which is a concept that can be used for comparing the fineness of different sands. The AFS (American Foundry Society) number, which is defined as $AFS \text{ Grain Fineness No.} = \frac{\text{Total product}}{\text{Total \% of Retained Grains}}$ after the vibration in the sieve analysis, indicates the average grain size of the base sand. Foundry sands usually fall into the range 150 – 400 μm, with 220 – 250 μm being the most commonly used. Direct conversion between average grain size and AFS grain fineness number is not possible, but an approximate relation is shown in **Table 2-2** [21].

Table 2-2. The relative values between average grain size and AFS grain fineness number [21].

AFS grain fineness number	35	40	45	50	55	60	65	70	80	90
Average grain size (μm)	390	340	300	280	240	220	210	195	170	150

There are different standards to measure the grain size distributions, such as, VDG 40 ^[22], DIN ISO 3310 part 1 ^[23], ASTM D2487-11 ^[24]. The VDG – 40 video grader as introduced by Prowell B. D., Zhang J. N., Brown E. R. ^[25], which can only measure two dimensions. Image analysis techniques are used to extract information about grading, shape, angularity, in some cases, texture. DIN ISO 3310 – 1 specifies the technical requirement and corresponding test methods for test sieves of metal wire cloth, which is applied to test sieves having aperture sizes ^[26]. ASTM D2487-11 defines 12 terms after sieving the solid particles, which is the ASTM version of the Unified Soil Classification System ^[24]. In this thesis, the DIN ISO 3310 part 1 was used to test the grain size distribution of different sands.

The size distribution and shape of the sand grains are important in controlling the quality of the mould. To determine the size, shape, and distribution of the sand grains, it is important to point out that the grain shape contributes to the amount of sand surface area and the grain size distribution controls the permeability of the sand cores.

As the sand surface area increases, the required amount of bonding material increases. A change of surface area, perhaps due to a change of sand shape or the percentage of core sand, will require a corresponding change in the amount of bonding agent.

Rounded grains have a low surface area to volume ratio and are therefore preferred for making cores because the less binder is required and a better decoring is observed.

Angular sands have the largest surface area and therefore require higher binder amounts. The angularity of a sand increases during recycling because the sands are broken down by thermal and mechanical shock.

The porosity of the cores controls its permeability, which is an ability of the core to allow gases generated during thermal decomposition of binder to escape through the core. The highest porosity can be obtained from grains with approximately the same size.

As the size distribution broadens, there are more grains that are small enough to fill the spaces between large grains. As grains break down through repeated reclamations, there are smaller grains, and the porosity of the mould decreases. However, if the porosity of the mould is too large, metal may penetrate sand grains and causes a burn-in defect.

Therefore, it is necessary to balance the sand distribution and continue to control the sand during foundry operation. Dust collectors during recycling can remove fines and determine the proper bond addition required for adjustment ^[27].

2.2.1.3 Thermal linear expansion

The coefficient of thermal expansion is defined as the change in a unit measure of material exposed to a change of 1 °C in temperature. The coefficient of linear expansion is thus the slope of the dilation temperature curve. The instantaneous coefficient of linear expansion is the slope at a specific temperature; while the mean coefficient is the mean slope between two designated temperatures. Coefficients of expansion may be presented in either volumetric or linear terms. The latter is most commonly used. To convert volumetric to linear expansion, the approximate relation of the linear coefficient being equal to one - third of the volumetric coefficient may be used ^[28]. The values for typical base sand are shown in **Table 2-3**.

Table 2-3 . Linear expansion coefficient of the mould base materials ^[29].

	20-300°C	20-600°C	20-800°C
Quarz sand	14	23	17
Kerphalite KF	5,3	6,5	7
Min Sand	4,2	4,5	4,8
Cerabeads	3,5	4	4,3
Zircon	3,4	4,1	4,5
δ- Al ₂ O ₃	6.2	7.2	7.4

Figure 2-3 shows thermal expansions curves with temperature up to 800 °C for different sands. The silica sands H32 show a jump in expansion to high values at about 600 °C. Zircon sand, Cerabeads sand, and Min sand are more stable when compared to the silica sand. This type of thermal expansions plays a significant role in the development of sand defects.

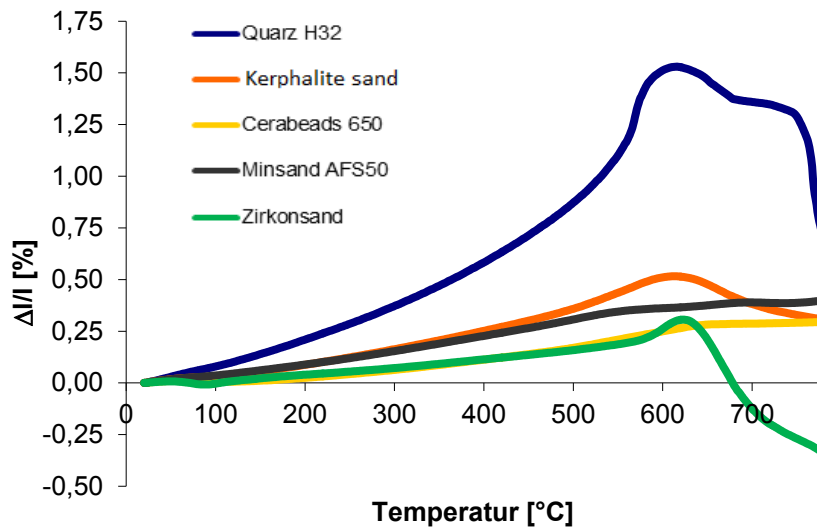


Figure 2-3: Thermal expansion of different sands bonded with sodium silicate (warm box hardened and microwave dried) with increasing temperatures ^[30].

The refractory ability is also mainly affected by the chemical composition. When more stable oxides are present, better properties can be obtained.

Silica sand (SiO_2); the first change in volume takes place at 573 °C, due to the displacive transformation of quartz α to quartz β , as shown in **Figure 2-4**, and involves an expansion of around 1.6 %. Quartz β undergoes the reversible transformation to tridymite at temperatures above 867 °C, which contracts around 0.3 %. At temperatures above 1470 °C tridymite transforms into cristobalite ^[31]. These phase transformations are influenced by trace elements as impurities of natural sand.

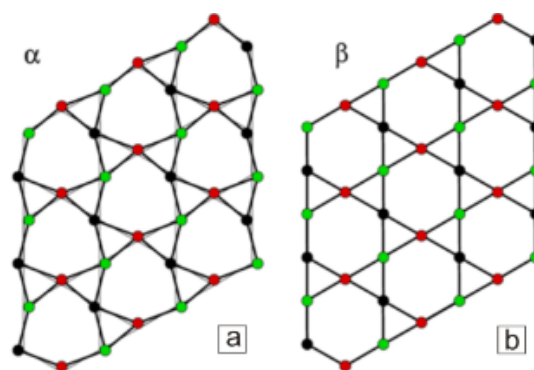


Figure 2-4: Silica structure phase transformation at 573 °C ^[32], (a) α -Quartz (trigonal) $\rho = 2.65 \text{ g / cm}^3$, (b) β -Quartz (hexagonal) $\rho = 2.30 \text{ g / cm}^3$ with a change point at 573 °C.

Alumina, Al_2O_3 , with a melting point of about 2053 °C, is chemically one of the most stable and mechanically one of the strongest refractory oxides, particularly at moderate application

temperatures. Alumina is stable in oxidizing and highly reducing atmospheres and can be used in atmospheres up to about 1800 °C. Alumina has a high thermal expansion coefficient, as shown **Table 2-3**, and a relatively high thermal conductivity.

Zirconia, ZrO_2 , with a melting point of about 2770 °C, has an unusually low thermal conductivity ($2 \text{ W m}^{-1} \text{ K}^{-1}$) in contrast to Al_2O_3 . It is also stable in oxidizing and moderately reducing atmospheres and is stable in contact with many metals and oxides ^[33]. At a temperature of 1200 °C and ambient pressure, a tetragonal structure becomes thermodynamically stable. At 2377 °C, the tetragonal structure changes into a cubic calcium fluoride structure. The mineral name zirconia is used for both the tetragonal and the cubic structures ^[34].

Kerphalite (Andalusite) is a natural ore, as Hagen R., Lamy C., Myhre B. and Peng H. ^[35] pointed out, it is composed of approximately 60 wt % Al_2O_3 , and 38 wt % SiO_2 , plus some inclusions containing iron and alkalis. Because of its contents of alumina and silica, this mineral easily forms Mullite when fired at high temperature. Mullite is an attractive bonding phase in alumina castable because its high melting point (1850 °C), and good mechanical properties such as low thermal conductivity, low thermal expansion and good chemical stability to be castables. Above 1280 °C, this mineral will yield 80 % of Mullite phase and 20 % of silica glass phase. A part of this liquid phase is expelled, but most of it (around 80 %) is confined in an interconnected capillary network in the Mullite ^[35].

Cerabeads (Mullite), is a refractory with chemical composition of $3Al_2O_3 \cdot 2SiO_2$. Mullite is a mineral with a very high melting temperature of 1840 °C. It is an acidic refractory mineral with a low thermal expansion coefficient ^[36].

MIN sand (Bauxite) refractory as reported by Sharma B. K. ^[37], has quite high heat resisting capacity, they are heat resistant from 1790 °C to 1880 °C, and can be heated up to 1700 °C 1750 °C. Min Sand is suitable as a mould material for these types of casting as it has high refractoriness (sintering temperature > 1,950 °C), it is not prone to mould material-metal reactions and is resistant to metal penetration even in highly thermally stressed castings. The heat resistance of MINsand is attributed to its high alumina content ^[38].

2.2.2 Chemical property

The pH value of a sample gives the water-soluble level of alkalinity or acidity of a given sand. This pH value is determined by its reactivity with resins used in the casting process. Sand with a pH value close to neutral (7.0) is the least reactive and therefore is best for core production ^[39].

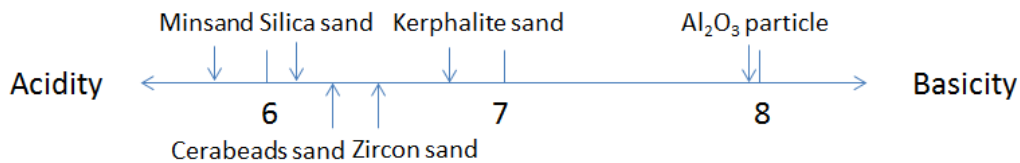


Figure 2-5: pH values of different base sands ^{[40][41]}.

The chemical properties are mainly manifested by chemical compositions, which can also influence physical properties.

2.3 Binders

The function of the binder is to produce cohesion between the refractory grains in the green or hardened state. Since most bonding materials are not highly refractory, the required strength should be obtained with a minimum addition to avoid gaseous decomposition products.

Organic binders in foundry industry are based on hot curing, gas curing and cold curing. In hot curing, hot box and warm box can use Furan-/ Phenolic/ Urea Resin combined with acidic hardener by heating to harden. In gas curing, epoxy with SO₂ and resol with CO₂ are utilized. In cold curing, Furan/ Urea resin with acid, Phenol/ Urea resin with acid, alkaline phenolic resin with high boiling ester are practiced ^[45]. The hardening of the organic binders can be obtained by chemical hardening, this kind of hardening is by linking of molecules to macromolecules that give the binder a fixed structure; this mechanism affects the organic resin binders ^[42].

Inorganic binders are generating more interests in recent years because of their advantage compared to commonly use organic binder systems. Their advantages include no emissions

during the whole production process as well as potentially higher quality castings and less rejects due to gas defects. Sodium silicates, also called “water glasses”, are most widely used. Combined with the growing sensitivity to enhance environmental protection under increasing restrictions for foundries, these advantages welcome a change from an organic binder systems to an inorganic binder system^[44]. The hardening of the inorganic binders can be obtained by drying the reaction products (crystals)^[44].

2.3.1 Chemical composition of binders and promoters

In this section, the following materials will be presented: organic binders, inorganic binders, including some promoters in the actual production process. Organic binders are focused on resin, while inorganic binders are based on water glass with different modules. Furthermore, water glass is discussed by different module ($\text{SiO}_2 / \text{Na}_2\text{O}$).

2.3.2 Organic binders

The established organic binder systems are based on resins with an aromatic polymer framework. Aromatic compounds are unsaturated cyclic carbohydrates with a high thermal stability. The aromatic backbone ensures sufficient thermal stability and a high dimensional accuracy at a low binder addition into sands. However, aromatic compounds are also the reason for critical emissions. Organic binder systems are used in the cold box, hot box and warm box process.

The binder bridges exhibit distinct difference between cold box process, hot box process and warm box process. In cold box process, binder bridges have linear structures and a plastic behaviour, while in the warm box and hot box process binder bridges have cross-linked structures and have a more brittle behaviour.

Cold box process

Numerous cold box processes are available and the main differences are in the chemical binder and hardening systems, together with the sand mixing and dispensing practice employed for both cores and block moulds. The setting time is sensitive to variations in sand temperature, so that sand heating, sand cooling or additional adjustment may be required to maintain the necessary process control.

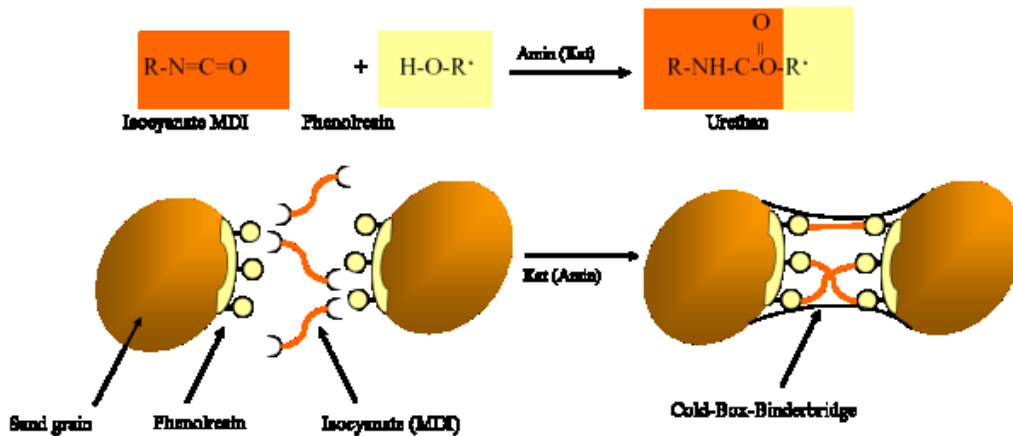


Figure 2-6: Phenolresin and isocyanate with Amin gas to form a Cold Box Binder bridge ^[45].

Figure 2-6 shows schematically that, the Polymers formed a linear structure in cold box process and can show a plastic behaviour especially at elevated temperatures. Because of this characterization, shake out operation requires more energy to separate the sand cores from castings.

Hot box process

The core box temperature is commonly maintained by integral gas or electric heating units, but stove cycling may also be employed to accelerate the full curing of cores with thicker sections after extraction.

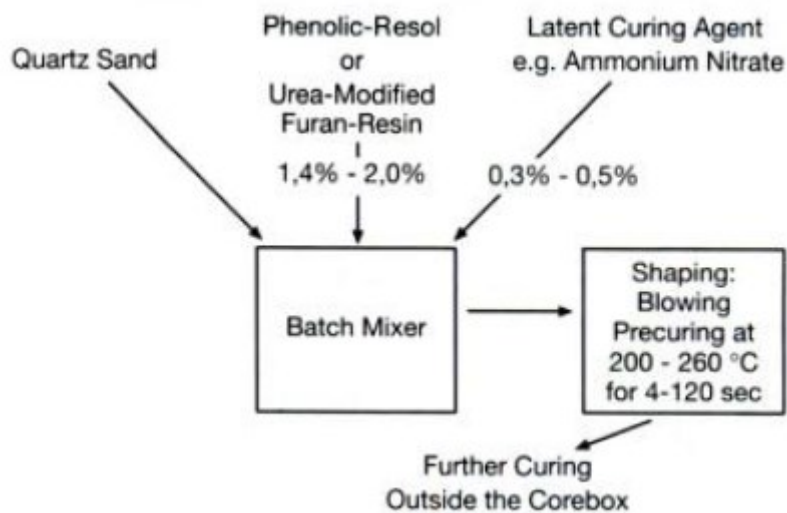


Figure 2-7: Hot box process for making cores ^[46].

Figure 2-7 shows hot box core making process. The binder is an aqueous Phenolic – Resol or Urea – modified Furan – Resin, the catalyst is an aqueous solution of ammonium salts, usually chloride and bromide. Sand is mixed with the liquid resin and catalyst and blown into a heated core box. The heat liberates acid vapour from the catalyst which triggers the hardening reaction. Hardening continues after removal of the core from the box causing the sand to be cured throughout. As reported by Brown J. ^[47], in Aluminum casting, special hot box resins are available which break down readily at aluminum casting temperature. And in ferrous casting, cores are usually coated to prevent burn – on. The rather high nitrogen can cause gas holes and fissures in iron casting and additions of 1 – 3 % of a coarse grained form of iron oxide are often used to minimize N – defects.

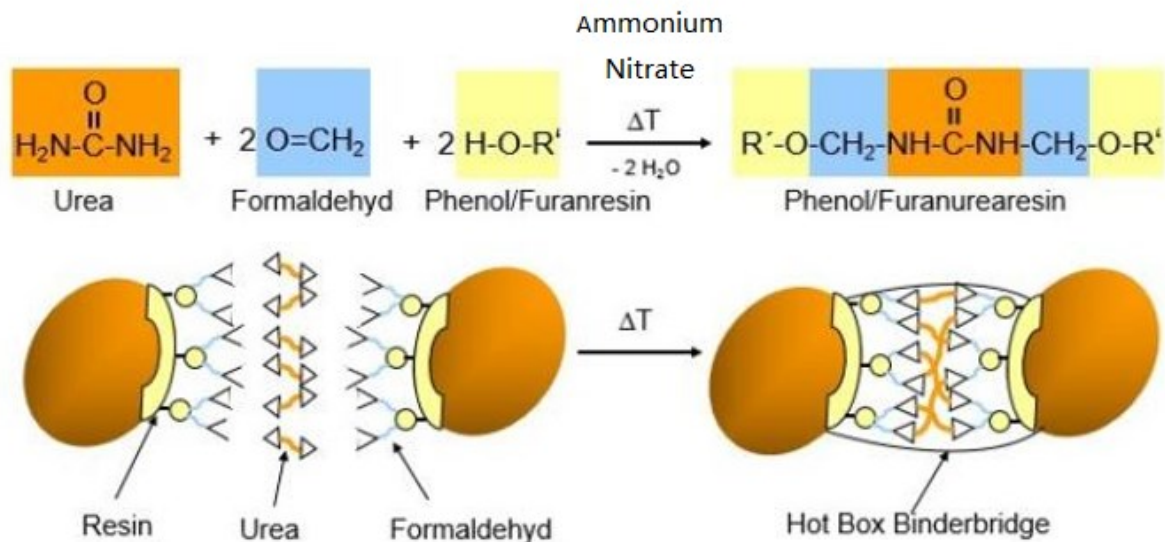


Figure 2-8: Urea and formaldehyde with phenol/furan resin and ammonium isolate as a latent coring agent under heating to form a Hot Box Binder Bridge ^[45].

Figure 2-8 points out that, formed Polymers have a cross-inked structure and have a brittle behaviour but higher stability at elevated temperatures. Because of this characterization, shake out operation needs less energy to separate the sand cores from casting.

Warm box process

The equipment and general approach employed in the warm box process are very similar to the case of hot box process, but a more reactive binder system enables core box temperatures in the range from 150 °C to 190 °C to be employed whilst maintaining short cure times. The cores feature very high strength and hardness with modest binder additions [48]. Comparing the hot box process with others, advantages and disadvantages can be listed as:

Advantages:

- (a) Good thermal stability for cores with high loads (e.g. water jackets).
- (b) Excellent flowability of the sands, only a low blow pressure is required.
- (c) Excellent surface roughness.
- (d) Classical shell cores are hollow, therefore they have a high gas permeability.
- (e) Unlimited bench life of the sand in core blowing machine.
- (f) Low gas release on contact with the melt.

Disadvantages:

- (a) Heated core tools necessary (higher cost, lower process stability).
- (b) Lower productivity in comparison to the cold box, especially for large cores.
- (c) Lower decoreability, especially for solid cores.
- (d) When used as single port cores, its dimensional accuracy, is limited.
- (e) Due to high resin amount, core gas amount is also high.
- (f) Production of cores with big differences in cross section is difficult.
- (g) Core production process releases gasses is required.

2.3.3 Inorganic binders

Sodium silica is a water soluble glass available from suppliers in wide range of types specified by the silica (SiO_2), soda (Na_2O) and water content. Sodium silicate can be hardened in a number of ways: by adding weak acids (CO_2 gas or organic esters), by adding various powders (di-calcium silicate, anhydrite, etc.) or by removing water [49].

Sodium silicate as binder

Sodium silicate is one of the most common binders used in air setting or self-hardening processes for moulding and core making. The CO₂ process, ferrosilicon process, cement process, dicalcium silicate process, and others make use of sodium silicate as binder, along with a solid or gaseous hardener. The water glass consist of three basic compounds: H₂O, SiO₂ and Na₂O (or K₂O). With increasing ratios of SiO₂ to Na₂O (SiO₂ / Na₂O), the viscosity of water glass increases ^[52]. The varieties suitable for the CO₂ process should contain total soluble silica (SiO₂) of 26 to 32%; total alkalinity (as Na₂O) of 11 to 13%, mass ratio(SiO₂/Na₂O) of about 2.2. ^[50]. Water glass is an aqueous solution with alkali silicate, with the chemical composition of xSiO₂·yM₂O·zH₂O. For M, alkali ions can be Li⁺, K⁺, or Na⁺ ^[51].

As listed in **Table 2-4**, a module (SiO₂ / Na₂O) under 2.5 reduces the beginning strength, but increases the ultimate strength of the cores and thus making decoring more difficult.

A module over 2.5 increases the beginning strength, but reduces the ultimate strength, thus favoring the disintegration during decoring. In practice, therefore, a modulus of about 2.5 is used as a compromise value ^[52].

Table 2-4: Properties of water glass module in the sand core ^[52].

Properties	Water glass module(SiO ₂ : Na ₂ O)	
	> 2.5	< 2.5
Viscosity	↑	↓
Reactivity	↑	↓
Alkali amount	↓	↑
CO ₂ consumptions	↓	↑
Over hardened	↑	↓
Beginning strength	↑	↓
Ultimate strength	↓	↑
Disintegration	↑	↓

Water glass-CO₂-Process

Sodium silicate ((Na₂SiO₃) or (Na₂O)n(SiO₂)) used as a major raw material in washing soap manufacture is obtained by high temperature(1650°C) fusion of pure silica(SiO₂) with washing soda(Na₂CO₃). It is a thick, viscous fluid which generates a strong bond when it is mixed with silica sand and reacts with CO₂ gas, which can also be reacted in air.

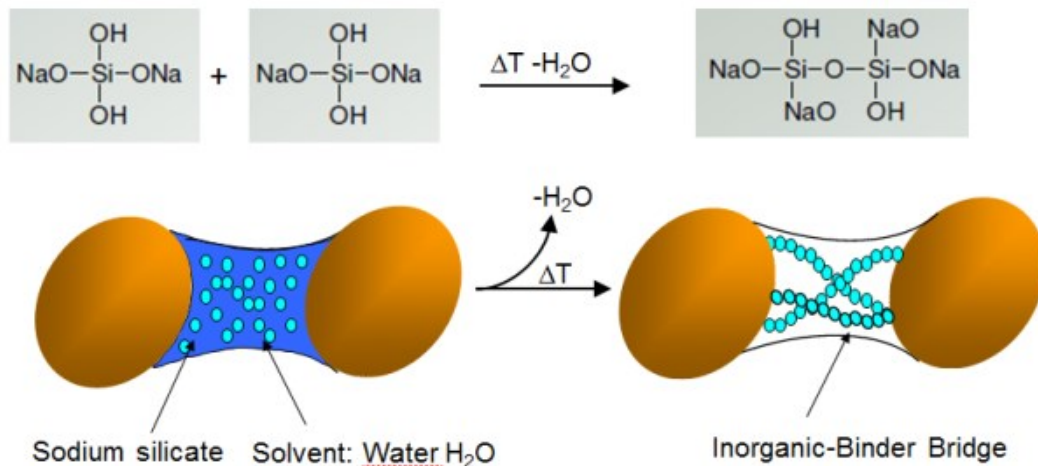
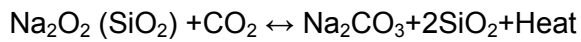


Figure 2-9: Formation of an Inorganic-Binder bridge ^[45].

The liberated SiO₂ is amorphous and results in an increase of viscosity and an increased bonding strength to the sand grains. This process is used both for moulding and core-making. Its advantage is a very fast cold chemical hardening with no requirement of baking as well as obtaining higher strength. However, the excessive bonding strength is one of the main drawbacks so that this process causes problems in decoring and cleaning as well as hot tears in castings ^[53].

Water glass-Warm box-Process

Water glass warm box process is aimed to improve the strength of the inorganically bonded sand cores. The water glass and sand mixture are heated by the heated tool after forming from sand core shooting machine, and with CO₂ to harden, by this combined treatment, the dehydration can faster than in the conventional process.

It has been reported that using 3% water glass (Na-basis) with heated metal tool and blowing with the hot air in 120 s or 45 s warm air and CO₂ can harden the sand cores ^[54]. Osterberg and Anderson ^[55] reported that, water glass sand mixture closed into the sand

mould box with temperature from 130°C-150°C, meanwhile, blowing 120 seconds hot air or CO₂, the strength can obviously be improved.

2.3.4 Dehydration

In all these processes, binders, which own the water solubility, have the reactions with additives or thermal energy. After the hardening process, moisture still exist in the sand cores. This results to less strength, compared to organic binder systems.

A drying process gives the possibility to improve the strength by dehydration. Dehydration can be achieved by many different mechanisms: drying by hot air, drying by a hot tool and drying by a microwave oven, etc. ^[56].

2.4 Thermal properties

Thermal conductivity

Thermal conductivity of the mould material is particularly crucial for the cooling rate of a casting part. Besides other factors (e.g. melt cleaning, degassing, grain refinement, modification, a correct fluid flow and the feeding technique) cooling rate has a large influence on the obtained microstructure. In general, higher cooling rates generate fine grains, small secondary dendrite arms in the microstructure, and thereby improved which in turn cause superior mechanical properties.

The thermal conductivity of the mould determines the heat removal from the solidifying casting when inaccurate data are used, the observed microstructure may develop quite differently to that expected from the simulation ^[57].

Temperature diffusivity

Thermal diffusivity α (m² s⁻¹) is another value to measure the heat removal velocity. It indicates the time interval of the temperature, which can be described by

$$\alpha = \frac{\lambda}{\rho * Cp} \quad (\text{eq. 1})$$

$$b = \sqrt{\lambda * Cp * \rho} \quad (\text{eq. 2})$$

The heat penetration coefficient b ($J / m^2s 0.5 K$) is the measurement for the rate of amount of heat flow, which influences the solidification in the foundry process ^[58].

After pouring a pure metal into an insulating mould (sand or ceramic) at pouring temperature T_P , the temperature along a line perpendicular to the mould- metal interface can be described as shown in **Figure 2-10**.

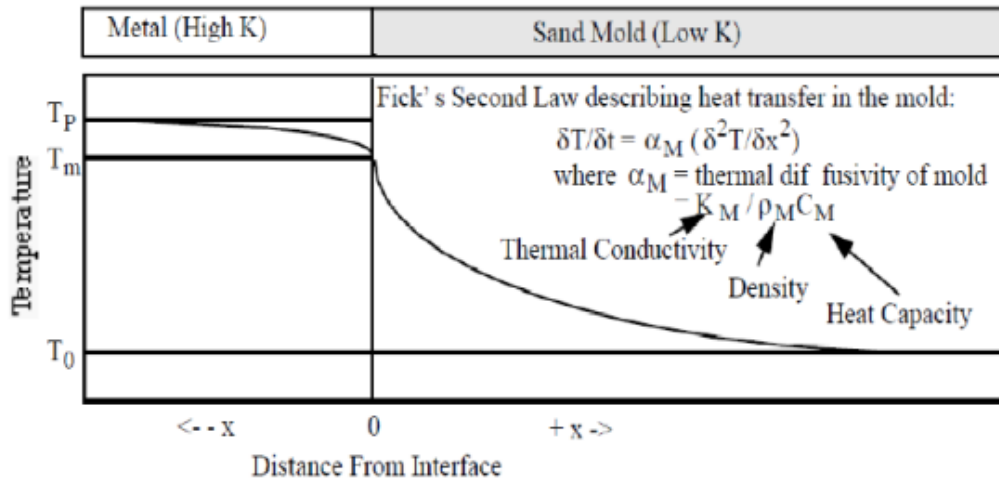


Figure 2-10: Temperature along a line perpendicular to the mould-metal interface ^[59].

In this case, the high thermal conductivity of the solidified metal results in the temperature of the metal at the interface dropping to T_m instantly upon pouring and staying there until solidification is complete. Intimate contact between the metal and mould means that the mould at the interface will also remain at T_m until solidification is complete ^[59].

2.5 Mechanical properties of sand cores

After a casting has been solidified and cooled down sufficiently in an expendable mould, the first step is freeing the casting from the mould. This operation is called as the 'shake out operation'. Because a great deal of heat and dust are involved in this operation. Shake out is usually done by means of vibratory knockouts, jolting grids and vibrators ^[60]. The mould is intensively jolted and broken up. The various cleaning operation usually performed on a casting are enumerated and discussed below: (1) rough cleaning (2) surface cleaning (3) trimming (4) finishing ^[61].

Due to the reasons mentioned above 'shake out operation' or 'Decoring' is done mechanically in closed atmosphere. Hammering and vibrating will loosen and break up cores. Stationary or portable vibrators are employed for this purpose. To knockout cores from heavy castings, it is advantageous to use air drills ^[62].

The energy required for successfully shake out of cores depends on the type of binder bridges between the sand particles, which will be part of the investigation here.

3 Experimental Methods

This chapter illustrates the methods to determine raw sands properties and sand cores properties, as well as technological tests of thermal physical properties obtained by iterated reverse simulation. These technological tests are 'dipping trail', 'ring mould' and 'Semi-sealed mould test', which can be related to actual casting processes. Magma 5 software was used to simulate the heat conductivity in quartz sand and compare those with the 'dipping trail' experiments for different sand cores. A method is described to measure the decoring and shake out behaviour of different sand cores after solidification. In order to further investigate the morphology of raw sands and the characterizations of binders' bridges of sand cores, optical microscopy and scanning electron microscopy equipped with energy-dispersive X-ray spectroscopy (SEM / EDX) were used.

3.1 Properties of raw sands

The grain size distribution of sands was measured by the granulometry using a sieve analysis. The shapes and the surface morphology of raw sands were investigated separately with optical microscopy (NIS-Elements 3.0) and SEM / EDX.

3.1.1 Grain size distribution

The size distribution is often of critical importance to cores and moulding sands. A sieve analysis (or gradation test) is a procedure used to assess the particle size distribution (also called gradation) of a granular material ^[63]. A sieve shaker with parameters in **Table 3-1** was used. In this experiment, the meshes are according to DIN ISO 3310/1 with a mesh size of 63 μm , 90 μm , 125 μm , 180 μm , 250 μm , 250 μm , 355 μm , 500 μm , 710 μm , 1000 μm and 1400 μm , respectively.



Figure 3-1: Sieve shaker used for granulometry and scale.

Meshed according to DIN ISO 3310/1 were selected and stacked in decreasing mesh size, from top to bottom, in a mechanical sieve shaker (Retsch AS 200). A pan was placed underneath the nest of sieves to collect the aggregate that passes through the sieves. The entire nest is then agitated, and the material whose diameter is smaller than the mesh opening passes through the sieves. After the aggregate reaches the pan, the amount of material retained in each sieve is then weighed and analyzed by computer, as shown in **Figure 3-1** ^[64].

Table 3-1 : Important parameters in the sieve analysis.

Parameters	Values
Amplitude (mm)	1,5
Sieving time (min)	10
Sieving height (mm)	50
Diameters (mm)	200
Vibration direction	Three dimension
Mesh Size (mm)	63--1400

3.1.2 Grain morphology 2D-shape factor

This parameter is used to define the roundness of an object. When the value is less than 1, this indicates a less rounded particle. A 2D-shape factor according to $S_f = 4\pi (\text{area}) / (\text{convex hull perimeter})^2$. NIS-Elements 3.0 was used to measure the values.

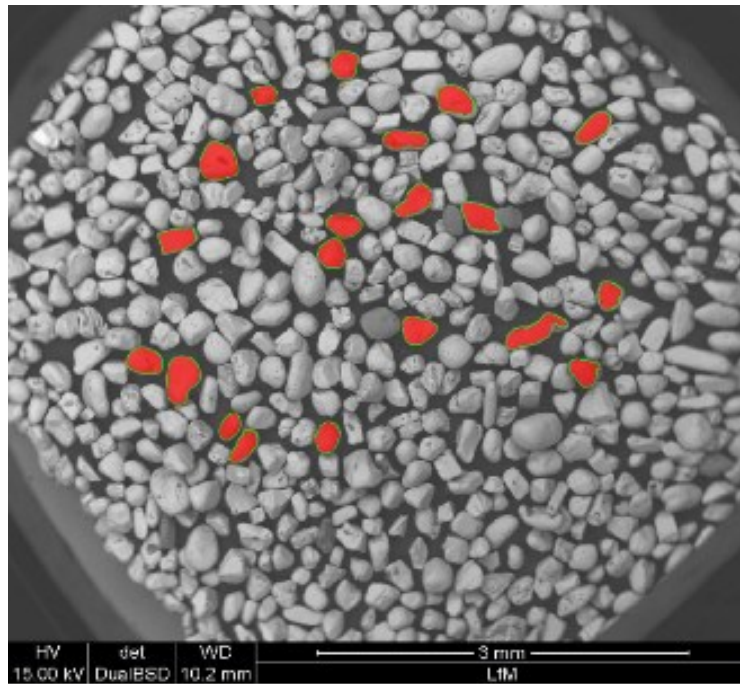


Figure 3-2: Binary shape of zircon sand particels.

Figure 3-2 shows the image analysis method used highlighting the morphology and size of an imported REM image REM. The shape factor values were determined by NIS-Elements 3.0 software, particles are more rounded if these values are close to 1.0.

3.1.3 Optical microscopy

Optical microscopy together with the stereomicroscopy (Leica Discovery. V 2.0 (**Figure 3-3 (a)**) with a version of Axiovison Rel.4.8) was used to analyze the surface, colour, shape and glossiness of sands in order to differentiate between sands.

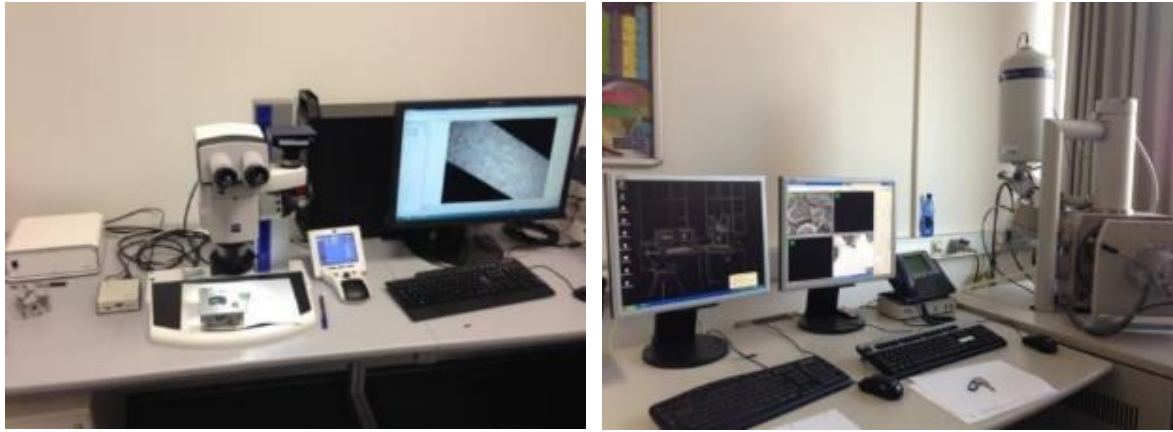


Figure 3-3: (a) Optical microscopy equipment (Zeiss discovery 2.0), (b) SEM / EDX equipment.

3.1.4 Scanning electron microscopy

SEM / EDX (FEI-Qanta 200), as shown in **Figure 3-3 (b)**, was used to observe the surface and shape of raw sands, and also to measure the chemical composition by EDX in order to distinguish the classifications and properties. Furthermore, SEM / EDX was also used to observe the bond methods and fracture surfaces of ‘binder bridges’, which has a significant influence on thermal properties and mechanical properties.

3.2 Technological investigation of thermal physical properties

Technological investigation of thermal physical properties were performed by ‘ring mould tests’, ‘dipping trial’ and ‘semi-sealed moulding test’. The dipping trials were performed to test the temperature distributions over time in sand cores submerged into a melt to compare thermal conductivities in different sand cores. An infinite heat supply was experimentally established as a boundary condition. With a steel ring mould at about 200 °C as a starting temperature, the temperature distribution over time during the ‘Ring mould test’ can be expected to be very close to the casting process such as in the Rotacast process, with the aim to optimize cooling rates at central cores of cylinder heads. In the semi-sealed moulding test experiments, it is also necessary to obtain the temperature over time in the centre of different sand cores obtained during solidification, which can be used to calibrate simulation models. Thereby, the temperature distribution in the sand cores with the subsequent decoring behaviour can be compared.

3.2.1 Core making process

Cylindrical sand cores for dipping trials and ring mould tests and trapezoidal sand cores were formed by a core shooting machine (Roperwerk Type: H11) in a preheated mould (warm box process at 150 °C). Outer cores were formed in a wooden mould using the inorganically cold box process (water glass+CO₂).

Cylindrical sand cores: H32 silica sands / Cerabeads sands / MIN sands / Kerphalite sands / Zircon sands were separately mixed with 2.5 wt. % water glass Betol® 39 T (see in **Table 3-2**) in a batch mixture (Zimmerman) for 2 minutes. A cylindrical shaped mould (Diameter 50mm and Height 25mm) was fixed on the core shooting machine and preheated before shooting operation at 6-8 bar. After 5 minutes, the cylindrical shaped mould was held for the sufficient hardening (**Figure 3-4 (b)**).

Trapezoidal sand cores: H32 silica sand was mixed with two organic (see in **Table 3-2**) and three different inorganic binders (see in **Table 3-2**) in a batch mixture (Zimmermann). The trapezoidal shaped mould was fixed on the core shooting machine and preheated before shooting. After shooting, the trapezoidal shape mould was held for 5 minutes to harden the cores (**Figure 3-4 (c)**).

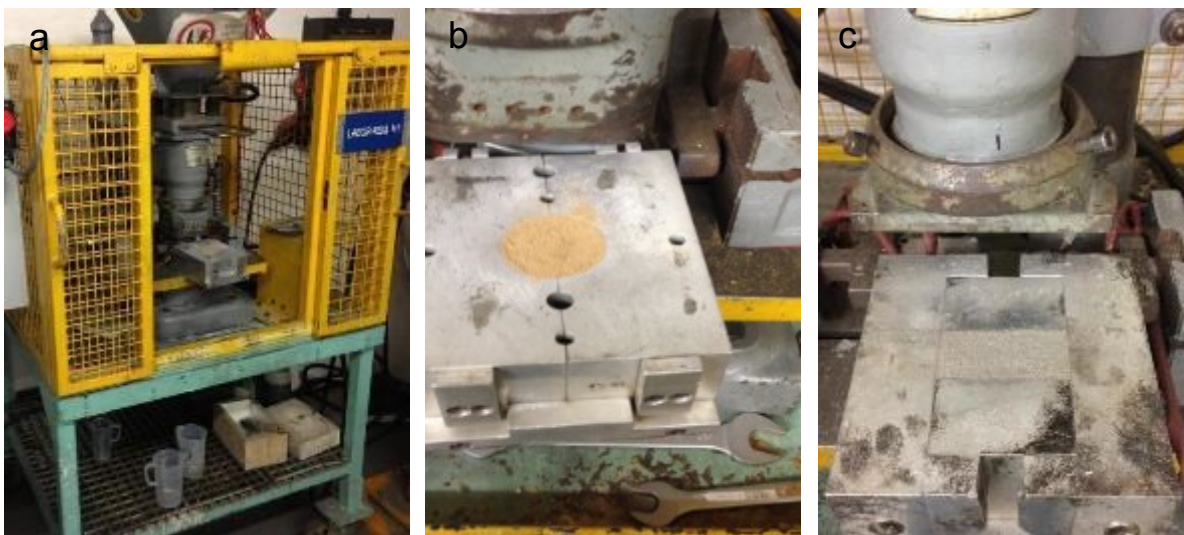


Figure 3-4: (a) Core shooting machine with the preheated mould (b). Installed cylindrical shape mould (c) Installed trapezoidal shape mould.

The mixed sands were shoot by a core shooting machine with 6-8 bars into the trapezoidal mould, which was preheated to the required parameters (**Table 3-2**). After 5 minutes drying in preheated mould, a trapezoidal sand core was formed.

Material for outer sand cores: H32 silica sands, water glass Betol[®] 52 T (Table 3-2), sand mixture device, and wooded mould.

Process: Outer cores were bonded by H32 silica sand and inorganic binder (water glass Betol[®] 52 T). The mixed sands were compressed into a wood mould (Figure 3-5), after forming, CO₂ was blown to harden sand cores for about 3 minutes.

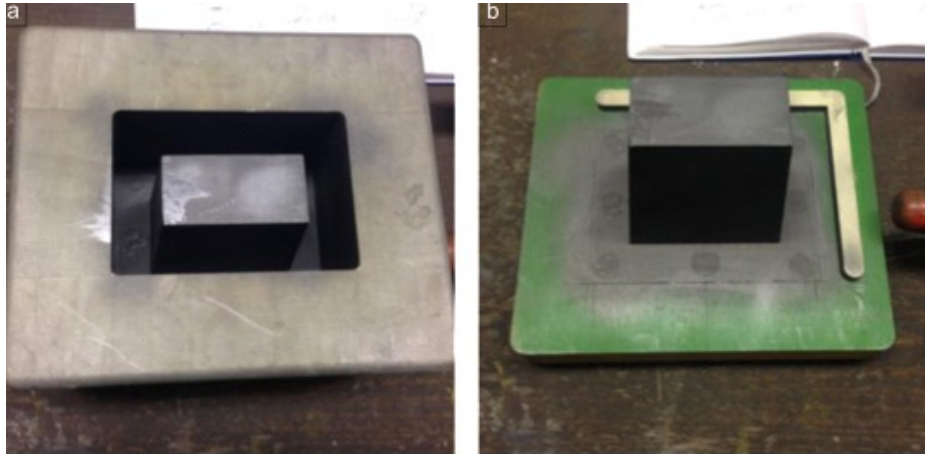


Figure 3-5: Wooded mould for making outer cores (a).the entirety wooden mould (b) the wooden foundation

Table 3-2: The parameters of producing five investigated internal cores.

Sand core	Base sand	Binder	Temperature	Time
Organically bonded sand core with modified urea-furan-phenolic resin using the warm box process	H32 silica sand	0.35 % urea-furan-phenolic resin	190 ± 10 °C	5 mins
Organically bonded sand core with an aqueous solution of phenol sulfonic acid, aluminum salts, sulfuric acid using warm box process	H32 silica sand	0.25 % aqueous solution of phenol sulfonic acid, aluminum salts, sulfuric acid	195 ± 10 °C	5 mins
Inorganically bonded sand core with modified silicate binder mixture and promoter (INOTEC™ - Promoter WJ 4000) using the warm box process	H32 silica sand	2.2 % modified silicate binder mixture and promoter (INOTECTM - Promoter WJ 4000)	180 ± 25 °C	5 mins
Inorganically bonded sand core with modified silicate binder mixture and promoter (Inotec Promoter EP 4174) using warm box process	H32 silica sand	2.2 % silicate binder mixture and promoter (Inotec Promoter EP 4174)	190 ± 25 °C	5 mins
Inorganically bonded sand core with water glass 39T @ using the warm box process	H32 silica sand	2.5 % water glass 39T @	190 ± 25 °C	5 mins
Inorganically bonded sand core with water glass 52T @ using water glass CO2 process	H32 silica sand	3.0 % water glass 52T @	-	5 mins

3.2.2 Dipping trials

3.2.2.1 Dipping trial of cylindrical sand core

Dipping trials were used to test the heat transport behavior of different sands submerged in an Al melt at constant temperatures.

Thermal couples were inserted into the specimens, which were set at 25 mm depth at three different positions. In order to measure the heat flow, the thermal couples were set at 25 mm, 15 mm and 5 mm from the edge of specimens, as shown in **Figure 3-6** (a). A welding wire held the sand cores for handling the thermal couples, as shown in **Figure 3-6** (b).

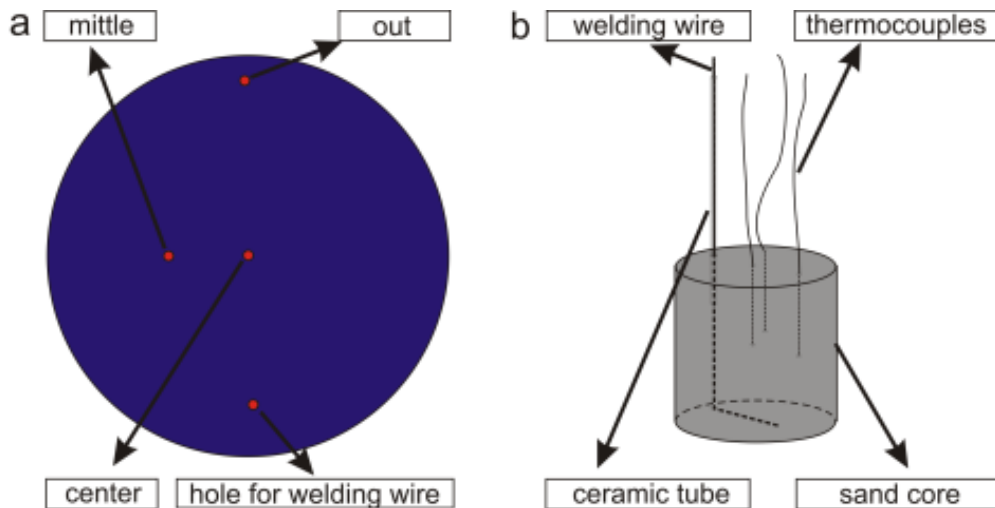


Figure 3-6: Sketch of positions of thermal couples.

Subsequently the specimens were held with the wire attached to a bracket (**Figure 3-7** (a)), and submerged into the Al melt (**Figure 3-7** (b)). Temperatures of Al-melts were set separately at 780 °C or 700 °C, with a holding time of 30 minutes. The temperatures time curves of each thermal couple at different measurement points were recorded with an analog - digital converter (DEWETRON data acquisition) (**Figure 3-7** (c) (d)).

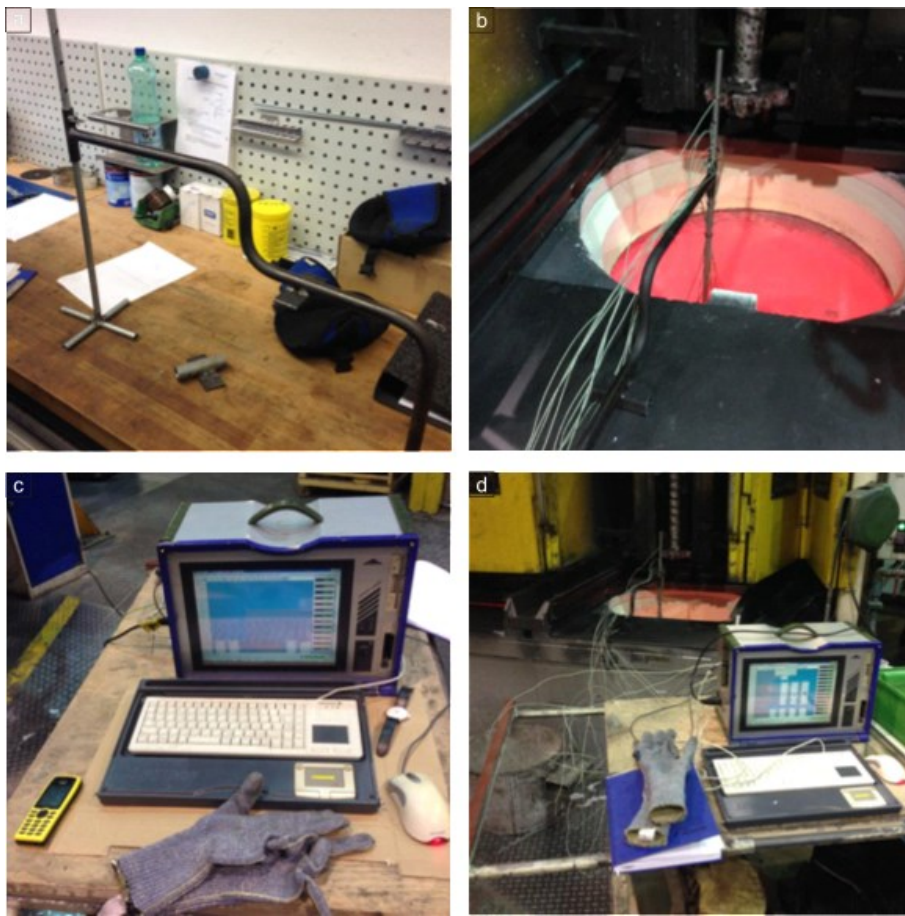


Figure 3-7: Device and process of dipping trails (a)The bracket for fixing the sand core and thermal couples; (b) The process of dipping into the melting Al alloy oven; (c) data acquisition to measure the temperature (Universalmaßgeräte DEWE – 2000; 1000894); (d) The measurement process of dipping trials.

3.2.2.2 Drying

Silica sand cores were dried in a Micro wave oven. The microwave oven can eliminate 80% to 90% water in the liquid medium. Three new H32 sand core were chosen, each was hardened using 2.5 wt. % water glass 39T and separately dried for 0 min/5mins/10mins.

3.2.3 Ring mould trials

The ring mould test is aimed to measure the temperature over time under a real solidification condition, and to measure the thermal conductivities of different sand cores during solidification. A steel ring mould ($D_{out} = 11.2$ mm, $D_{inner} = 8.9$, $H = 8.9$ mm) is arranged to provide a limited solidification time by an outside die acting as a heat sink while

the temperature distribution was measured in a cylindrical core located in the centre of the ring mould. Thereby these tests can be used to simulate a real casting condition, for example, the Rotacast process. The design of the cores was similar to that used in ‘dipping trials’, however without welding wires.

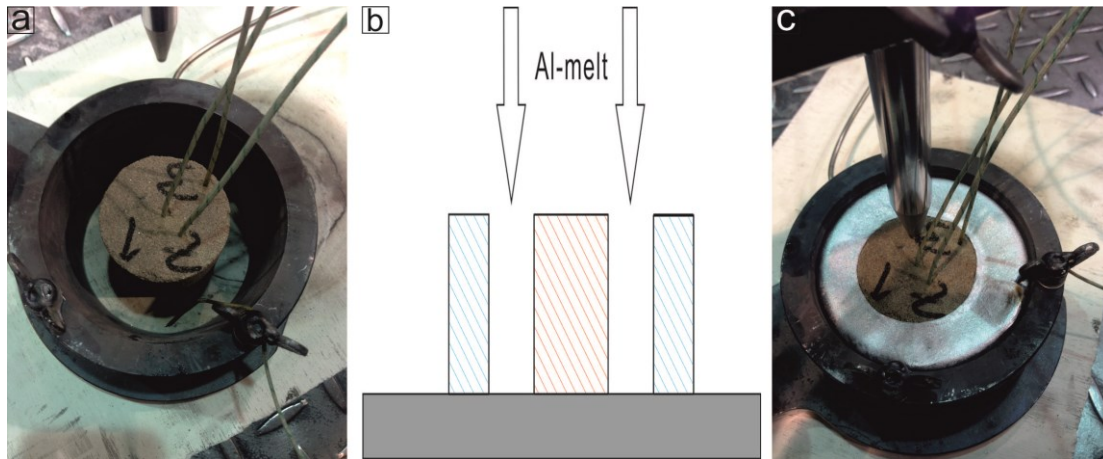


Figure 3-8: Sketch of the ring mould test with thermal couples. (a) Three thermal couples fixed into sand core and linked one thermal couples between steel ring mould and sand core

The sand cores with three thermal couples at 5 mm, 15 mm and 25 mm were set at the centre of a preheated ring steel ring (**Figure 3-8 (a)**) to 200 °C. A further thermal couple to measure the ring mould temperature during solidification was implemented. **Figure 3-8 (b)** shows the sand cores and the steel ring placed on the top of a refractory plate, and the Al – melt poured into the semi – enclosed space between ring mould and sand core. **Figure 3-8 (c)** shows the device during the solidification.

The temperature of the casting alloy was set at about 720 °C-740 °C, while the ring mould temperature was preheated to 200 °C. Experiments were stopped after 30 minutes. The temperatures over time in the core and the steel ring were recorded with a data acquisition system.

3.3 Mechanical properties

Shake out operation after casting is a significant process, which can impact the production efficiency in foundries. The retained strength of sand moulds is related to the base sand, binder, additives, and temperature exposure.

3.3.1 Semi-sealed mould test – casting box

The semi-sealed mould test is aimed to investigate the decoring behaviour for different core compositions. An internal trapezoidal core and an outer core were fixed on a steel plate, as shown in **Figure 3-9**. The internal core was used for subsequent decoring trials.

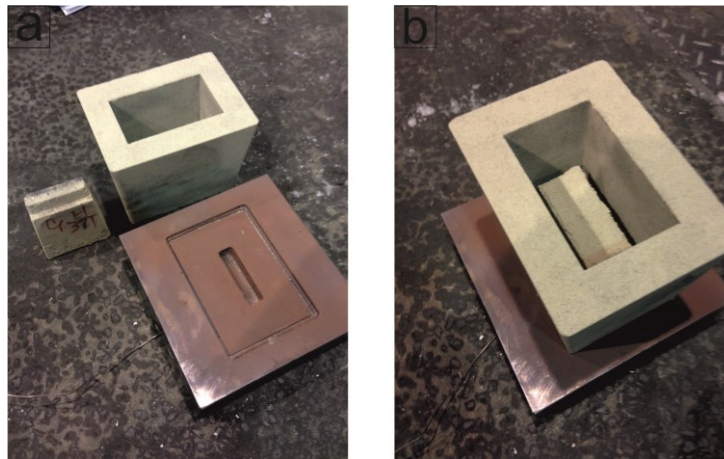


Figure 3-9: (a) internal core, outer core and steel plate (b) casting box before pouring Al-melt.

Molten Al ($T = 720\text{ }^{\circ}\text{C} \sim 740\text{ }^{\circ}\text{C}$) alloys were poured into the mould so that the internal core was totally submerged (**Figure 3-10 (a)**) and (**Figure 3-10(b)**).

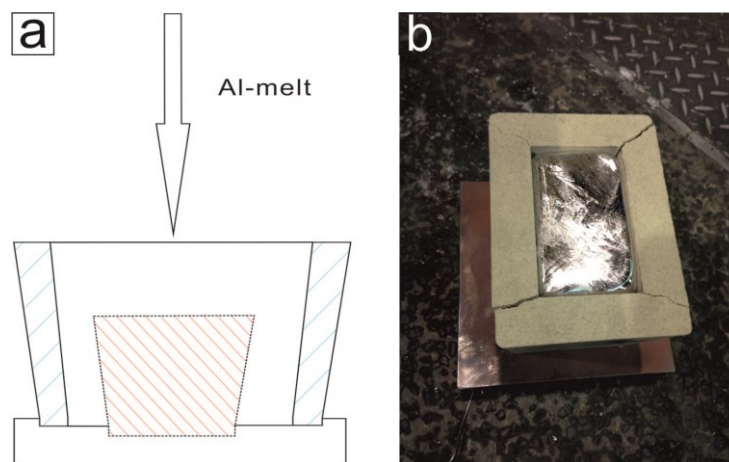


Figure 3-10: (a) The sketch of pouring Al – melt into fixed inner core and sand mould (b) Al – melt solidified in a sand mould.

After solidification, the outside core was carefully removed, and the Al casting with internal core was subsequently decored (shake out operation) under controlled conditions.

3.3.2 Shake out trials

For shake out trials the Al casting with internal core was placed on a robust funnel on top of a table (see in **Figure 3-11 (a)**) and hit with an impact device (300g, according to DIN1014). The sand of the internal core fell down through the funnel (see in **Figure 3-11 (b)**). Thereby for each impact a weight fraction of decored material was obtained, its weight was determined on a scale (PBJ6200-2M).

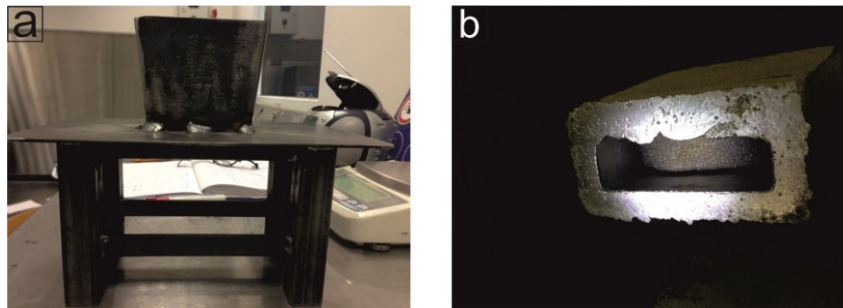


Figure 3-11: (a) modified shake out device (b) Specimen after shake out operation.

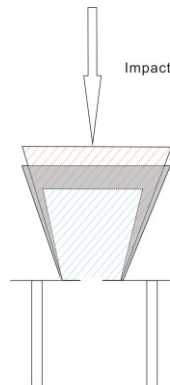


Figure 3-12: The schematic shake out operation with impact device.

Each type of sand core was exposed to three different manual impacted energies (light / middle / heavy) (see in **Figure 3-12**) and for each kind of impact energy, the samples were hit one two or three times.

3.4 Simulation of dipping trial

MAGMA 5 has well-developed thermal and fluid dynamic codes which can be used to predict shrinkage and gas porosity as well as stresses during solidification. Thermal properties correction and boundary condition justification can be performed due to the solidification simulation results [65]. MAGMA5 software was used to obtain thermal conductivity λ values for different sand cores. Thereby the temperature time curves at defined locations can be calculated for quartz sand and related to other sand based on their thermal physical properties (thermal conductivity λ , density ρ , and heat capacity C_p).

25 virtual thermal couples were defined in core samples to compare simulated temperatures to real temperature curves. The locations of virtual and real thermal couples are given in (Figure 3-13 (a)). From the edge to the centre, each 1 mm one thermal couple was set; the geometry is shown in Figure 3-13 (a) and (b).

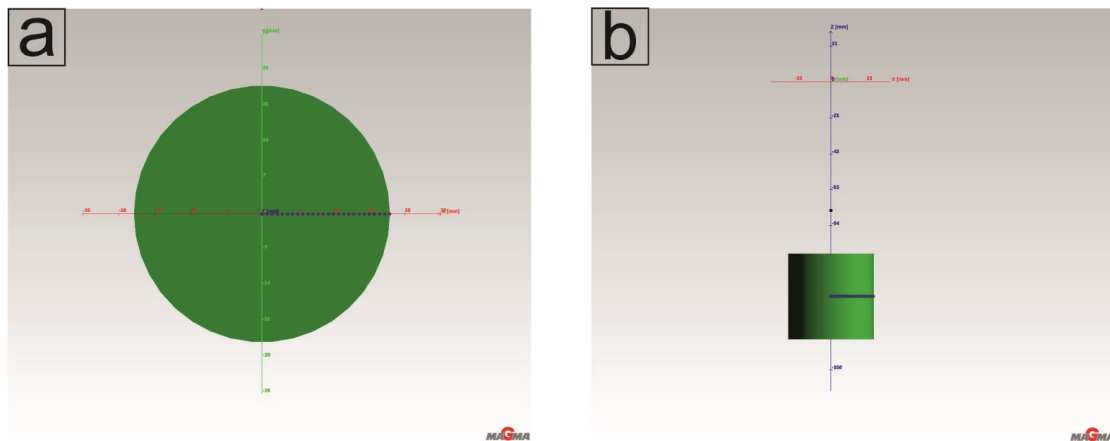


Figure 3-13: (a) 25 thermal test points in the sand core. (b) Geometry of simulated sand core with 25 thermal couples in sand core

The thermal conductivity λ of H32 silica sand from 0° C to 800° C ($\lambda_{\text{silica sand}}^{\text{Magma}}$) (Figure 3-14) was imported in Magma software as a reference.

As well-known Fick's Second Law [60], it describes heat transfer in the sand mold,

$$dT / dt = \alpha (d^2T / dx^2) \quad (\text{eq. 3})$$

where α is thermal diffusivity of mold (eq. 2); so that,

$$dT / dt = \frac{\lambda}{\rho * C_p} (d^2T / dx^2) \quad (\text{eq. 4})$$

A quotient Q was defined as a coefficient to adjust the thermal conductivity $\lambda_{\text{sand cores}}$ till the simulated and experimental dT / dt (temperature time curves) overlapped. So eq. 4 shorted as

$$(dT / dt)_{\text{silica sand in Magma}} = \frac{Q * \lambda_{\text{silica sand in Magma}}}{\rho * Cp} (d^2T / dx^2) \quad (\text{eq. 5})$$

where $Q * \lambda_{\text{silica sand in Magma}}$ was defined as the thermal conductivity of the investigated sand cores, density ρ and specific (Table A - 21) heat capacity Cp (from Table A - 16 to Table - 20) were as given values, according to (eq. 5), thermal conductivities of the investigated sand cores were defined as $\lambda_{\text{MIN sand}} = Q_{\text{MIN sand}} * \lambda_{\text{silica sand Magma}}$, $\lambda_{\text{Cerabeads sand}} = Q_{\text{Cerabeads sand}} * \lambda_{\text{silica sand Magma}}$, $\lambda_{\text{Kerphalite sand}} = Q_{\text{Kerphalite sand}} * \lambda_{\text{silica sand Magma}}$, $\lambda_{\text{Zircon sand}} = Q_{\text{Zircon sand}} * \lambda_{\text{silica sand Magma}}$, $\lambda_{\text{silica sand}} = Q_{\text{silica sand}} * \lambda_{\text{silica sand Magma}}$, so if the $(dT / dt)_{\text{simulation}}$ and $(dT / dt)_{\text{experiment}}$ overlapped by controlling Q values, the thermal conductivities of investigated sand cores were obtained.

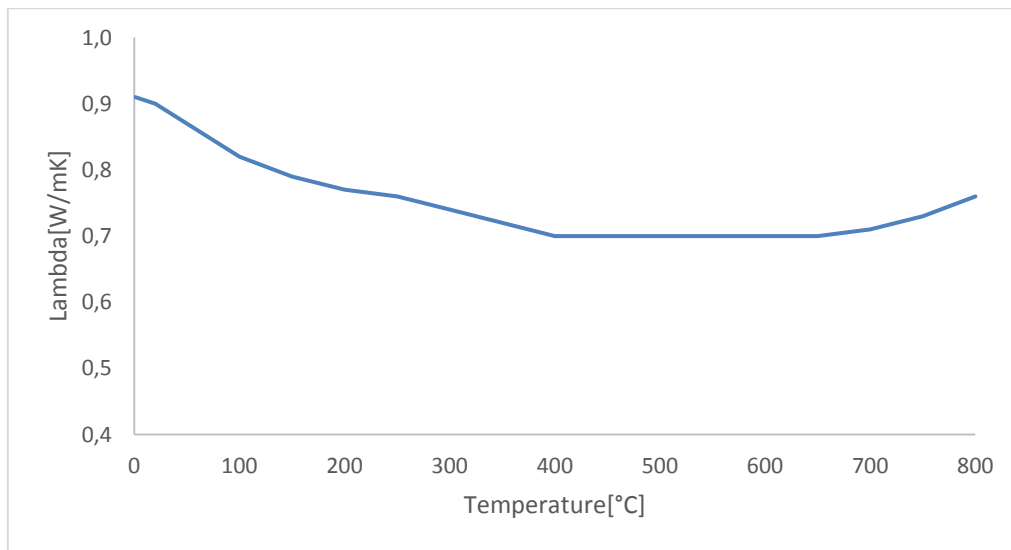


Figure 3-14: $\lambda_{\text{silica sand}}$ value with temperature.

4 Results

In this chapter the morphology of the raw sands and the binder bridges in sand cores were investigated using optical microscopy and SEM. The thermal and mechanical experiment results were obtained by 'dipping trials', 'ring mould trials' and 'semi-sealed mould tests' in thermal experiments and by a scaled down mechanical shake out operation in decoring experiments.

4.1 Raw sands

4.1.1 Grain size distribution

Grain size distributions of five different sands were obtained by sieve analysis described in Chapter 3. The grain size distributions are shown in Table A-1, Table A-2, Table A-3, Table A-4 and Table A-5 and are illustrated in **Figure 4-1**.

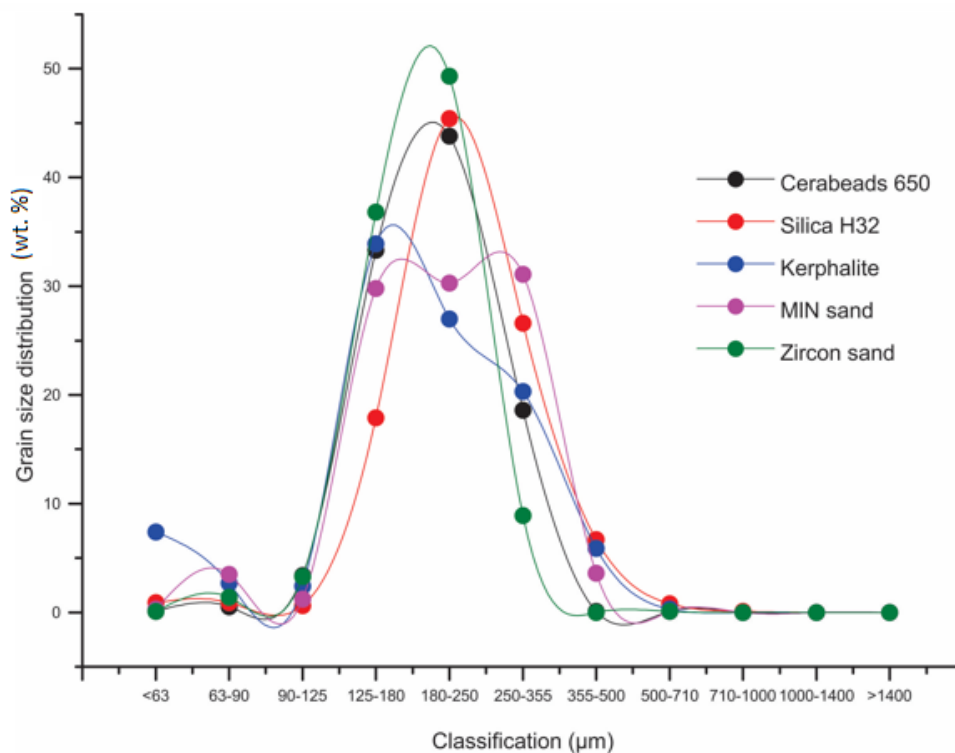


Figure 4-1: Grain size distribution of five different base sands.

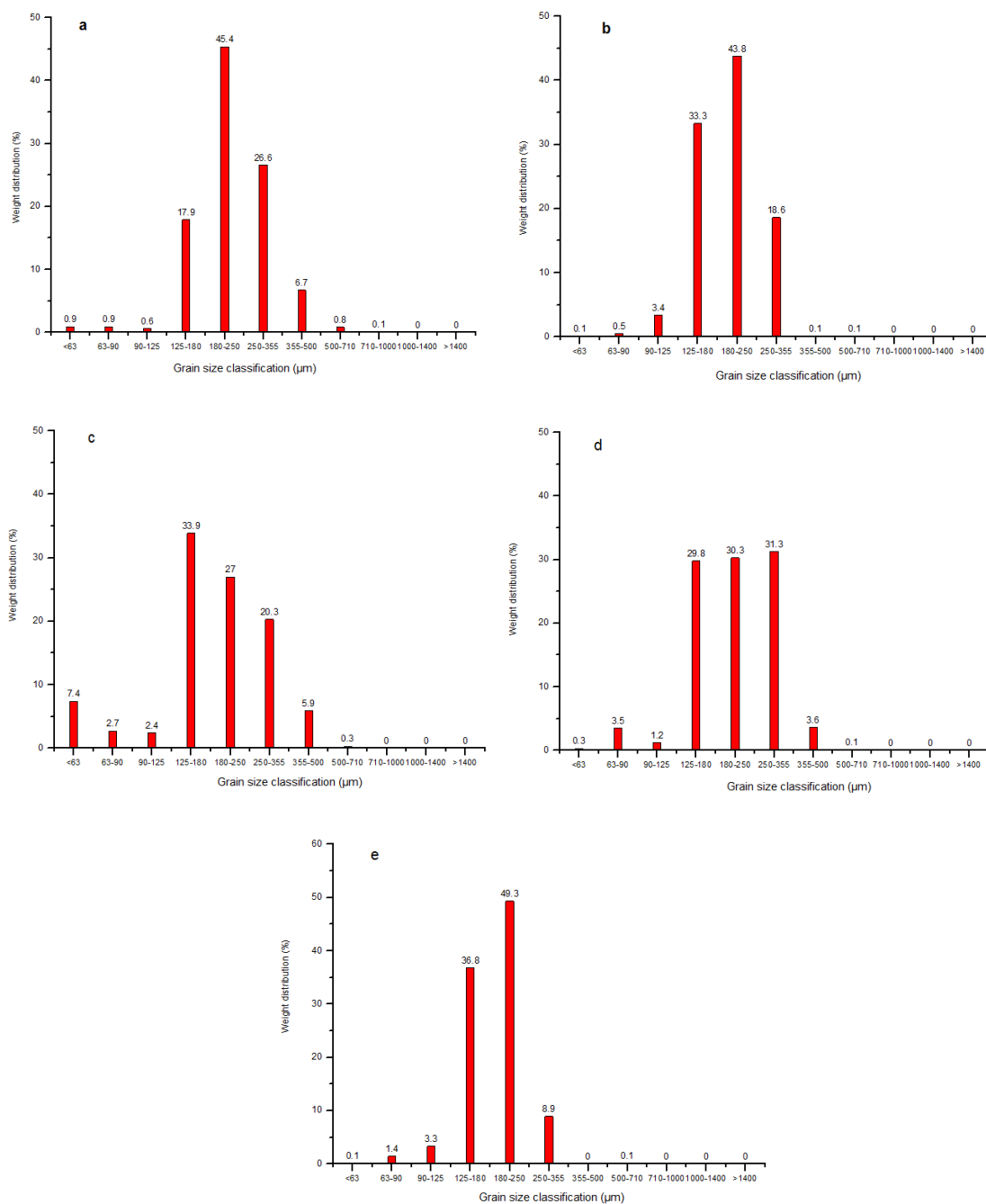


Figure 4-2: Grain size distribution by weight in five investigated raw sands. (a) H32 silica sand grain size distribution (b) Cerabeads sand grain size distribution (c) Kerphalite sand grain size distribution (d) MIN sand grain size distribution (e) Zircon sand grain size distribution.

As shown in **Figure 4-1** and **Figure 4-2**, grain sizes in these five sands were mainly distributed between 90 µm and 710 µm. For the silica sand H32, the grain size distribution ranged from 125 µm to 180 µm at 17.9 wt. %, from 180 µm to 250 µm at 45.4 wt. %, from 250 µm to 355 µm at 26.6 wt. %, larger than 355 µm over 6 wt. %. For the dark spheroidal Min sand, the grain size distribution ranged from 125 µm to 180 µm at 29.8 wt. %, from 180

μm to 250 μm at 30.3 wt. %, from 250 μm to 355 μm at 31.1 wt. %, and over 355 μm , or smaller 125 μm at 4 wt. %. For the yellowish spheroidal Cerabeads sand, the grain size distribution ranged from 125 μm to 180 μm at 33.3 wt. %, from 180 μm to 250 μm at 43.8 wt. %, from 250 μm to 355 μm at 18.6 wt. %. For the synthetic gray Kerphalite sand, the grain size distribution ranged from 125 μm to 180 μm at 33.9 wt. %, from 180 μm to 250 μm at 27.0 wt. %, from 250 μm to 355 μm at 20.3 wt. %, below 125 μm at about 10 wt. %. For the Zircon sand, the grain size distribution ranged from 125 μm to 180 μm at 36.82 wt. %, from 180 μm to 250 μm at 49.39 %, from 250 μm to 355 μm at 8.9 wt. %, below 125 μm of about 5 wt. %.

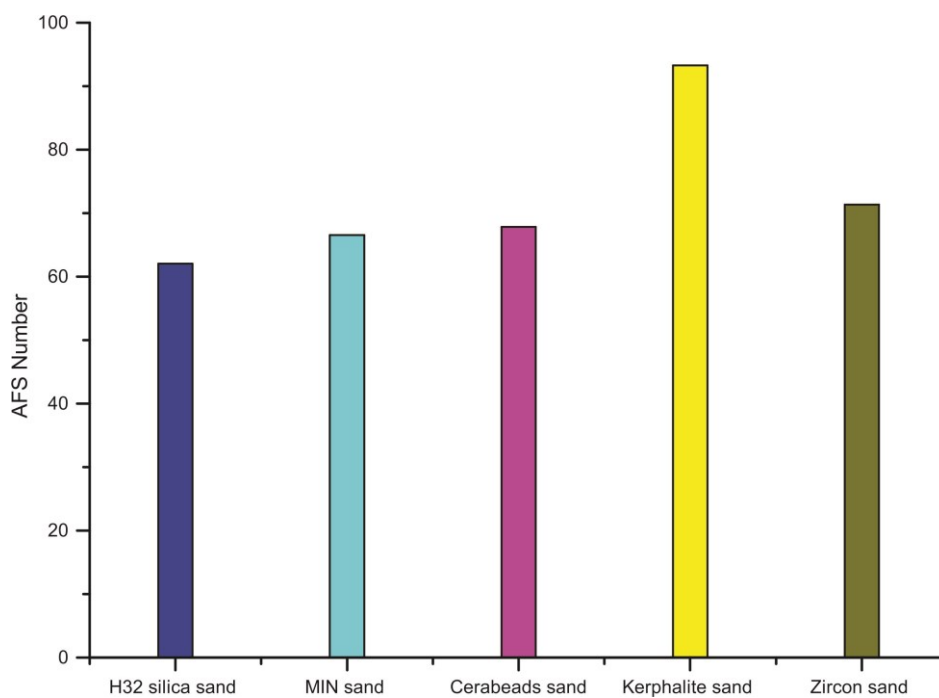


Figure 4-3: AFS Number of five different base sands.

Figure 4-3 shows the AFS number (see section 2) of five different base sands. Kerphalite sand exhibit the largest average grain size in these five base sands with the AFS number of 93.3. Zircon sand has the AFS number of 71.4. The H32 silica sand has the smallest average grain size with the AFS number of 62.0. AFS numbers of MIN sand and Cerabeads sand are 66.6 and 67.8, respectively. As mentioned in chapter 2, the AFS grain fineness number and average grain size are relevant, this relationship in investigated five sands is shown in **Figure 4-4**.

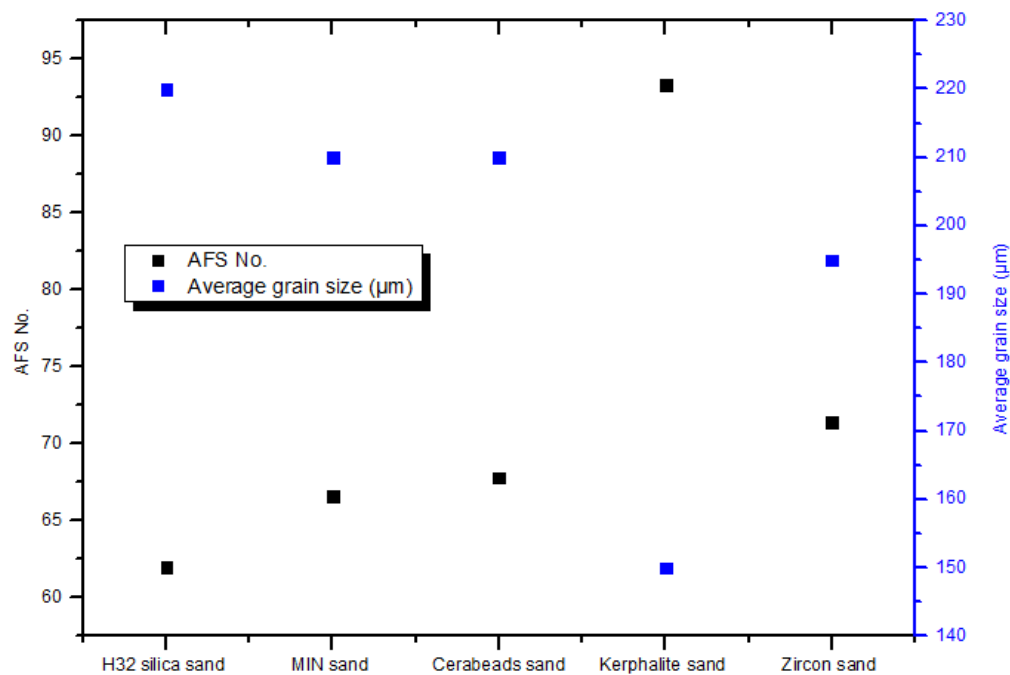


Figure 4-4: The relationships between AFS grain fineness number and average grain size in five sands.

Figure 4-4 shows that, H32 silica sand exhibits a maximal value (about 220 µm) of average grain size and a minimal value of AFS grain fineness number (62.0). This means, H32 silica sand has the largest grain size. And the Kerphalite sand has a minimal value (about 150 µm) of average grain size and maximal value of AFS grain fineness number (93.3). This means, the Kerphalite sand has the smallest grain size. MIN sand and Cerabeads sand exhibit a similar average grain size of about 210 µm. Zircon sand exhibits an average grain size of 195 µm as a second smallest in these five base sands.

4.1.2 Grain morphology 2D-Shape factor

2D-shape factors of five base sands were measured manually of scanning electronic micrograph as described in Chapter 3. Red zones covered the manually chosen sand particles. The shape factor was calculated for each highlighted red zone, as shown in **Figure 4-5**.

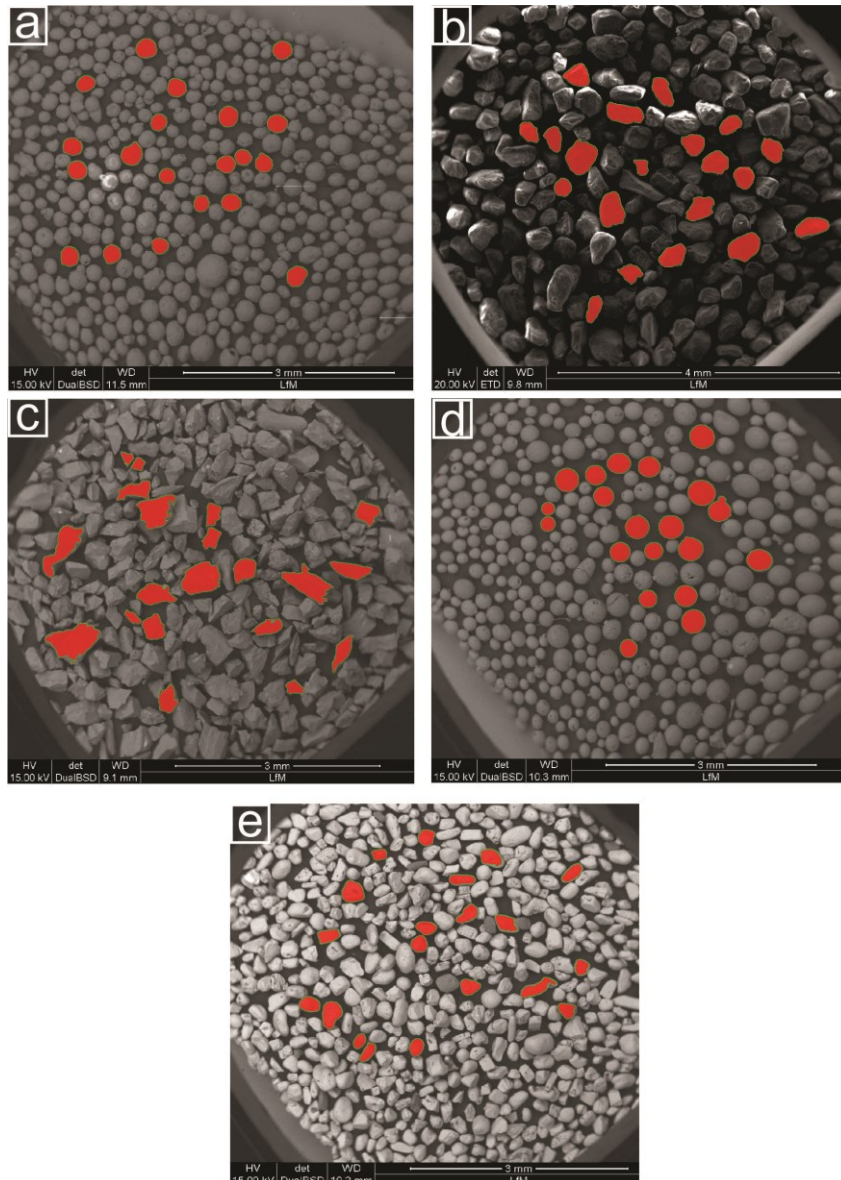


Figure 4-5: Tested sand particles in each base sand to measure shape factor (a) Cerabeads sand (b) H32 silica new sand (c) Kerphalite sand (d) MIN sand (e) Zircon sand.

In **Figure 4-5**, examples of sand particles in each base sand to measure shape factor are shown. The covered red areas are the manually chosen sand particles for roundness analysis.

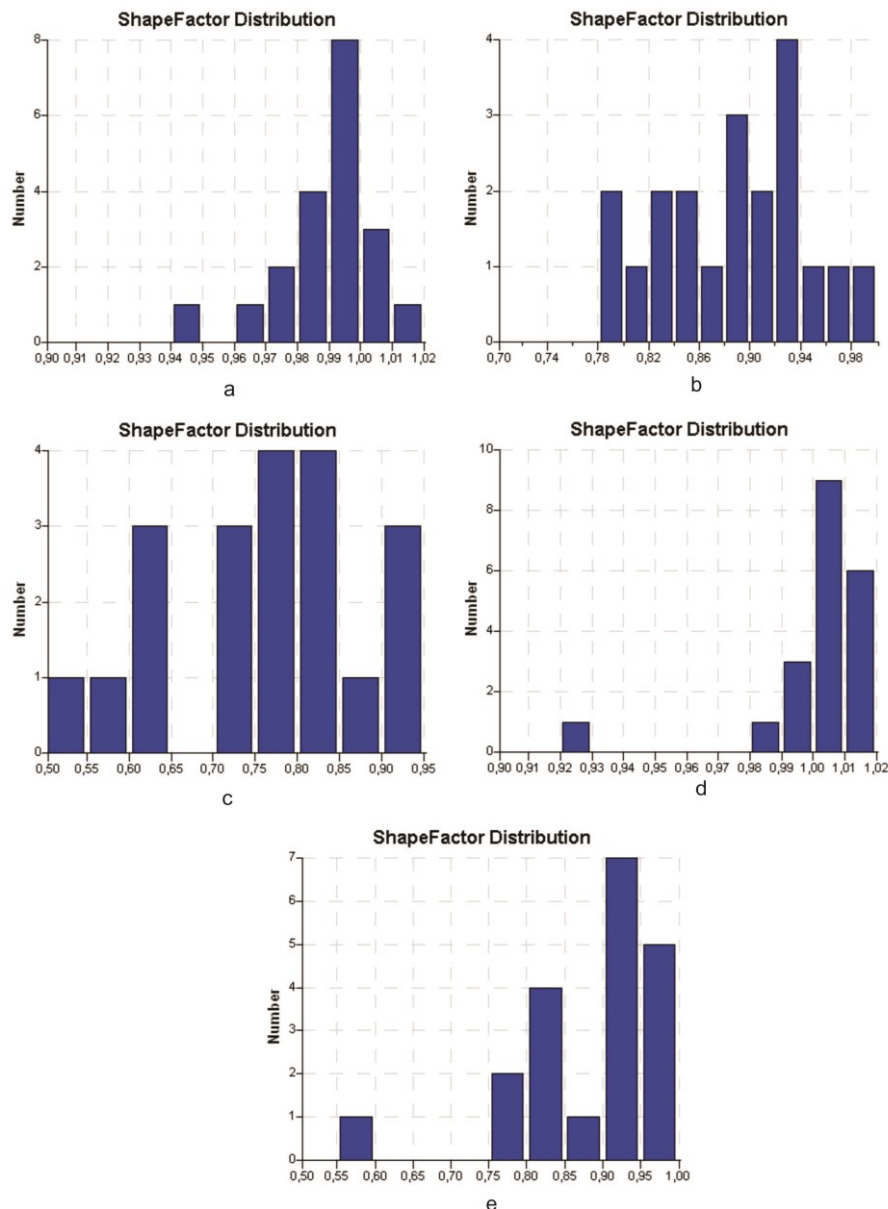


Figure 4-6: Shape factor distribution of five different base sands (a) shape factor distribution of Cerabeads sand (b) shape factor distribution of Silica sand (c) shape factor distribution of Kerphalite sand (d) shape factor distribution of MIN sand (e) shape factor distribution of Zircon sand.

Particles were individually chosen and measured by image analysis for their mean values of shape factors for each base sand. A Shape factor distribution in each base sand is given in **Figure 4-6**. As **Figure 4-6 (a)** shows, Cerabeads sand particles exhibit shape factor values over 0,94. Furthermore, the shape factor of 17 particles is close to 1,0. This means, the Cerabeads sand particles are mostly round. As **Figure 4-6 (b)** shows, 20 silica sand particles exhibit shape factor values over 0,78. In silica sand the shape factor distribution gives a roundness of sand particles from 0,78 to 1,0. This indicates that silica sand exhibits

also some irregular sand particles. As **Figure 4-6 (c)** shows, Kerphalite sand particles have shape factor values less than 0.65, others are distributed between 0.75 and 0.95. As **Figure 4-6 (d)** shows, one MIN sand particle has a shape factor value less than 0.60, others are all around 1.0. These values indicate that, MIN sand exhibit mostly regular round particles, with some exception. As **Figure 4-6 (d)** shows, Zircon sand particle exhibits a shape factor value less than 0.60. Others are unevenly distributed from 0.75 to 1.0.

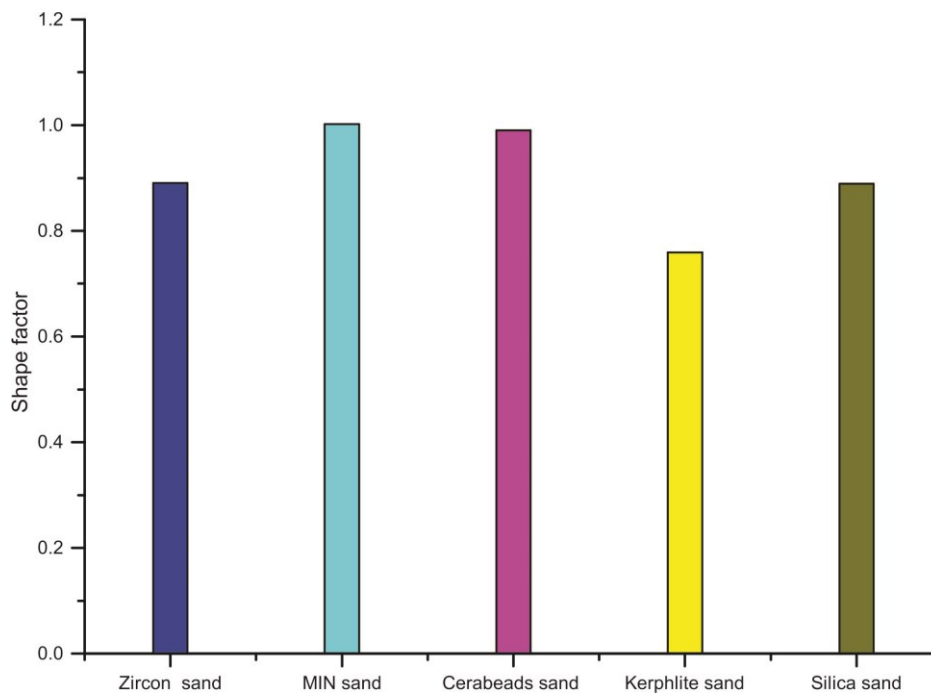


Figure 4-7: The shape factors of different raw sands.

In **Figure 4-7**, the mean 2-D shape factors of five different sands are given. After calculating a mean value of 20 different sand particles, the value of shape factor in MIN sands was 1.0, Cerabeads sands had a value closer to 1.0, silica sands and Zircon sands had values closer to 0.9, and shape factor value of Kerphalite sands was the lowest, was closer to 0.75.

4.1.3 Optical microscopy

A variety of sands were compared and their visual appearances are shown in **Figure 4-8**. In some cases the optical transparency, leading to shining and glancing surfaces, made it difficult to investigate the morphology by optical microscopy in detail.

Figure 4-8 shows the grain shapes and colours obtained by Optical Microscopy: a) Cerabeads are the yellowish spheroidal; b) silica sand grains are transparent; c) gray

Kerphalite sand grains are irregular with more edges and corners; d) MIN sand grains are black spheroidal; e) zircon sand grains exhibit a smooth surface with light pink colour.

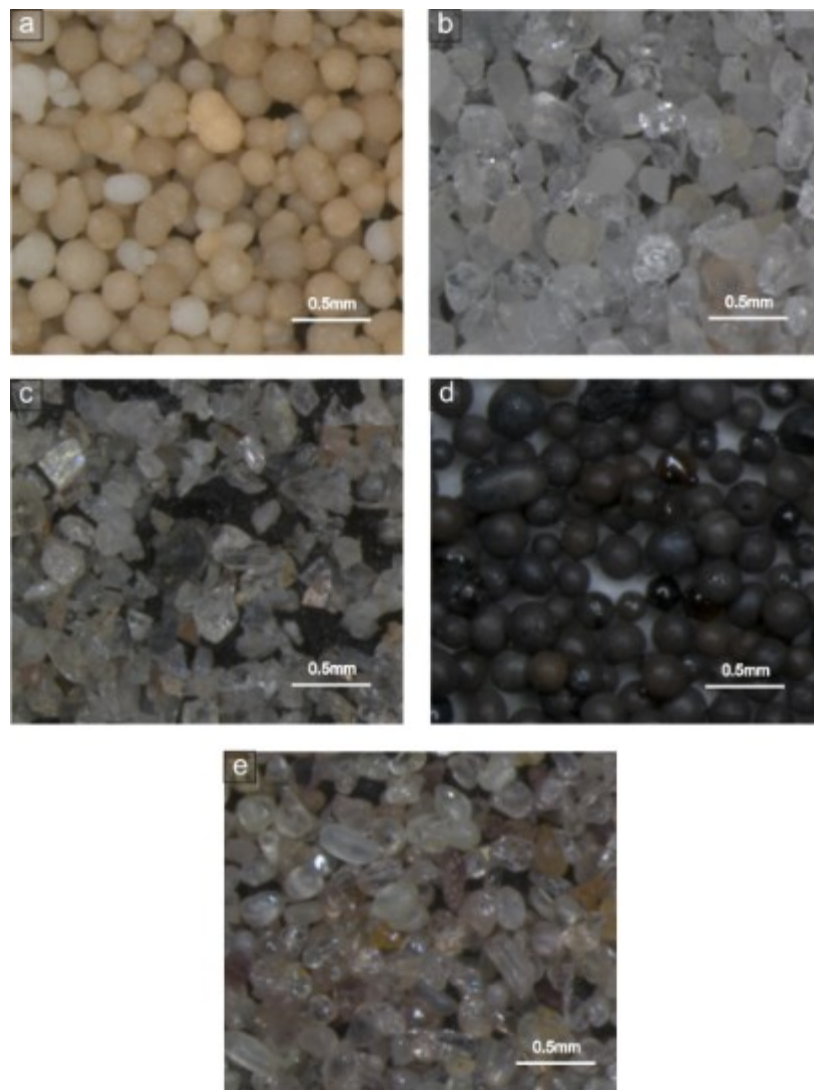


Figure 4-8: Microscopy images of raw sands (a) Cerabeads 650 raw sand (b) Silica sand H32 (c) Kerphalite or Andalusit raw sand (d) MIN sand (e) Zircon raw sand.

4.1.4 Scanning electron microscopy

The morphology of five different raw sands and binder bridges in sand cores before and after thermal shock were observed by scanning electron microscopy. The morphologies of five base sands were observed by SEM, and chemical compositions were determined by EDX. The observation of binder bridges in sand cores is aimed to analyze the binder connection before and after Al – casting.

4.1.4.1 Raw sands

Figure 4-9 (a) and **Figure 4-9** (b) show synthetic Cerabeads sand grains exhibiting a rounder shape than silica sand grains as illustrated by the shape factor (**Figure 4-7**). The morphology was mainly round and in some cases agglomerates led to irregular particles, as shown in **Figure 4-9** (c). The surface of Cerabeads sand shows a microstructure with a fine surface roughness (**Figure 4-9**(d)).

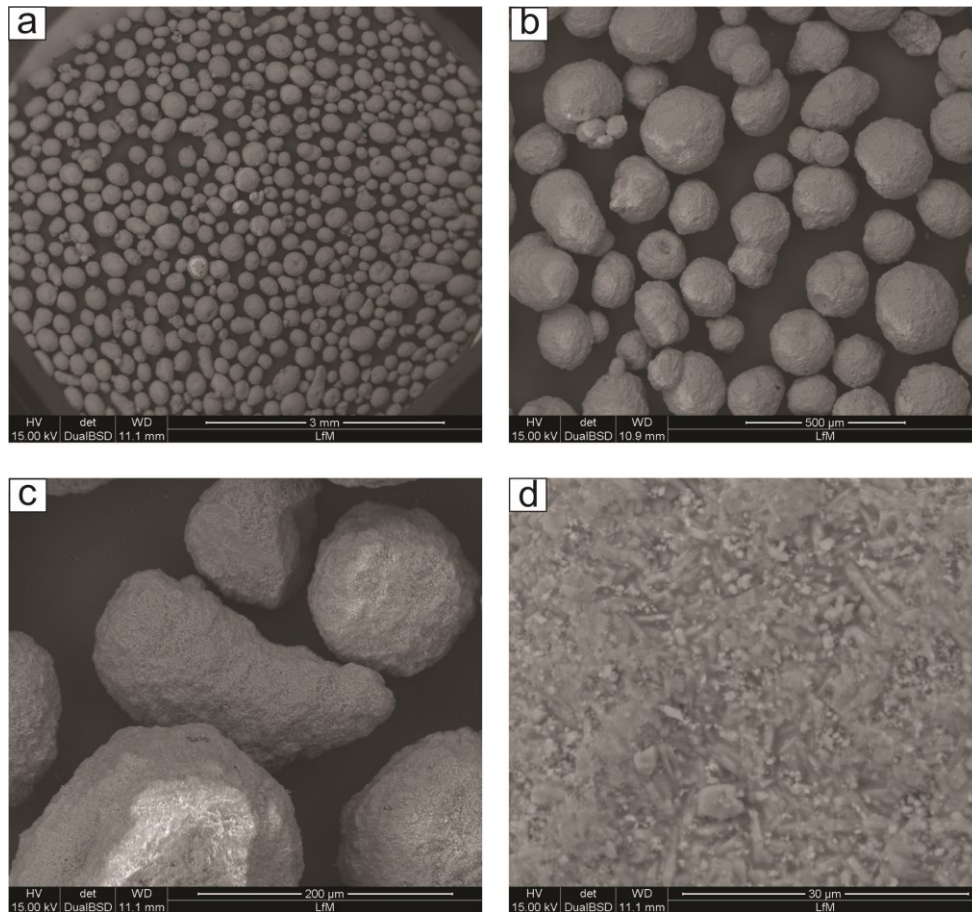


Figure 4-9: Different sand particles of Cerabeads raw sand (a) Different size of rounded sand particles (b) Single particles and bonded particles (c) morphology of sand particle (d) surface of Cerabeads sand particle.

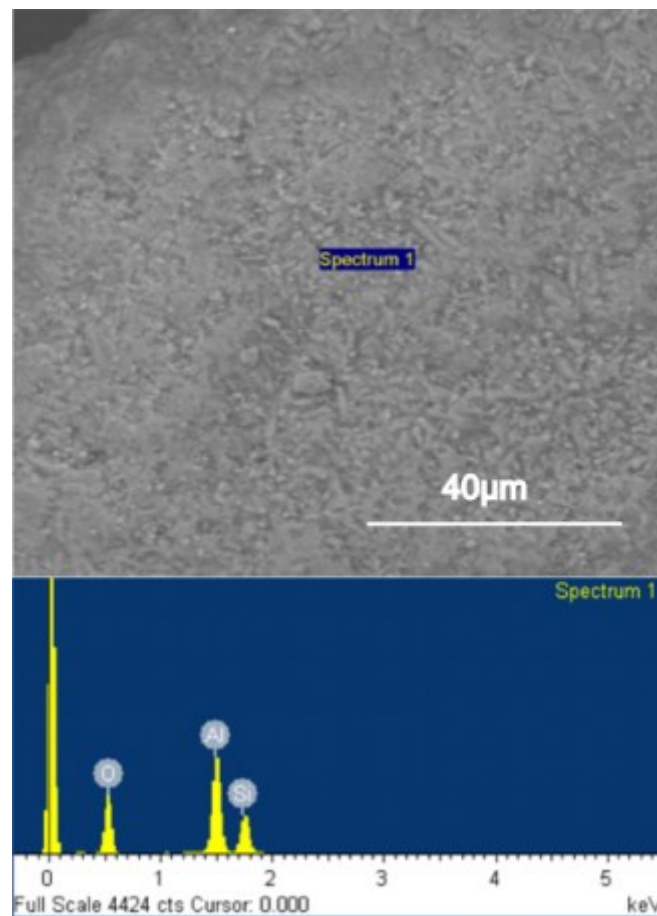


Figure 4-10: View of Cerabeads sand and their chemical compositions.

Figure 4-10 shows the SEM and EDX analysis of a Cerabeads sand particle. A fine surface roughness was observed by SEM. The chemical composition of Cerabeads sand particle was determined by EDX, as 24.15 at. % Al, 13.54 at. % Si and 61.66 at. % O as SiO_2 and Al_2O_3 .

Figure 4-11 shows the observed smooth surfaces with some fractured rough areas of silica sand. The irregular shape is shown in **Figure 4-11 (a)**. **Figure 4-11 (b)** shows some rough fractured surface on the silica sand particle surface. **Figure 4-11 (c)** shows an irregular sand particle with distinct faces. **Figure 4-11 (d)** shows a round grain with a smooth surface.

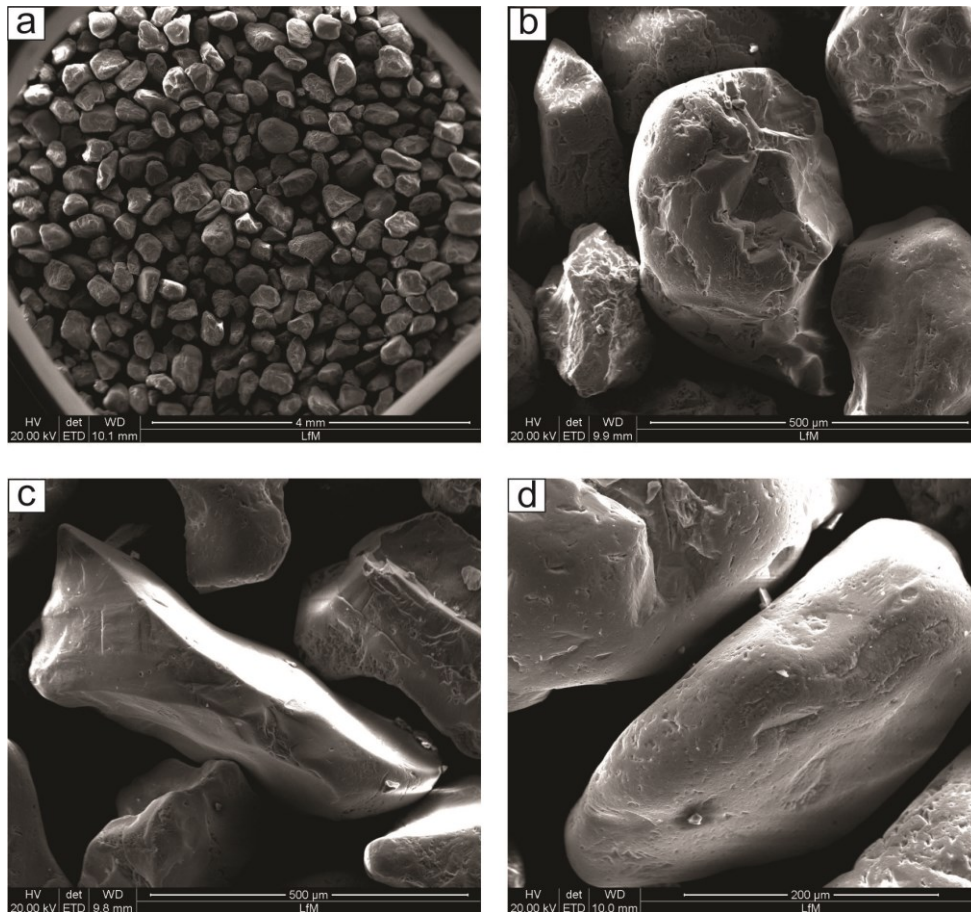


Figure 4-11: Different sand particles of H32 raw sand (a) Shapes of H32 silica sands (b) rough surface and fracture (c) the particle with distinct faces (d) smooth round surface.

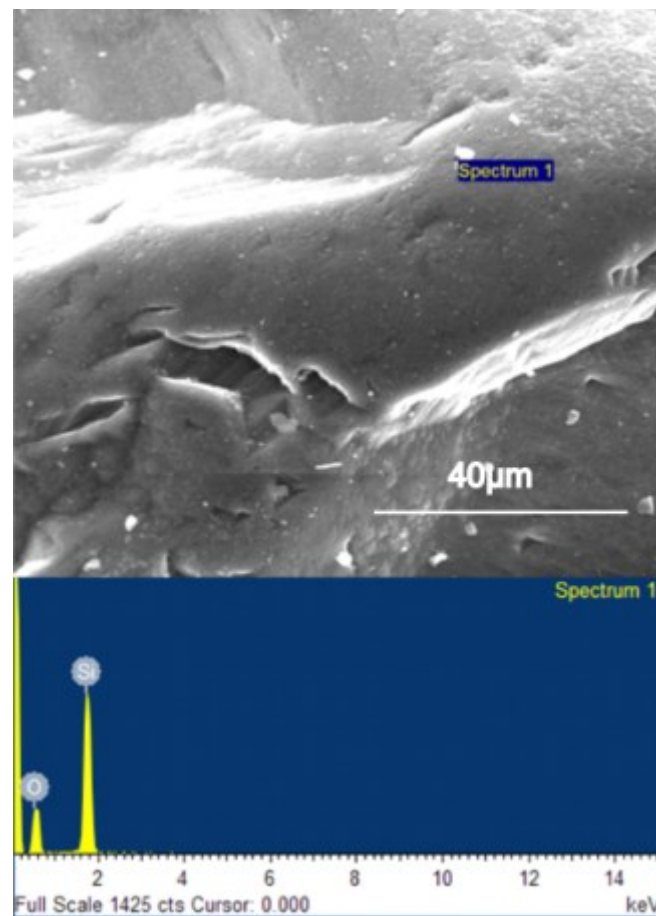


Figure 4-12: The fractured surface and groove on silica sand particle and its chemical compositions.

Figure 4-12 shows SEM and EDX analysis of a silica sand particle. A fracture on the surface was observed by SEM. The chemical composition of silica sand particle was determined by EDX, as Si of 36.15 at. % and O of 63.85 at. %, silica sand H32 contains mostly SiO_2 .

Figure 4-13 (a) shows Kerphalite sand grain with sharp edges and corners. A cubic shape particle was observed (**Figure 4-13** (b)). Some fractures and cracks were observed on the surface of particles (**Figure 4-13** (c) and **Figure 4-13** (d)).

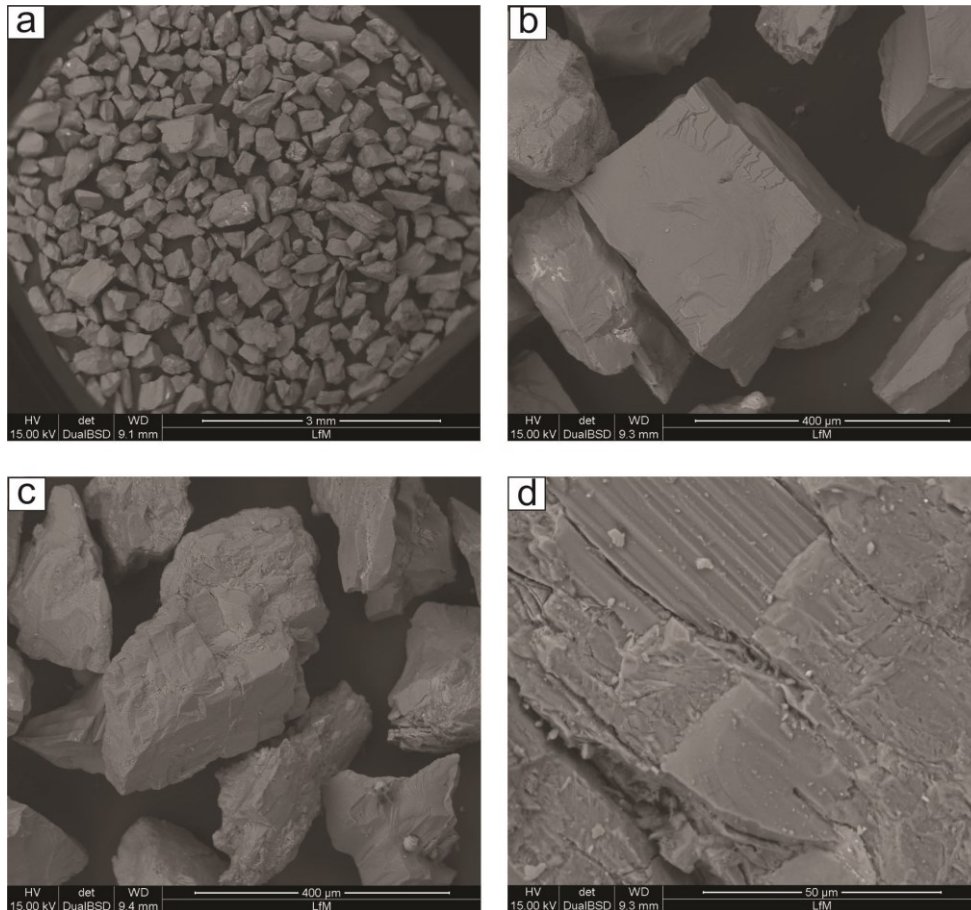


Figure 4-13: Different sand particles of Kerphalite raw sand. (a) Different size sand particles with sharp edges and corners (b) an obvious cubic shape particle (c) morphology of an irregular and sharply pointed particles sand particle (d) surface of Kerphalite sand particle.

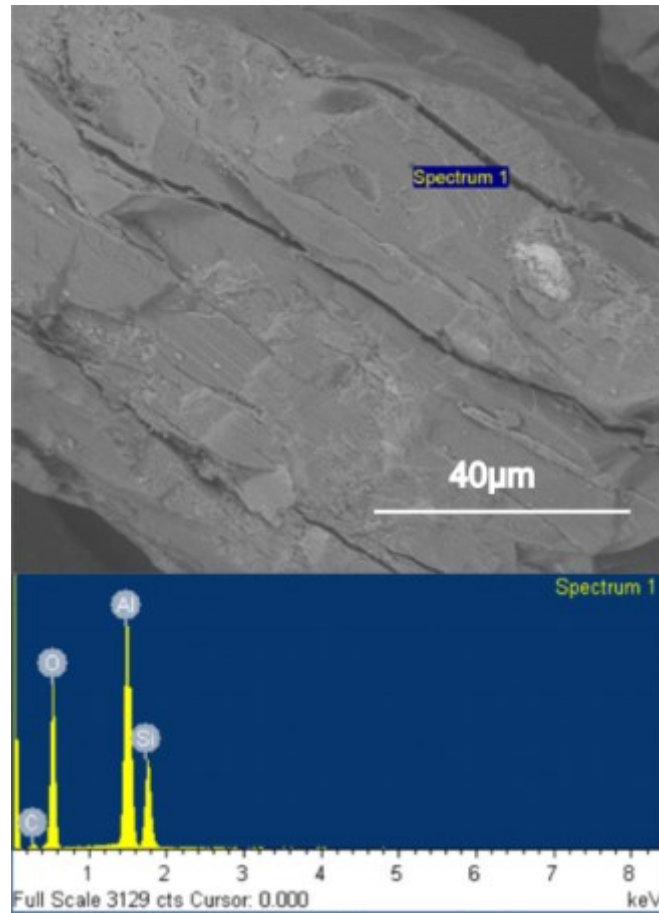


Figure 4-14: View of Kerphalite sand and their chemical compositions.

Figure 4-14 shows SEM and EDX analysis of a Kerphalite sand particle. A rough surface with many broken layers on the surface was observed by SEM. The chemical composition of Kerphalite sand particle was determined by EDX, as Al of 20.80 at. %, Si of 10.15 at. %, O of 57.66 at. % and C of 11.39 at. %.

Figure 4-15 (a) shows different sizes of round MIN sand particles. **Figure 4-15** (b) shows different surface morphologies of MIN sand particles, which were observed near to perfect spheroidal. Agglomerated particles were also observed as shown in **Figure 4-15** (c). Also a dendrite structure resulting from some Al_2O_3 growth was observed on the surface (**Figure 4-15** (d)).

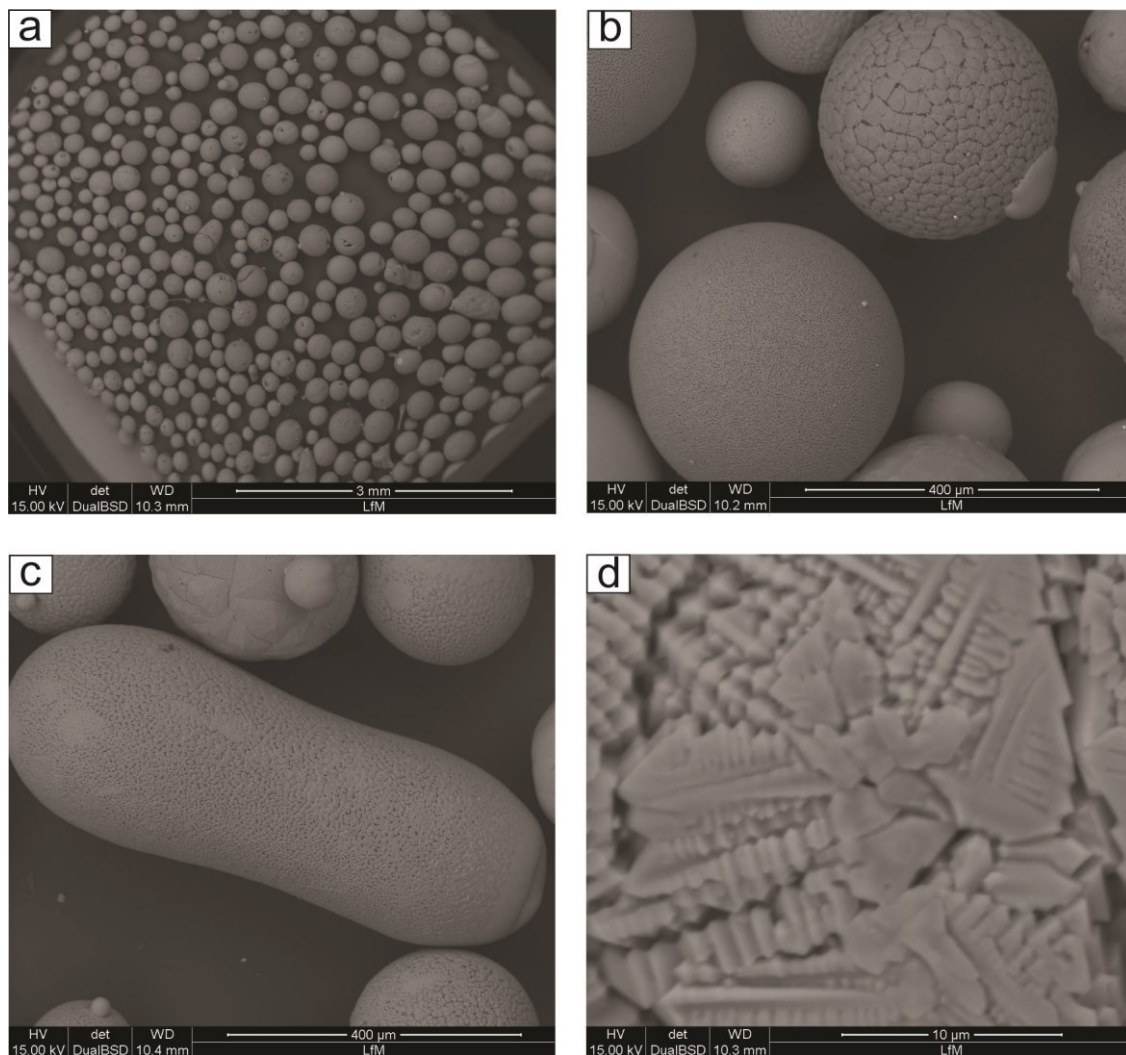


Figure 4-15: Different sand particles of MIN raw sand. (a) Different size sand particles with round particles (b) some spheroidal particles (c) Agglomeration of two particles (d) surface of MIN sand particle

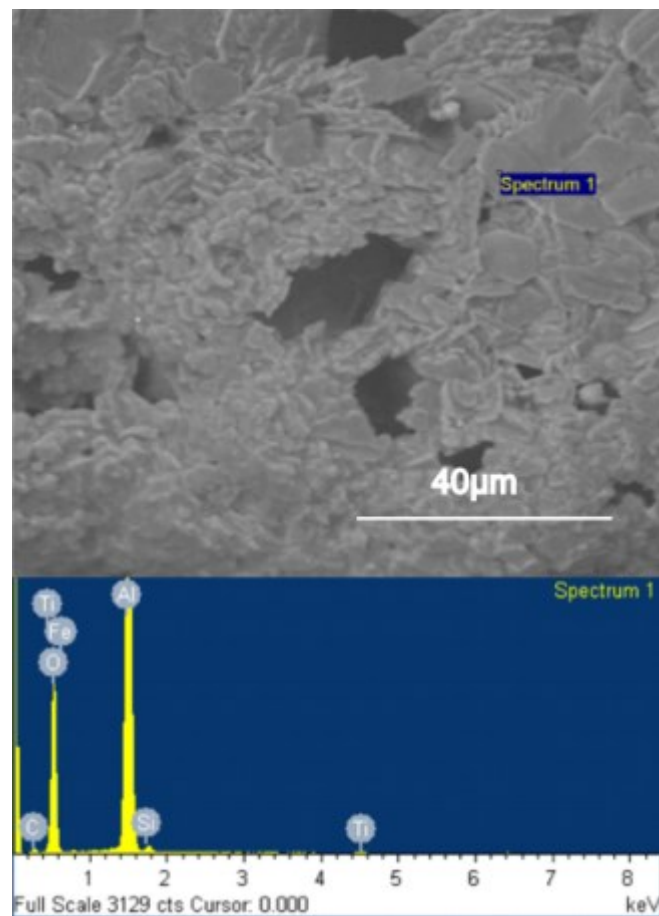


Figure 4-16: View of Min sand and their chemical compositions.

Figure 4-16 shows SEM and EDX analysis of a Kerphalite sand particle. A rough surface with many cavities on the surface was observed by SEM. The chemical composition of MIN sand particle was determined by EDX, as O of 63.49 at. %, Al of 28.30 at. %, C of 6.85 at. %. Cavities were observed on the particle surface, which may particularly strengthen the adhesion between sand particles and binder.

Figure 4-17 (a) shows irregular shaped zircon sand particles with rounded edges. Zircon sand grains exhibit pre-fractures and grooves on the surfaces as shown in **Figure 4-17** (b), some particles exhibit round edges and cleaved fracture surface as shown in **Figure 4-17** (c) and smooth surface was observed as shown in **Figure 4-17** (d).

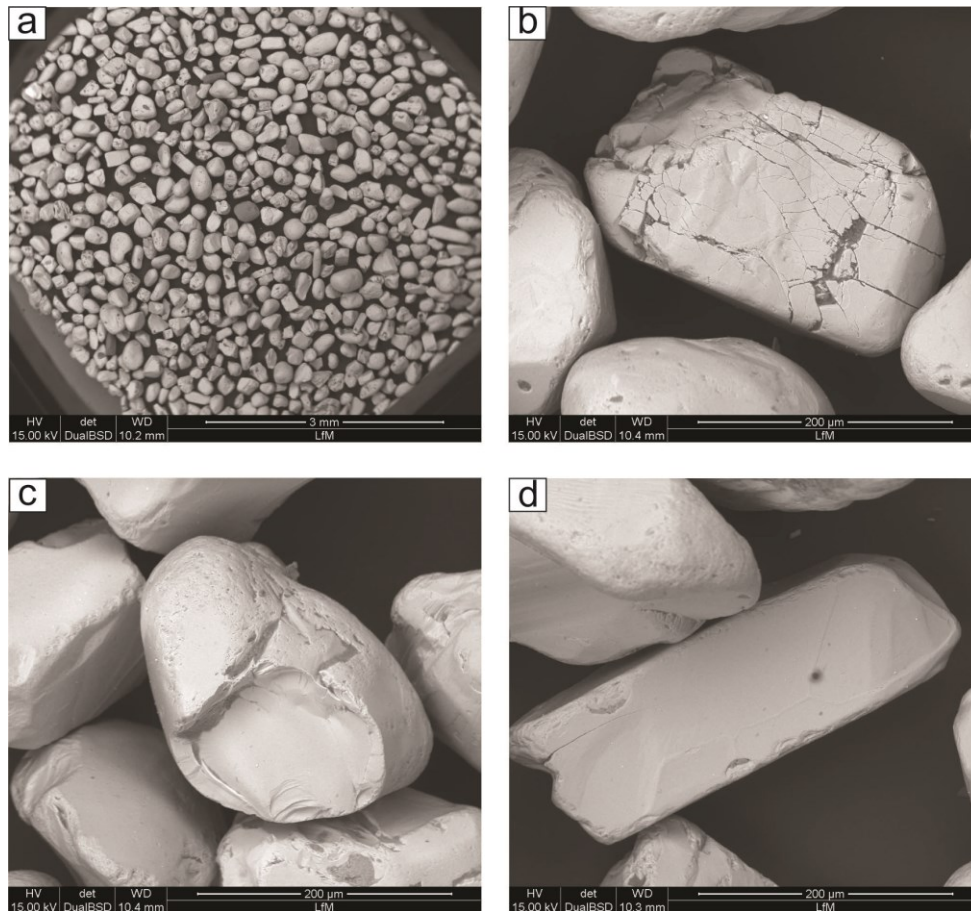


Figure 4-17: Different sand particles of Zircon raw sand (a) Rounded edges irregular particles (b) pre-fractures and grooves on the surfaces (c) fractures on the surface (d) smooth surface.

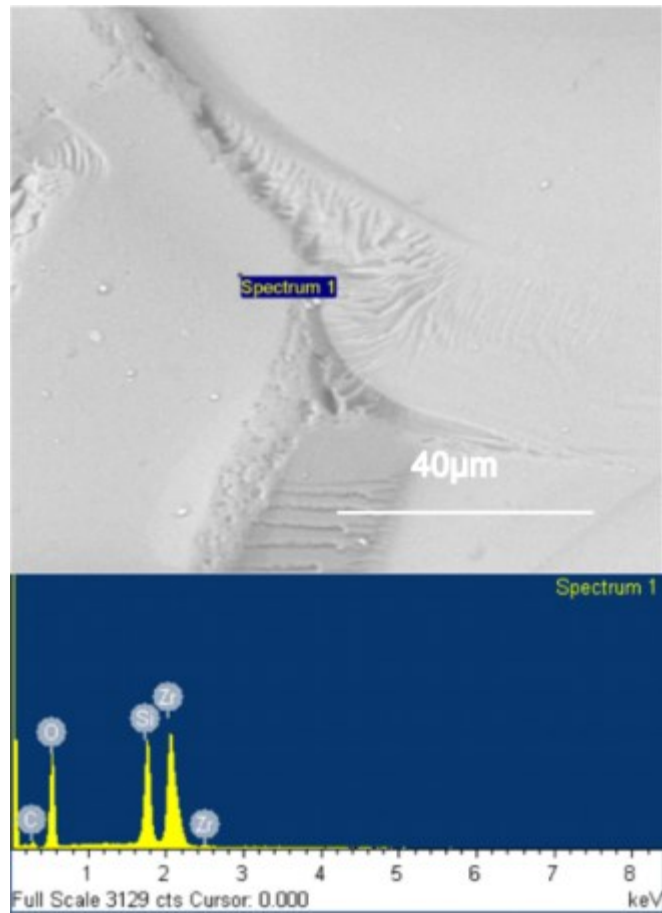


Figure 4-18: the Micro view of zircon sand and chemical compositions.

Figure 4-18 shows SEM and EDX analysis of a zircon sand particle. A smooth surface with the broken edges was observed by SEM. The chemical composition of the zircon sand particle was determined by EDX, as Zr of 10.8 at. %, Si of 9.91 at. %, O of 65.30 at. % and C of 14 at. %.

4.1.4.2 Organically bonded sand cores

Organically bonded sand cores were produced with modified urea-furan-phenolic resin (as shown in Fehler! Verweisquelle konnte nicht gefunden werden. and Fehler! Verweisquelle konnte nicht gefunden werden.) using the warm box process. A second batch of organically bonded sand cores were produced with an aqueous solution of phenol sulfonic acid, aluminum salts, sulfuric acid (Fehler! Verweisquelle konnte nicht gefunden werden. and Fehler! Verweisquelle konnte nicht gefunden werden.) using the warm box process. The organic binder bridges exhibit different morphologies before and after contact with the Al melt.

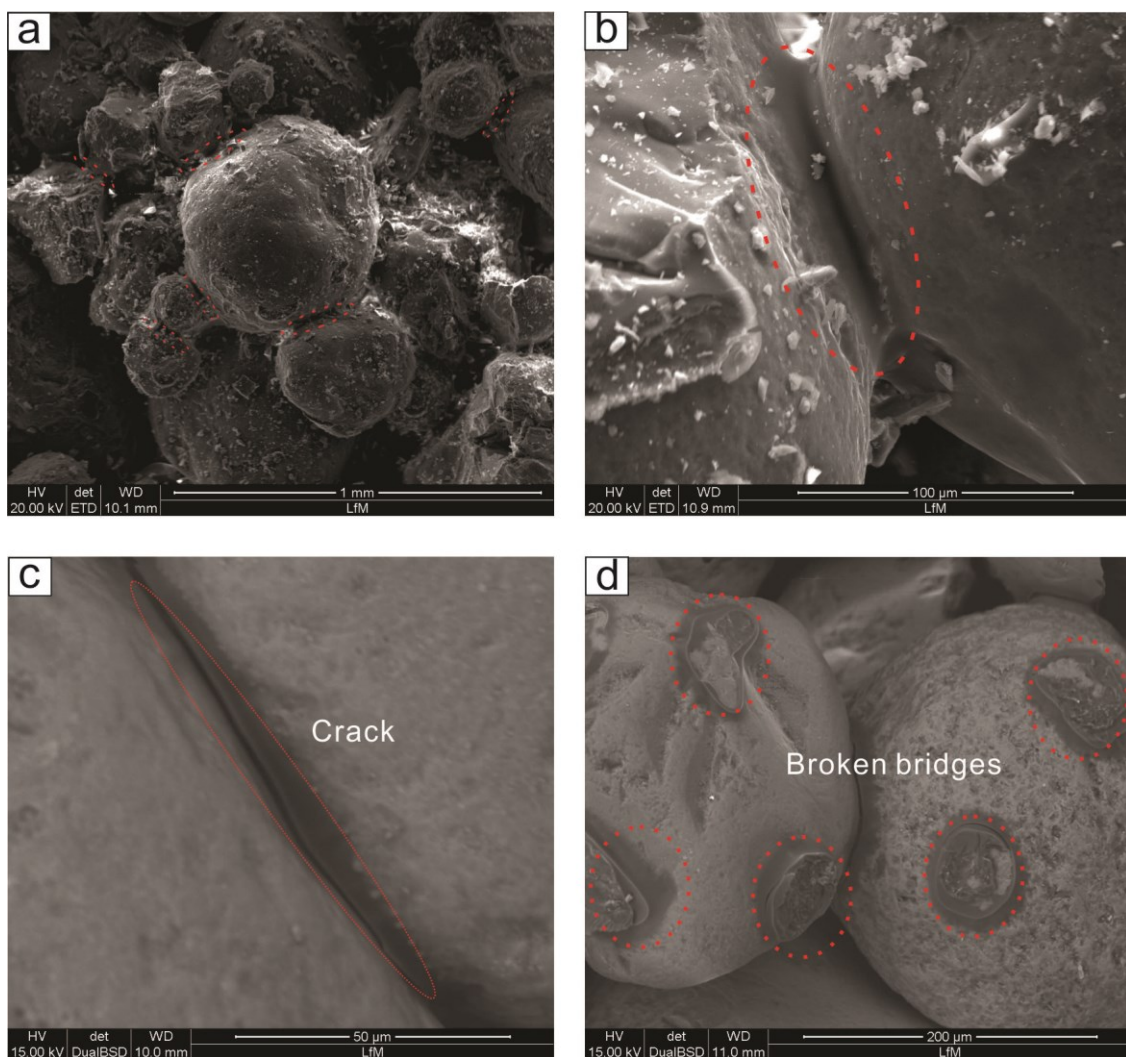


Figure 4-19: (a) and (b) Organically bonded sand core with modified urea-furan-phenolic resin using the warm box process before casting, (c) a crack in the binder bridge between two sand particles after Al casting (d) broken binder bridges with fully covered intersection and partly covered intersection.

Figure 4-19 (a) and (b) shows the binder bridges before thermal exposure during casting. A crack was already present between sand grains in the case of the organically bonded sand core before casting. Furthermore, many fine (small silica) particles were also present on the surfaces, which were also bonded between and onto sand particles with the binder. In **Figure 4-19** (c), the ‘broken binder bridges’ can be clearly observed between sand particles, illustrated by the dotted line. **Figure 4-19** (d) shows the separated broken binder bridge on the sand particle surface. These broken binders were observed with ring shaped ridges and fractures. Except for the broken binder bridge, other areas of particle surface were smooth with no residue of thermally decomposed binder on the surface.

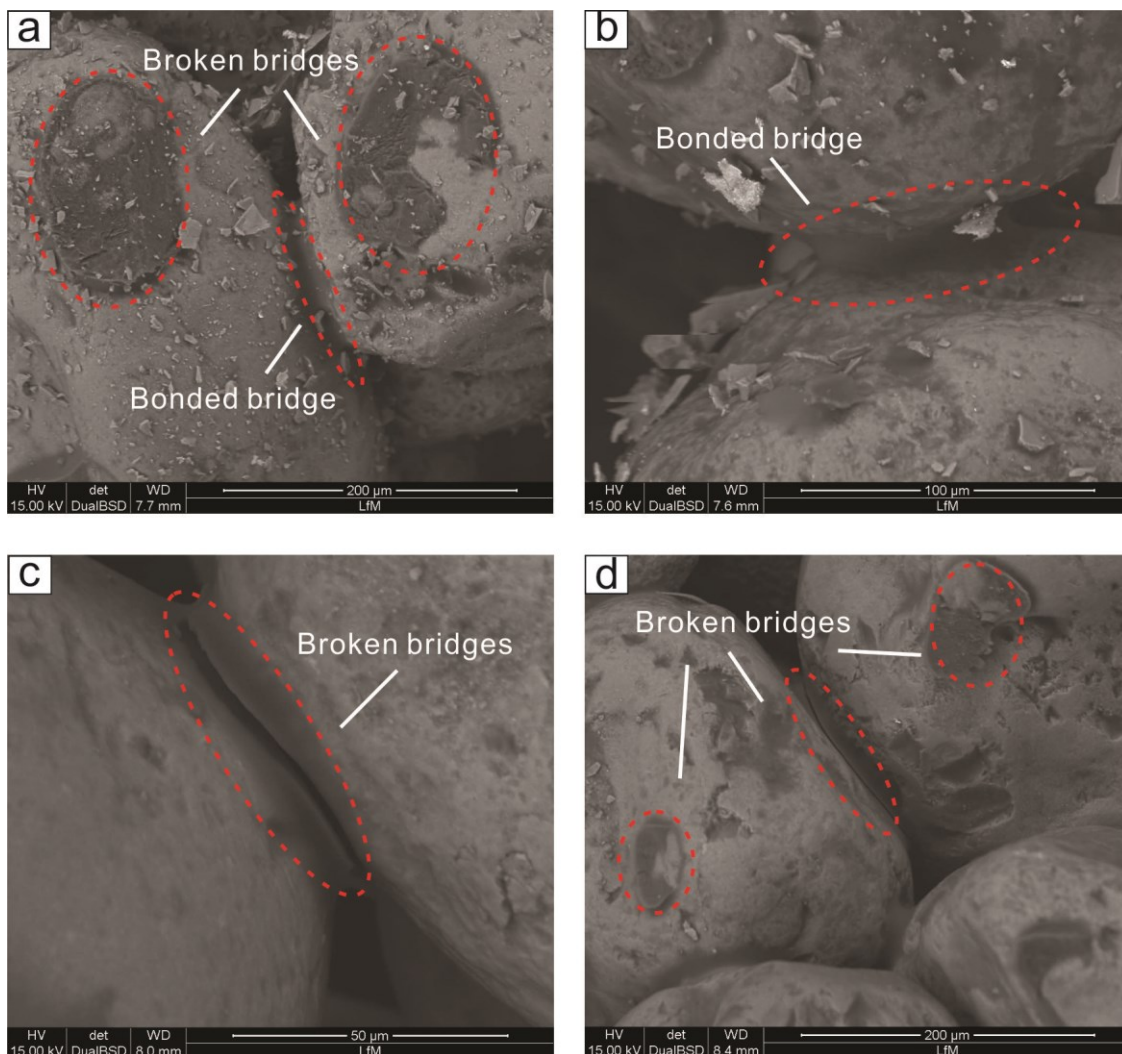


Figure 4-20: (a) and (b) Organically bonded sand core with an aqueous solution of phenol sulfonic acid, aluminum salts, sulfuric acid using the warm box process before casting, (c) and (d) organically bonded sand cores after casting.

Figure 4-20 (a) and (b) shows the organically bonded sand cores before thermal exposure. It can clearly be seen that, two binder bridges were broken in **Figure 4-20** (a). While in **Figure 4-20** (b), the binder bridges between particles are still holding the particles together. Otherwise, SiO₂ fine particles (many small particles on the surface) were also observed. **Figure 4-20** (c) shows the obviously broken binder bridge between two particles. In **Figure 4-20** (d), surfaces were cleaner after thermal exposure with smooth surface without binder bridges, while the binder bridges were broken into two parts. Some binder bridges are connected to the sand; the other one is adhered to other sands, which was similar to organically bonded sand cores with modified urea-furan-phenolic resin in warm box process.

4.1.4.3 Inorganically bonded sand cores

Two types of inorganically bonded sand cores were both bonded with same modified silicate binder mixture but with different promoters (see chapter 3, in Fehler! Verweisquelle konnte nicht gefunden werden.). The inorganically binder was pure water glass (39T). All these inorganic binder cores were produced by the warm box process. The binder bridge connection before and after casting were observed by SEM. They exhibit distinct differences from the organically bonded cores.

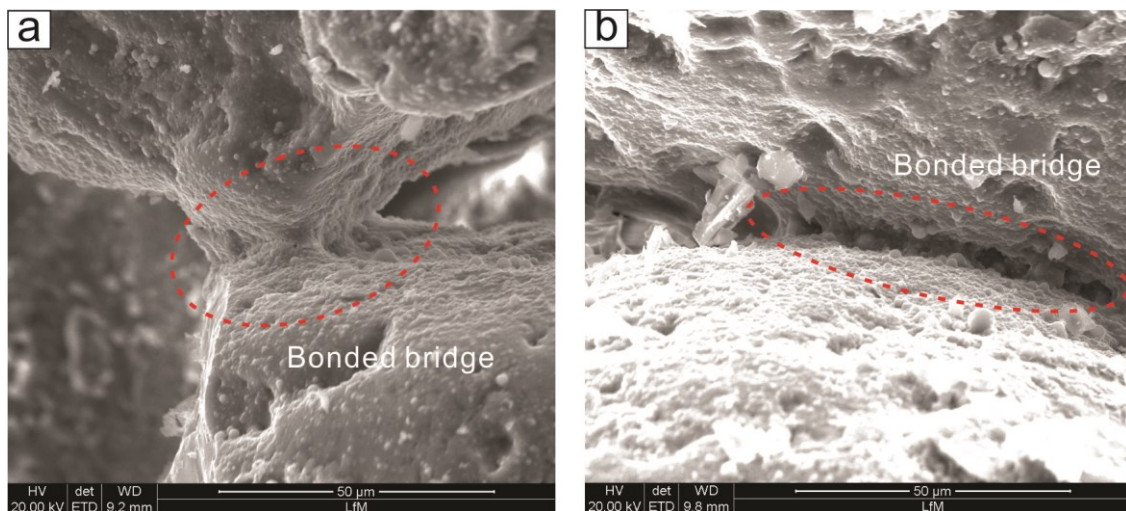


Figure 4-21: (a) and (b) Inorganically bonded sand core with modified silicate binder mixture and promoter (INOTECTM - Promoter WJ 4000) using the warm box process before casting.

Figure 4-21 (a) shows that inorganic binder covered the sand particles. At a contact point between two sand grains the excess binder resulted into the formation of a binder bridge smaller in cross section compared to organically bonded sand cores, shown in **Figure 4-21** (b).

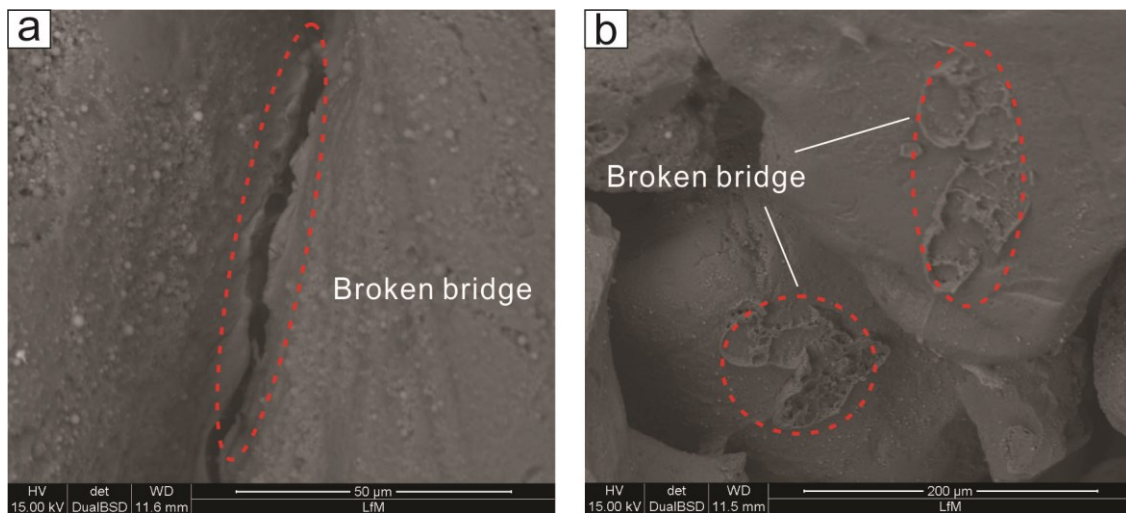


Figure 4-22: (a) and (b) Inorganically bonded sand core with modified silicate binder mixture with promoter (INOTEC™ - Promoter WJ 4000) using the warm box process after casting.

Figure 4-22 (a) shows that, after thermal exposure, inorganic binder bridges were broken between the sand particles. In **Figure 4-22** (b), on the sand grain surface, broken binder bridges were observed. The fracture surface of inorganic binder bridges appears to be different to that of the broken organically binder bridges.

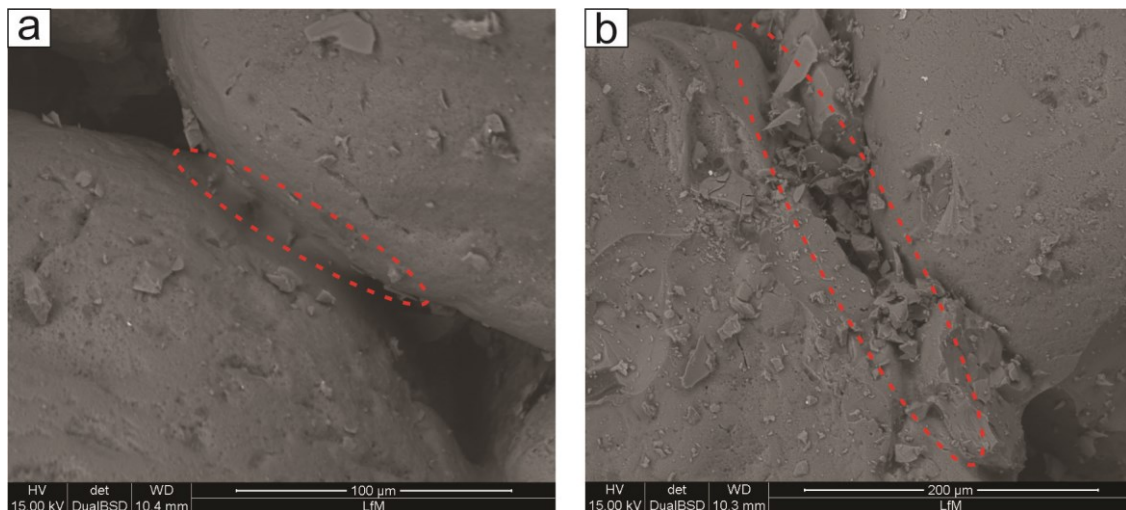


Figure 4-23: (a) and (b) inorganically bonded sand core of modified silicate binder mixture and promoter (Inotec Promoter EP 4174) using warm box process before casting.

Figure 4-23 shows that the inorganic binder bridges have essential differences to organic binder bridges before thermal exposure to the Al melt. They bonded particles tightly, and amounts of dust were observed between sand particles and on the sand grain surface (**Figure 4-23** (b)).

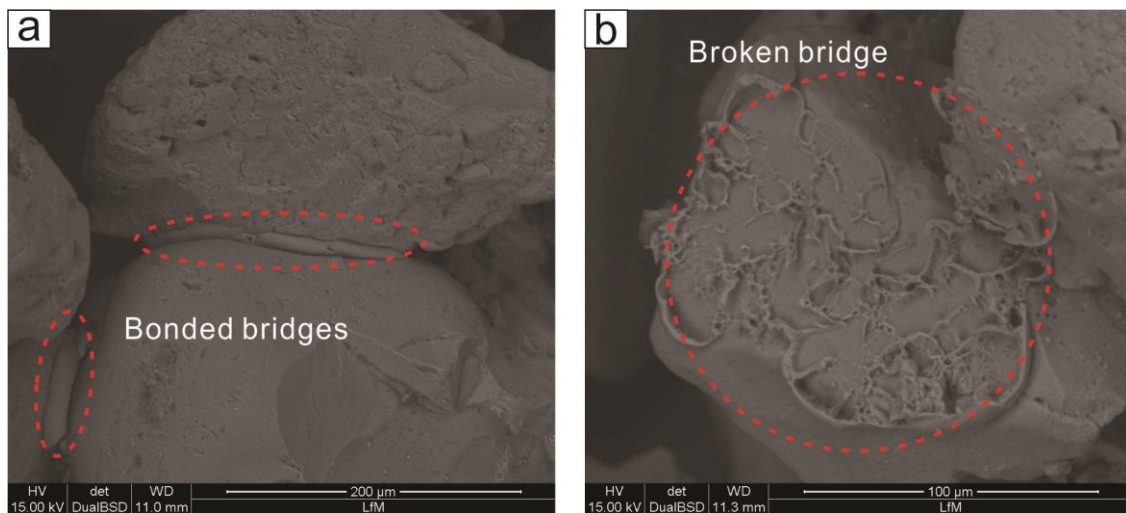


Figure 4-24: (a) and (b) inorganically bonded sand core of modified silicate binder mixture and promoter (Inotec Promoter EP 4174) using warm box process after casting showing an unbroken binder bridge and a typical inorganic fracture surface indicating a brittle behaviour.

Figure 4-24 (a) shows that, after thermal exposure, bonded bridges were observed between sand particles. In **Figure 4-24** (b), a broken bridge exhibited river pattern on the surface of sand particle.

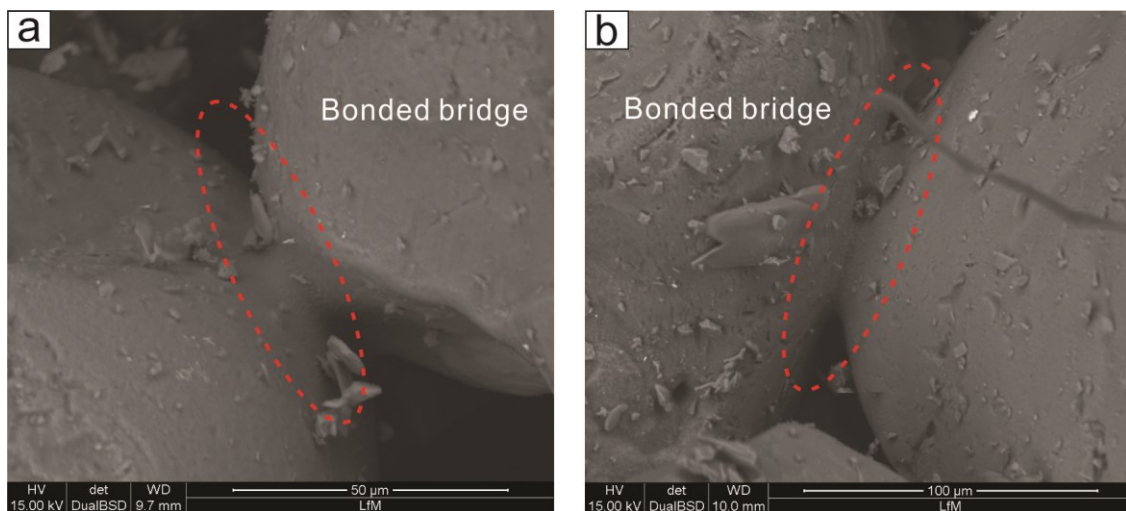


Figure 4-25: (a) and (b) inorganically bonded sand core with water glass 39T[®] using the warm box process before casting.

Before casting, bonded bridges were bonded tightly between particles as shown in **Figure 4-25** (a) and (b). The binder covered sand particles, and many dust particles were bonded onto the surface.

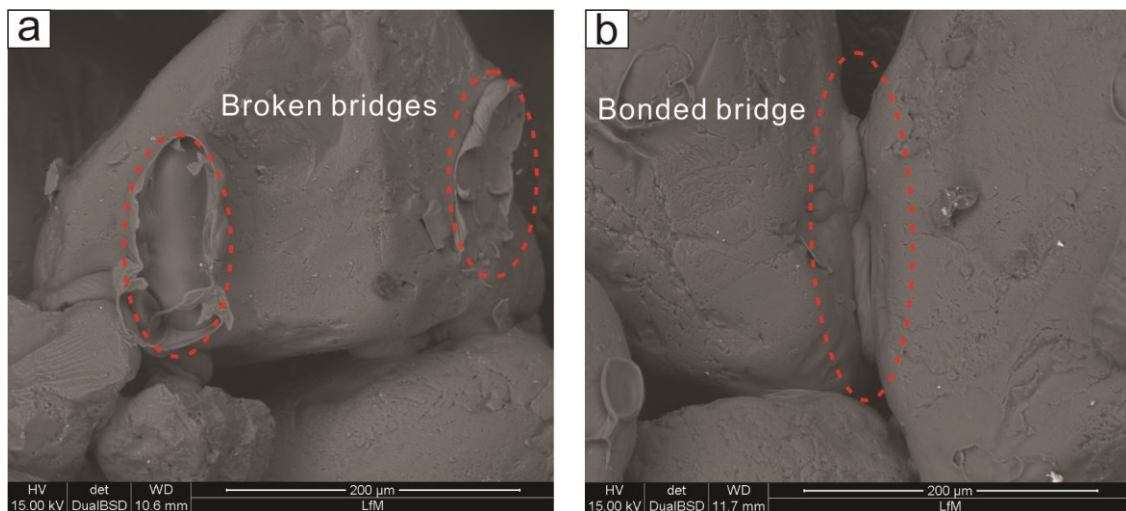


Figure 4-26: (a) and (b) inorganically bonded sand core with water glass 39T[®] using the warm box process after casting.

After casting, binder bridges using water glass 39T[®] were connected like a ring or 'suction pad' in between sand grains (**Figure 4-26** (a)). The binder formed a ring in which a cavity between sand particles were found. After casting, some binder bridges were still bonded, as shown in **Figure 4-26** (b).

Inorganic binder bridges and organic binder bridges have different morphologies and structures between sand particles. Inorganically bonded binder bridges formed **Figure 4-26** (a) in case of pure water glass only a ring or (b) a ring with riverine pattern (**Figure 4-24** (b)) between sand particles in case of addition of silicic acid, sodium salt and Sodium hydroxide.

In contrast organically bonded binder bridges formed either a fully covered cross-section (**Figure 4-19** (d)). Or a partly covered cross-section between sand grains after thermal exposure (**Figure 4-20** (a)). These different features become distinctly apparent after thermal exposure once the fracture surface of the binder bridges are exposed.

4.2 Thermal properties

Thermal properties were investigated by 'dipping trials' and 'ring mould tests'. During the dipping trial described in chapter 3, the temperature over time curves of five different sand cores were obtained when the sand cores were submerged into the Al melt. A water peak was investigated by 'microwave drying of cores'. During the ring mould trials, important parameters were obtained to simulate the temperature behaviour of different sand cores in the real casting process.

4.2.1 Dipping trials

4.2.1.1 The curves of the temperature over time

Figure 4-27 shows the typical temperature time curves after dipping into Al melt at 780 °C. The temperature distribution in MIN sand core changed over time and was recorded at three positions (see in chapter 3 **Figure 3-6**). At the position located nearest to the Al-melt, the temperature increase was faster than at other positions, the temperature increase in the centre point was the slowest. At the mid-point location temperature time curves lies in between the center and outside core. The reason for this phenomenon was the heat flow reached the nearest thermal couple firstly, while the thermal couple in the centre of sand core need more time until the heat flow reached the sand core centre.

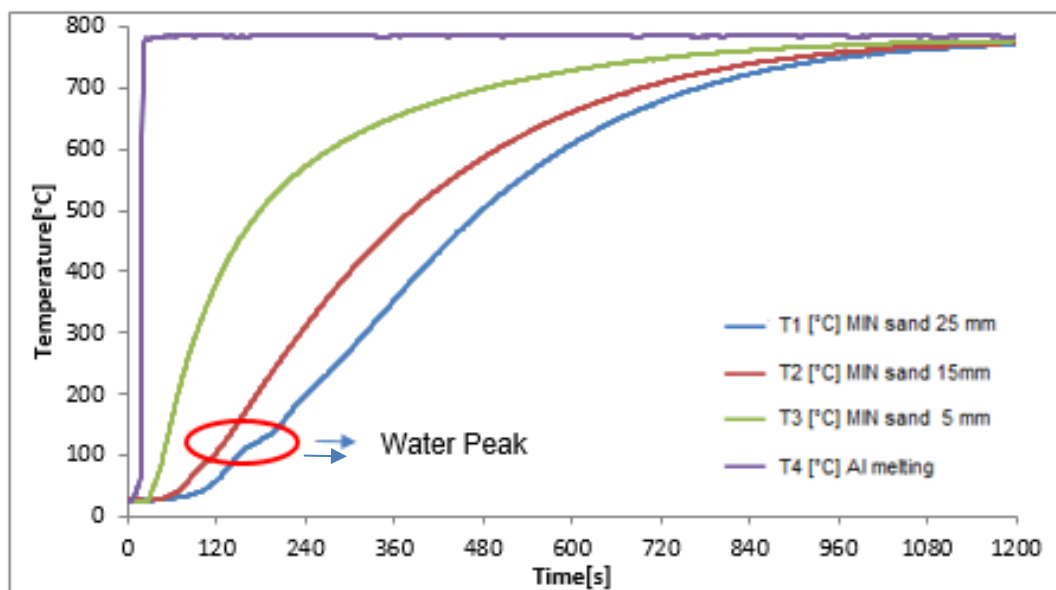


Figure 4-27: Temperature over time curves of MIN sand specimen dipping trial in 780 °C Al- melts.

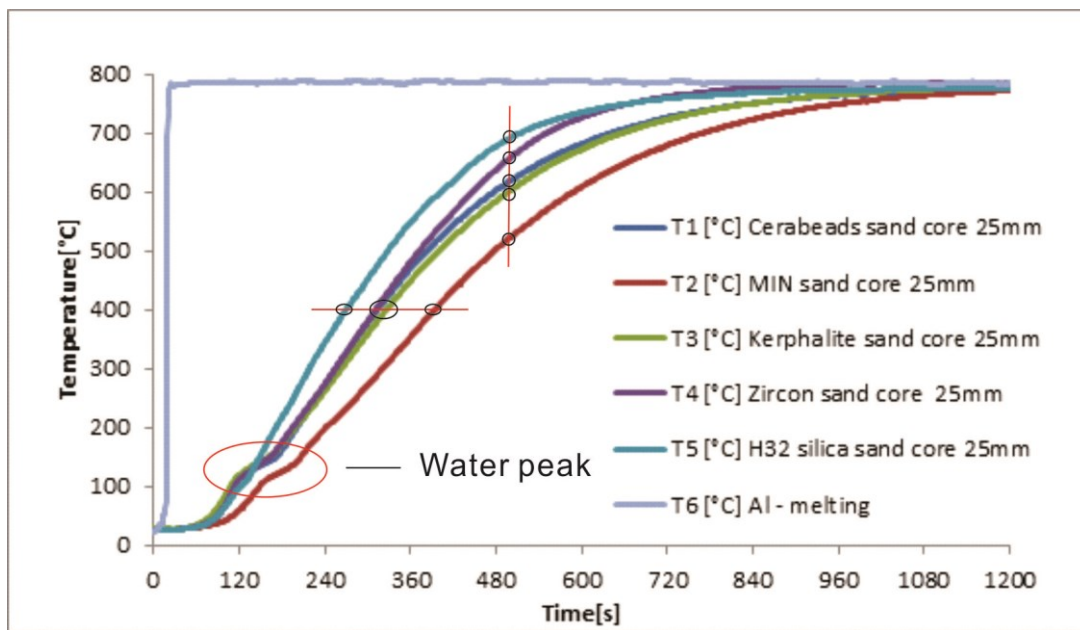


Figure 4-28: Temperature distribution in different sands at the 25 mm testing point during dipping trial in 780 °C Al - melt.

Figure 4-28 shows the temperature curves over time in five different base sand cores with thermal couples at the centre dipped into Al – melt at 780° C. Interestingly the temperature – time curves exhibit a clear saddle point at ca. 100 °C indicating a water peak which occurs firstly. Water peaks appeared at about 120 s after dipping samples into the Al melt in all sand cores except for MIN sand cores, which showed a water peak later at about 150 s dipping time into the Al melt. The water peaks held for about 60 s in sand cores except for silica sand cores, in which the water peak lasted about only 20 s.

In **Figure 4-28**, the temperature of tested point at the centre (25 mm) of different sand cores were compared at 480 s. It is clear to see that, the measured temperature in the silica sand core was the highest at about 700° C, and in the MIN sand core, the lowest at about 500°C. From the temperature time curves it is apparent that the heat flow into the core center occurs fastest for silica sand, followed by zircon sand, Cerabeads sand, Kerphalite sand core and MIN sand in descending order.

The differences of time to achieve a certain temperature was also compared in **Figure 4-28**. To reach a temperature of 400 °C the silica sand core required about 250 s, the MIN sand core 380 s, the Cerabeads and zircon sand 300 s and Kerphalite sand 320 s during the dipping trial.

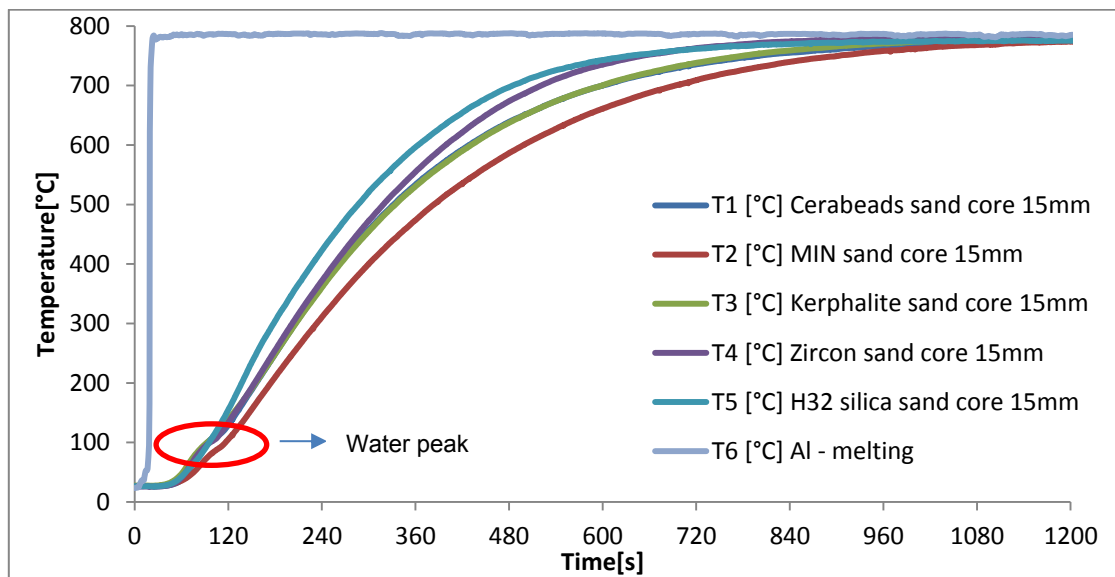


Figure 4-29: Temperature time curves in different sands at 15 mm testing point during dipping trial in 780 °C Al- melt.

Figure 4-29 shows the temperature curves over time for five different sand cores of different base sands with a water glass binder at the 15mm test point after dipping into the Al melt at 780° C. A saddle point was observed for each sand core during dipping trials in temperature over time curves, indicating also a water peak at the 15 mm point which occurred earlier and held for less time compared to the water peaks in the centre of sand cores. **Figure 4-30** shows temperature time curves in different sands at the 5 mm testing point in dipping trials at 780 °C in the Al melt. Here, the water peak is not clearly apparent during the dipping trials.

In **Figure 4-28**, **Figure 4-29** and **Figure 4-30**, it can clearly be seen that, the gradient of the temperature time curves are different for different base sands. The gradient of temperature time curve at 25 mm testing point in dipping trial is larger than at 15 mm testing point, which is larger than at 5 mm testing point. This means, the cooling rate ($\frac{dT}{dt}$) for all three testing points arrange as $\frac{dT}{dt}(\text{at } 5 \text{ mm}) > \frac{dT}{dt}(\text{at } 15 \text{ mm}) > \frac{dT}{dt}(\text{at } 25 \text{ mm})$.

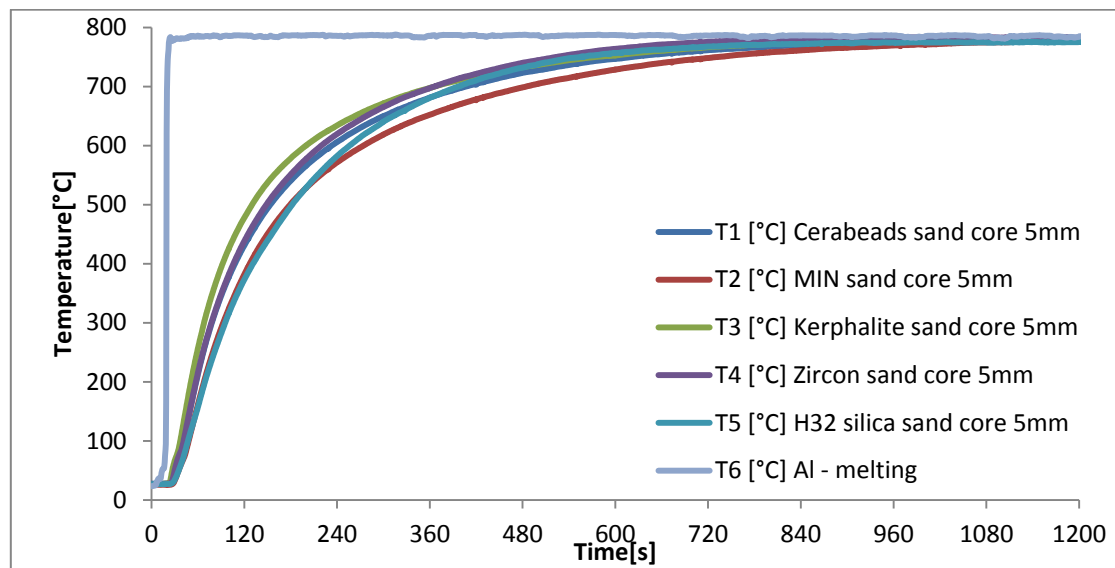


Figure 4-30: Temperature time curves in different sands at 5 mm testing point in dipping trial in 780 °C Al - melt alloys.

In **Figure 4-28**, **Figure 4-29**, the temperature curves over time during the dipping trials in silica sand core are over the curves of other sand cores, and the temperature curves in MIN sand core are below the curves of other sand cores. These curves are resulted by cooling rate differences in different sand cores, it is apparent that the cooling rate is fastest for the silica sand core, followed by zircon sand, Cerabeads sand, Kerphalite sand and MIN sand in descending order as $\frac{dT}{dt}(\text{silica sand}) > \frac{dT}{dt}(\text{zircon sand}) > \frac{dT}{dt}(\text{Cerabeads sand}) > \frac{dT}{dt}(\text{Kerphalite sand}) > \frac{dT}{dt}(\text{MIN sand})$. The results are shown in **Table 4-1**.

Table 4-1: Comparison of dT / dt in different base sands.

Sand type	dT / dt (° C / s) at 480°C
MIN Sand	1.05
Kerphalite sand	1.22
Cerabeads Sand	1.25
Zircon Sand	1.32
H32 Silica sand	1.41

4.2.1.2 Water peak

At the centre position (25mm from the edge), the water peak at about 100 °C was observed clearly. By using a Micro wave oven, dried samples were subsequently tested in a dipping trial to see possible effects of drying on the water peak at the same position.

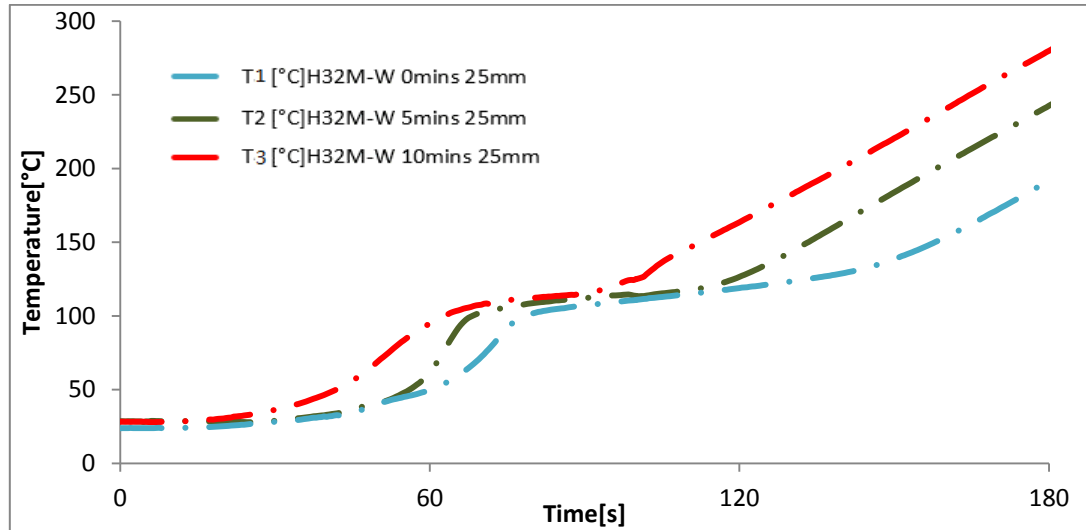


Figure 4-31: The water peak in H32 silica sand cores with different drying times by microwave (0 mins / 5 mins / 10 mins), the sand specimens dipping into Al – melt at 780 °C.

The results after the dipping into Al - melt at 780 °C is shown in **Figure 4-31**. At 100° C, The temperature curve over time of a 10 mins - dried sample (T3) holds a water peak for about 30 s, the temperature curve over time of a 5 mins – dried sample holds a water peak for about 60 s, and the temperature curve over time for undried sample holds a water peak for about 90 s. It's very clear that, more drying respectively dehydrating resulted in a shorter water peak.

4.2.2 Ring mould test

Figure 4-32 shows the temperature behaviour in the ring mould test for a silica sand core. The tested points were the same as in the dipping trials mentioned before. In **Figure 4-32**, the initial temperature of the sand cores were always at room temperature. The pouring temperature was set similar to the actual temperature in the pouring process for Al castings at 720 °C to 740 °C.

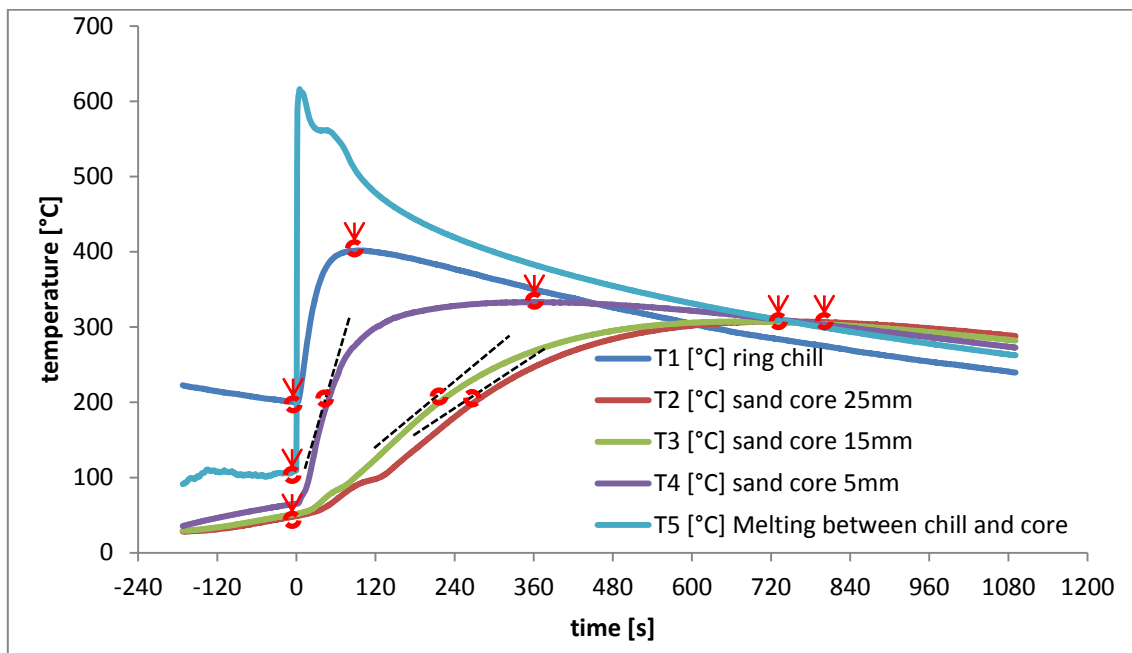


Figure 4-32: The significant points in the curves in the ring mould test.

In the foundry process, measuring the temperature time curve and thereby the thermal conductivity in the sand cores are of great importance to control the properties of Al casting during the solidification.

The significant test points are the beginning temperature of ring mould and sand cores / Al-melt; the maximal values of different positions in sand cores; and the highest cooling rate (at 200°C) in the sand core during solidification, as shown in **Table 4-2**.

	$T_{\text{Ring mould}}$	$T_{\text{air in mould}}$	$T_{\text{Core centre}}$	$T_{\text{at 15mm}}$	$T_{\text{at 5mm}}$
$T_{\text{Pouring time}} \text{ } ^\circ\text{C}$	200	113	49	52	66
$dT / dt_{200^\circ\text{C}} \text{ } ^\circ\text{C/s}$	-	-	0,52	0,61	1,94
$t_{200^\circ\text{C}} \text{ } \text{S}$	-	-	287,5	242,0	69,0
$T_{\text{Max.}} \text{ } ^\circ\text{C}$	397	633	302 °C	300 °C	326
$t_{\text{Max Temp.}} \text{ } \text{S}$	95,0	3,5	761,0	684,5	416,0
$T_{\text{Casting melting}} \text{ } ^\circ\text{C}$	734		Core size	H: 50 mm	D: 50 mm

Table 4-2: The process parameters during the ring mould test.

T_{Max} and $dt / dt_{200^{\circ}C}$ in **Table 4-2** are important parameters to influence the solidification and the quality of castings.

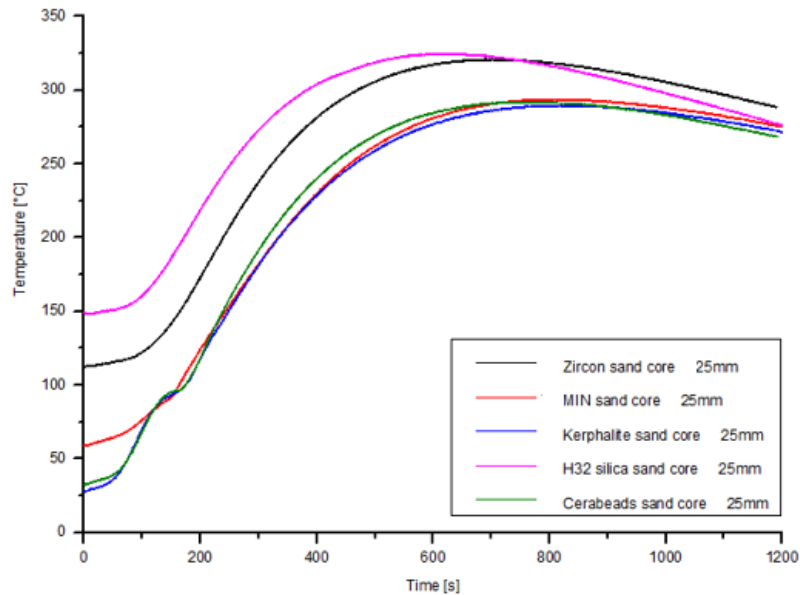


Figure 4-33: Temperature time curve at the centre position for ring mould tests with different core sand types with water glass Betol® 39 T.

Figure 4-33 shows temperature time curves at the centre position for ring mould test in five different sand core types. During the ring mould test, the temperature curve in the centre of sand core raise up gradually to a maximal value, until the temperature decreased. The initial temperature in sand cores was set over $100^{\circ}C$ and below $100^{\circ}C$. When the initial temperature in silica sand cores and zircon sand cores were over $100^{\circ}C$. No water peak was observed in these two sand cores during solidification in a ring mould test. In contrast, in the case of Kerphalite and Cerabeads sand cores, water peaks were observed at $100^{\circ}C$ due to the lower initial sand temperature.

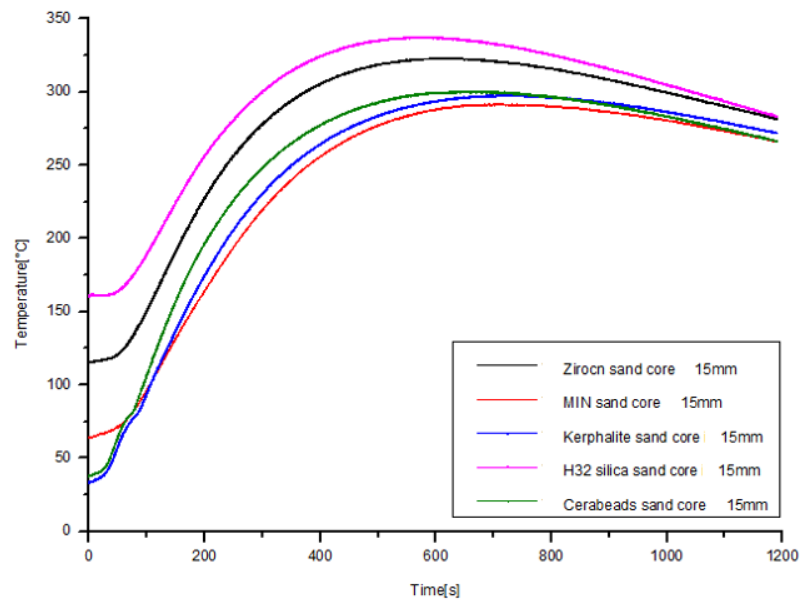


Figure 4-34: Temperature time curve at the position of 15 mm for ring mould tests with different core sand types with water water glass Betol @ 39 T.

Figure 4-34 shows temperature time curves at the 15 mm position for ring mould test for five different sand types. The temperature time curve at this position had the same trend as in the centre of the sand core.

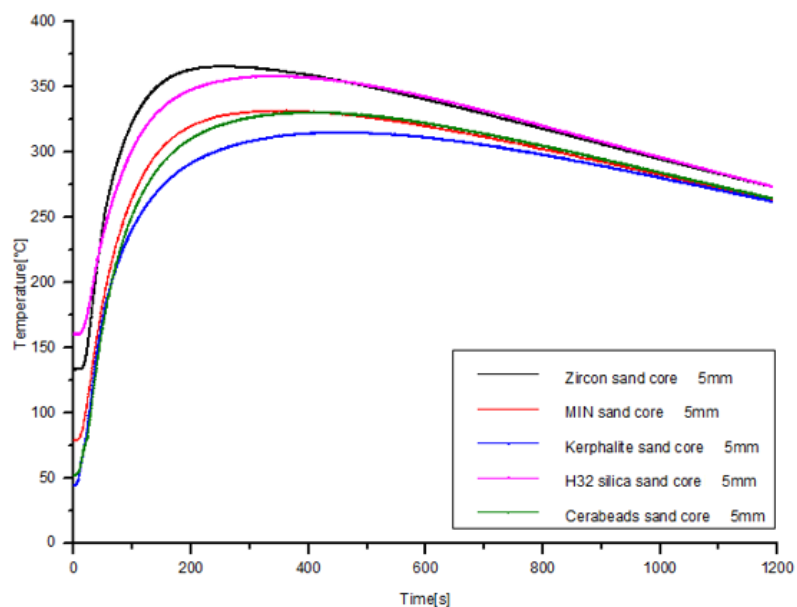


Figure 4-35: Temperature time curve at the position of 5 mm for ring mould tests with different core sand types bonded with water water glass Betol @ 39 T.

Figure 4-35 shows temperature time curves at the 5 mm position for ring mould test for five different sand types. No water peak in this position in five sand cores (**Figure 4-33**, **Figure 4-34** and **Figure 4-35**) was observed. This demonstrate clearly, high temperatures were present at the location nearest the edge of sand cores resulting in an immediate evaporation of the water. The testing point at 5mm to the edge had the highest temperature gradient. Furthermore, a higher starting temperature of the cores resulted into a higher absolute maximal temperature. This can be an important factor affecting the casting quality.

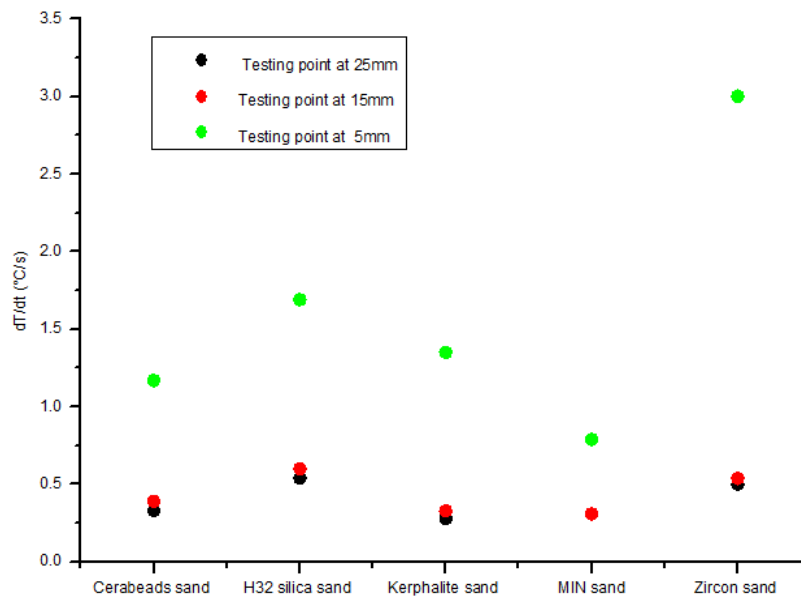


Figure 4-36: Comparison of dT / dt ($_{(0-250^{\circ}\text{C})}$) in different sands and different position.

Figure 4-36 shows a comparison of cooling rate dT / dt ($_{(0-250^{\circ}\text{C})}$) in different sands at different positions. At the 5 mm testing point, the dT / dt had higher values than at the 15 mm and 25 mm testing point. The maximal value of 3.0 ($^{\circ}\text{C} / \text{s}$) is at the 5 mm testing point in zircon sand. The cooling rate dT / dt of the 25 mm testing point had a higher values than at 15 mm, but both values are very close. The minimal values of 0.28 ($^{\circ}\text{C} / \text{s}$) occurred at the 25 mm test point in the Kerphalite sand core.

4.2.2.1 Comparison with different initial temperatures

As discussed in the previous section, the water peak was very sensitive to a core temperature at 100°C during the casting process. The initial temperature of sand cores was set differently, which led to differences of holding times of the water peak. In order to reduce the water peak holding time, two different trials were employed: (a) to dry the sand samples (b) and to keep sand samples in ring mould until their temperature was over 100°C.

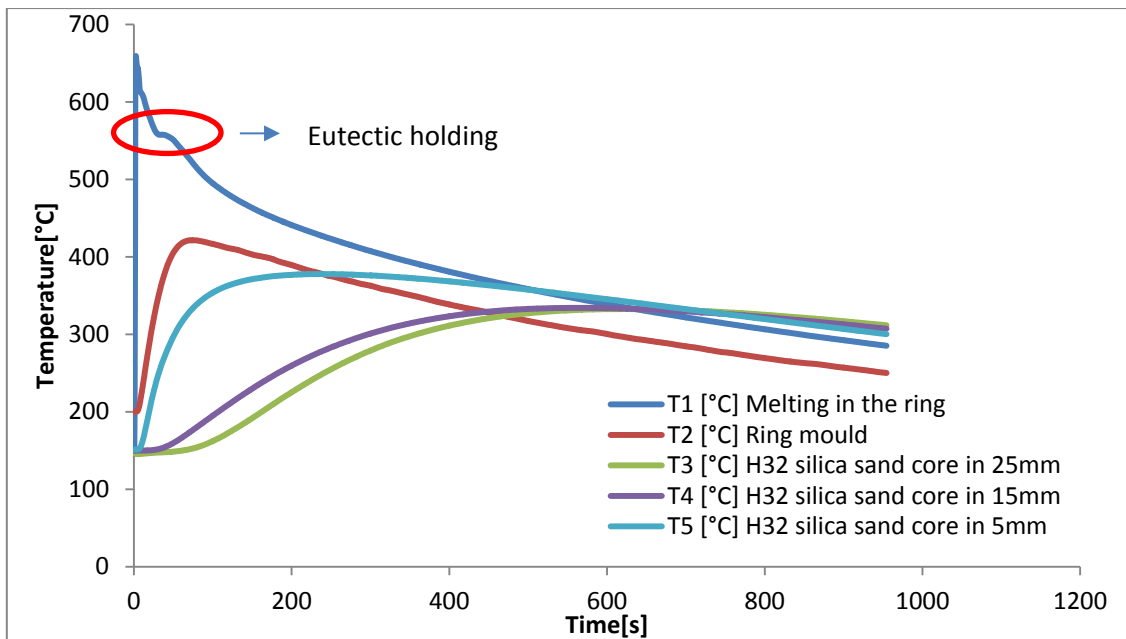


Figure 4-37: Ring mould test of with water glass 39T bonded H32 silica sand with an initial temperature over 100 °C with micro wave oven treatment.

Figure 4-37 points out that, the holding time of water peak was sharply reduced by using the micro-oven to dry the sand core for 10 minutes.

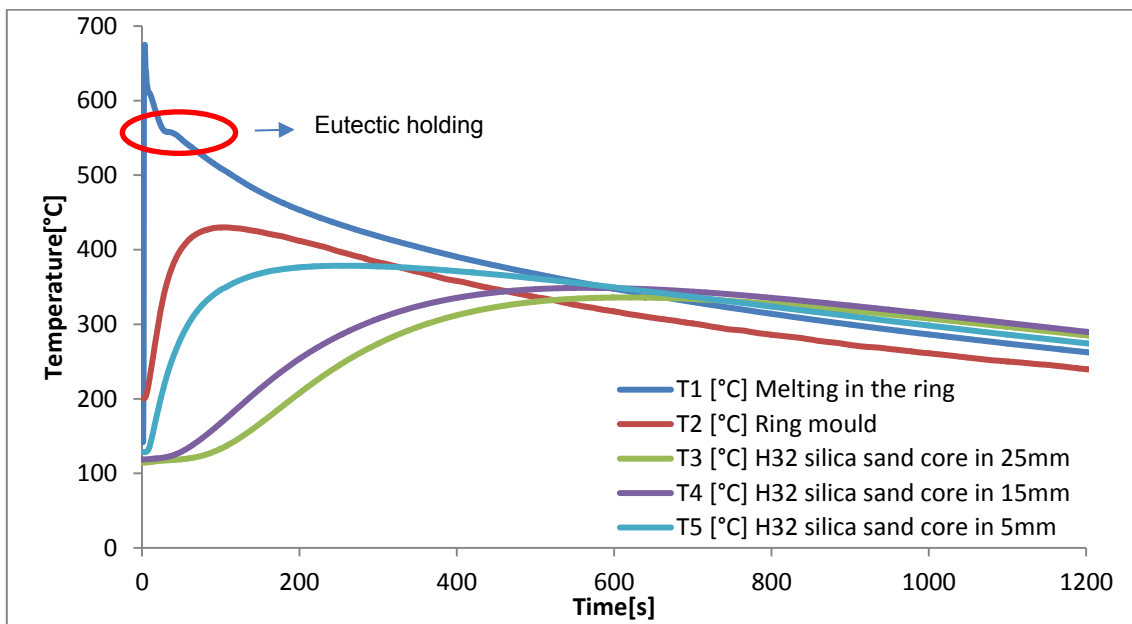


Figure 4-38: Ring mould test of with water glass 39T bonded H32 silica sand with an initial temperature over 100 °C without micro wave oven treatment.

As shown in **Figure 4-38**, if the initial temperature of sand cores was over 100°C in the preheated ring mould, even without the micro oven treatment, the water peaks were not present.

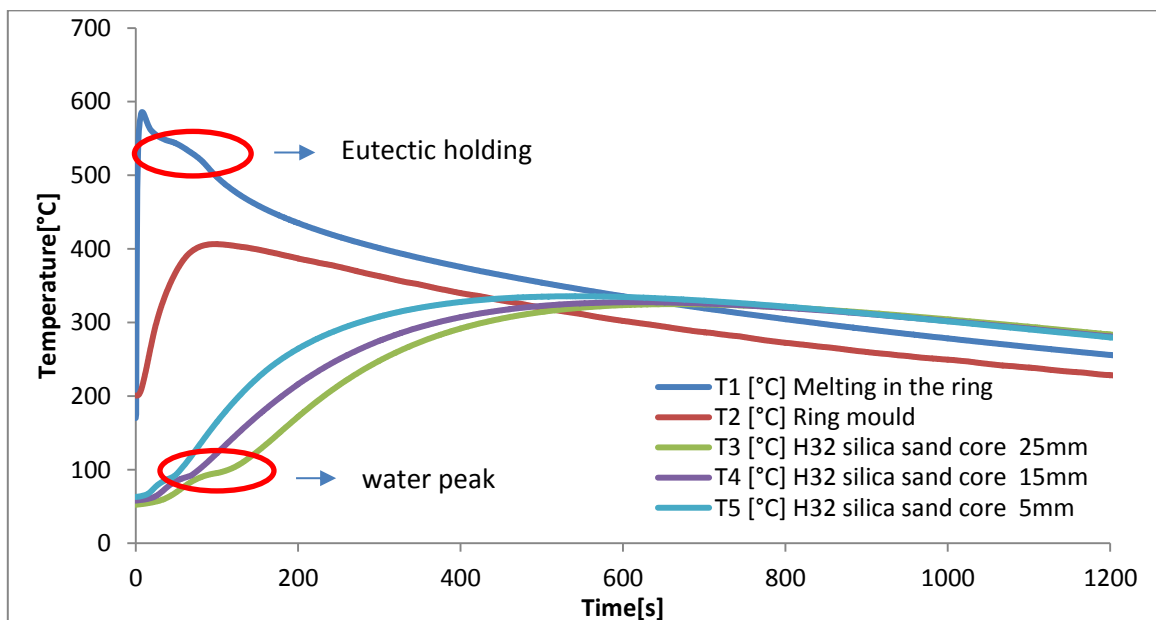


Figure 4-39: Ring mould test of with water glass 39T bonded H32 silica sand with an initial temperature below 100 °C without micro wave oven treatment.

In **Figure 4-39**, the water peak was observed to be at about 100 °C, which was measured by thermal couples at three different positions in the sand cores. With micro wave oven treatment of 10 minutes, the water peaks were still present.

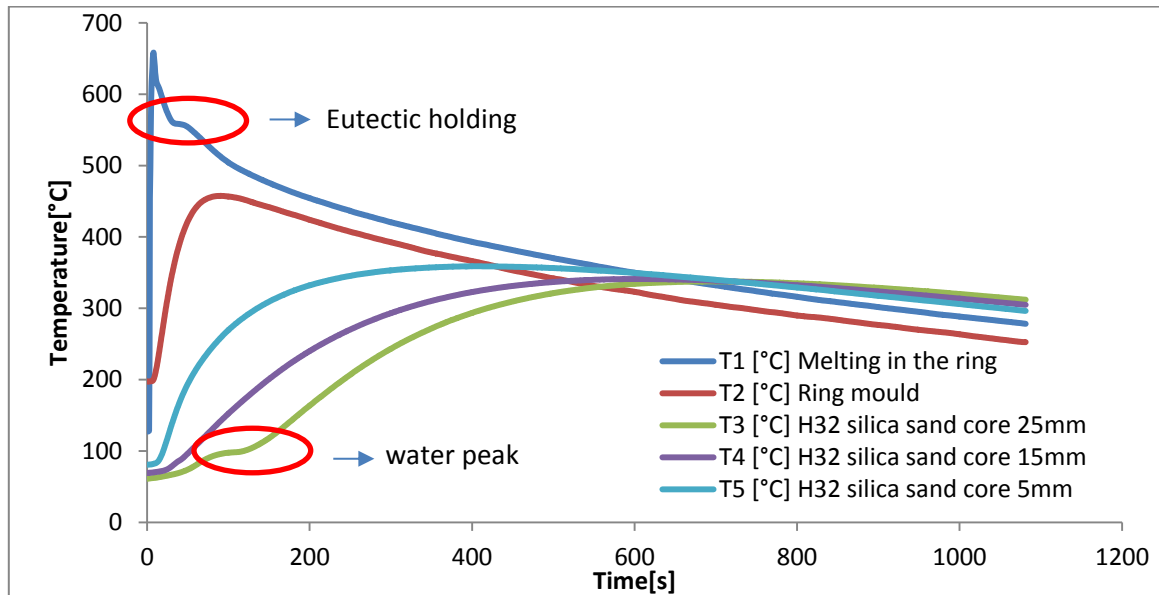


Figure 4-40: Ring mould test of with water glass 39T bonded H32 silica sand with an initial temperature below 100 °C with micro wave oven treatment.

In **Figure 4-40**, the water peak was still observed at 100 °C in the centre of sand sample with micro oven treatment of 10 minutes. However the water peak was not obvious at other test points.

4.3 Decoring behaviour

Mechanical experiments which have been explained in detail in the experimental methods have been performed to distinguish the de-coring behaviour among the different sand bonded cores. Experimental results indicate that the organically bonded sand cores were easily shaken out. In contrast, inorganically bonded sand cores were more difficult to be de-cored. The experiments have been repeated three times for each type of sand core with different impact energy. The de-cored sand was gathered and the weight determined.

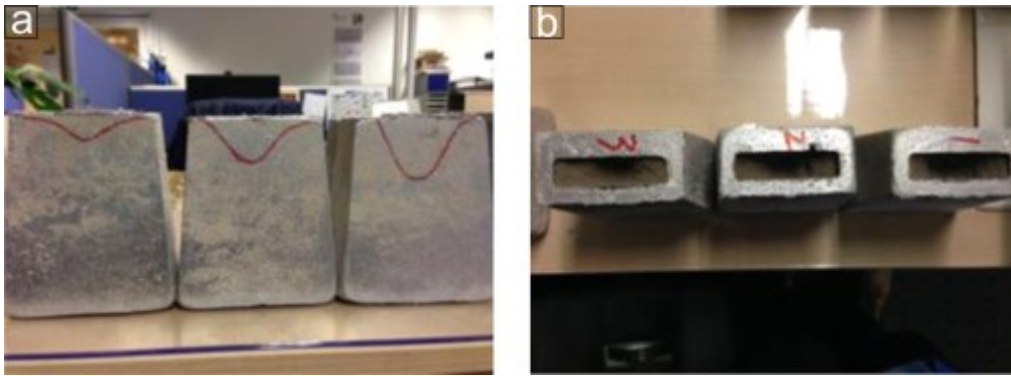


Figure 4-41: (a) and (b) Features of three different impact energies and times by impact device in organically bonded internal core.

Figure 4-42 shows schematically, that with the repeated impacts, the amount of fallen sand was increased, while the residual sand adhered to the Al – casting.

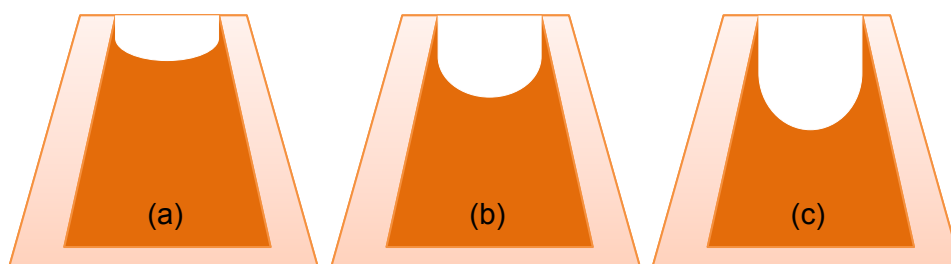


Figure 4-42: Schematic cross section of specimens after the decored sand removed Al casting (a) one impact (b) two impacts (c) three impacts.

After the experiments, the shapes of the residual sand agglomerates in the casting box were examined with increasing impacts. Repeated impacts, resulted in more agglomerates as well as fine sand, and a deeper decoring crater in the core, as shown schematically in **Figure 4-42**. It is to note that the core has a tenancy to adhere to the casting for all sands investigated.

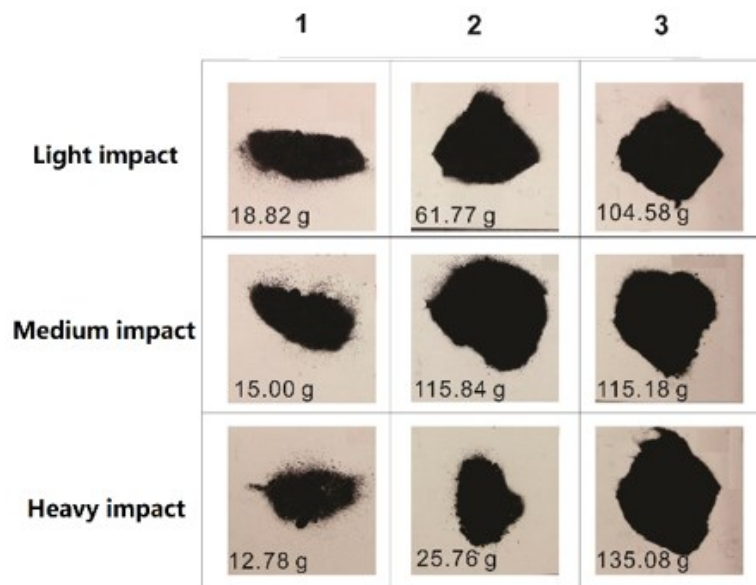


Figure 4-43: Decored sands samples from organically bonded sand core with modified urea-furan-phenolic resin in warm box process after impacting.

In **Figure 4-43**, three organically bonded sand cores with modified urea-furan-phenolic resin (warm box) have been de-cored from Al-casting with different impacted times and energy. With higher impact energy, the amount of fallen sand from internal cores increased.

The decored sand exhibits black colour and fine particles with small agglomerates and the amount for each impact is given in **Figure 4-44**.

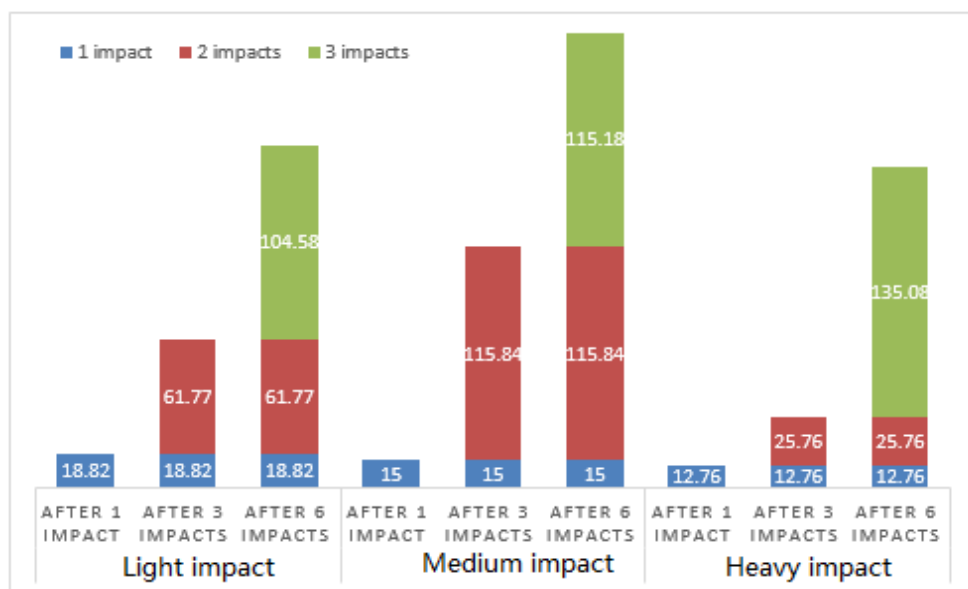


Figure 4-44: Decored sands samples from organically bonded sand core with modified urea-furan-phenolic resin in warm box process after impacts.

Figure 4-44 shows the amount by weight of decoated sand for different impact energies and number of impacts. A maximal value of 135.08 g was obtained by heavy impacts repeated three times. For the medium impact energies, the weight of fallen sand after two times impacts and three times impacts have nearly same value of 115 g.

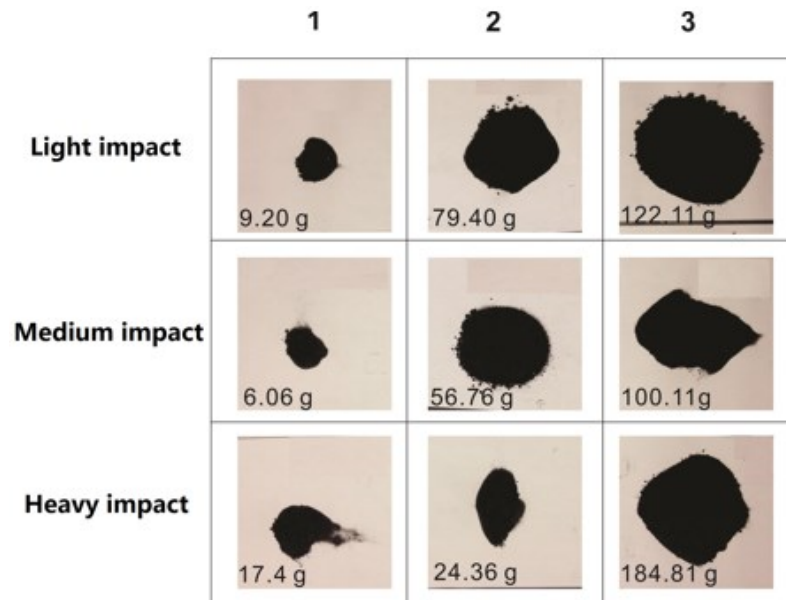


Figure 4-45: Decoated sands samples from organically bonded sand core with an aqueous solution of phenol sulfonic acid, aluminum salts, sulfuric acid (warm box) after impact.

Figure 4-45 shows the decoating behaviour of three organic sand cores bonded with an aqueous solution of phenol sulfonic acid, aluminum salts, sulfuric acid (warm box). The amount of fallen sand from cores increased with more impact energy similar to organically bonded sand cores with modified urea-furan-phenolic resin (warm box). The decoated sands exhibit black colour resulting from the decomposed binder but also more agglomerates.

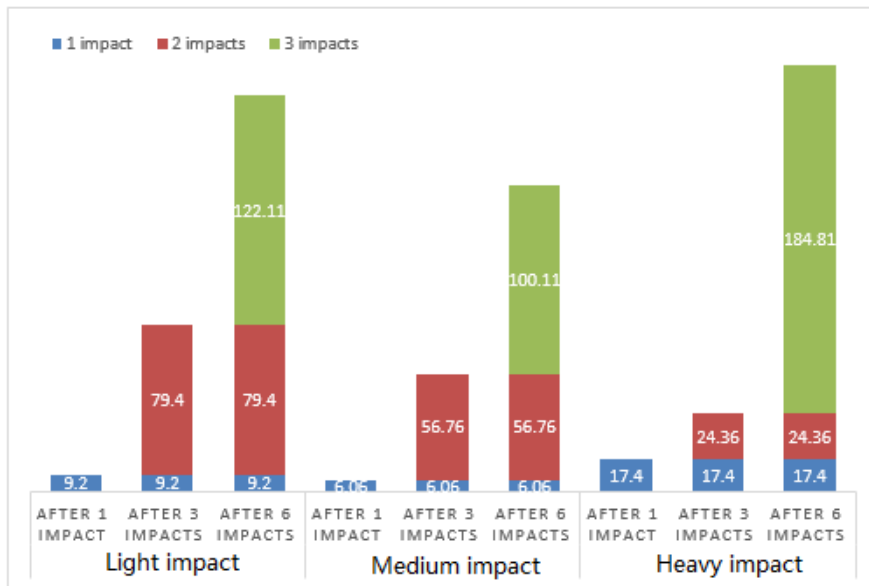


Figure 4-46: Decored sands samples from organically bonded sand core with an aqueous solution of phenol sulfonic acid, aluminum salts, sulfuric acid in warm box process after impact.

Figure 4-46 shows the amount by weight of decored sand for different impact energies and number of impacts from organically bonded sand core with an aqueous solution of phenol sulfonic acid, aluminum salts, and sulfuric acid (warm box). The maximal value of 184.11 g of decored sand core is observed after three heavy impacts. The amount of decored sand core was higher with increasing impact times for different impact energies.

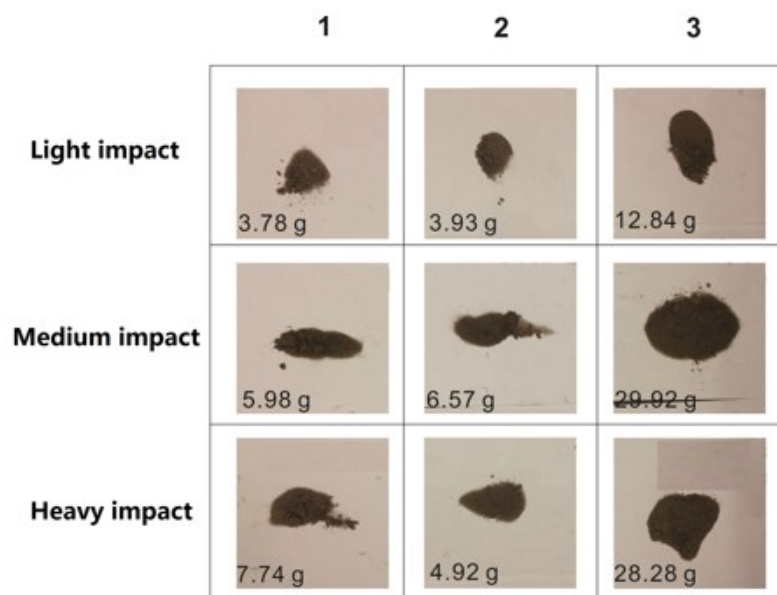


Figure 4-47: Decored sands samples from inorganically bonded sand core with modified silicate binder mixture and promoter (INOTEC™ - Promoter WJ 4000) in warm box process after impact.

Figure 4-47 shows three inorganically bonded sand cores with modified silicate binder mixture and promoter (INOTEC™ - Promoter WJ 4000) (warm box) de-cored from Al-casting with different impacted times and energy.

The amount of decored sand from cores increased with more impact energy similar to organically bonded sand cores (warm box), except for the amount of 29.92 g obtained by medium energy for three repeated impacts compared to the amount of 28.28 g obtained by three repeated heavy impacts.

The decored sands exhibited gray colour as a result of the decomposed promoters and fine sand without agglomerates, the amount is shown in **Figure 4-48**.

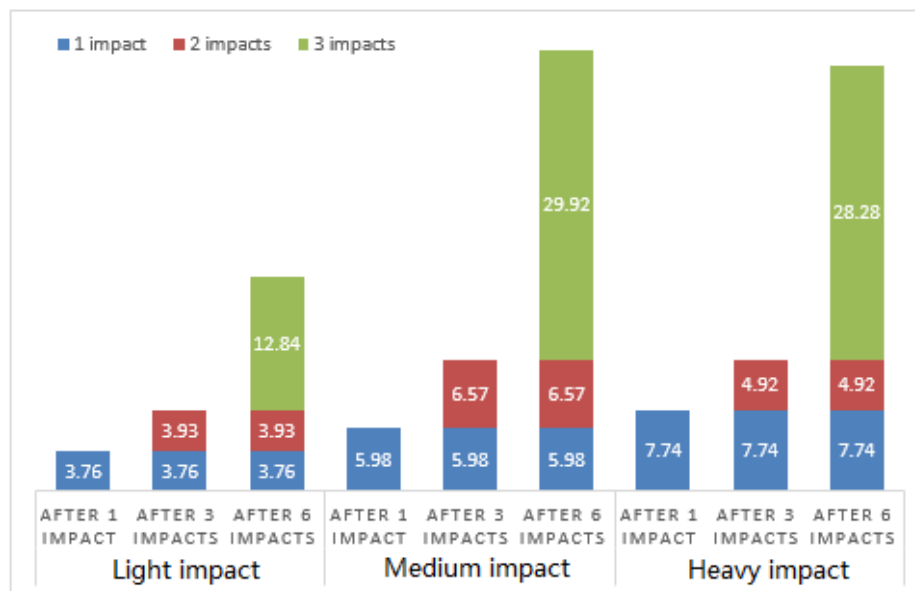


Figure 4-48: Decored sands samples from inorganically bonded sand core with modified silicate binder mixture and promoter (INOTEC™ - Promoter WJ 4000) in warm box process after impact.

Figure 4-48 shows the amount by weight of decored sand for different impact energies and number of impacts from inorganically bonded sand core with modified silicate binder mixture and promoter (INOTEC™ - Promoter WJ 4000) (warm box). A maximal value of 29.92g for decored sand was obtained by a medium impact energy for three times, which is only 1.64 g more than by heavy impacts for three times. All the values for different impacts numbers and energies were much less than obtained in organically bonded sand cores.

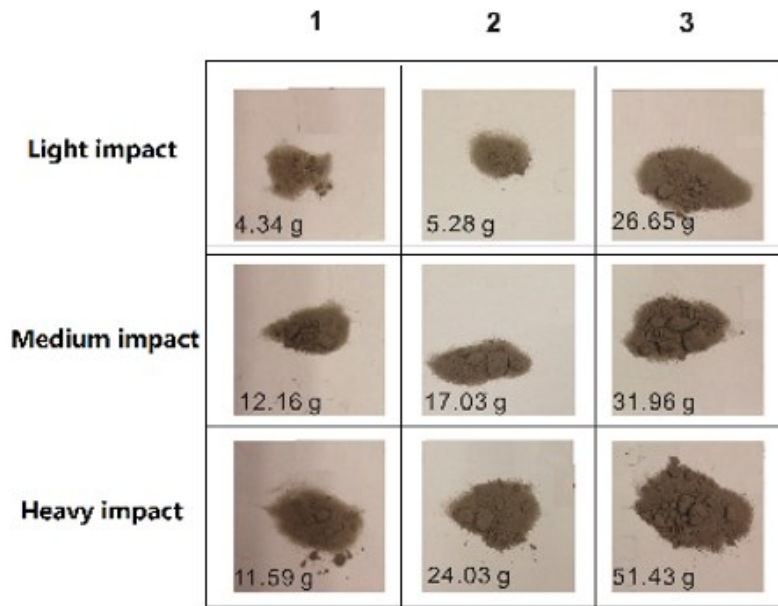


Figure 4-49: Decored sands samples from inorganically bonded sand core of modified silicate binder mixture and promoter (INOTEC™ Promoter EP 4174) in warm box process after impact.

In **Figure 4-49**, three inorganically bonded sand cores of modified silicate binder mixture and promoter (INOTEC™ Promoter EP 4174) (warm box) de-cored from Al-casting with different impacted times and energy are shown. The amount of decored sand from cores increased with more impact energy similar to organically bonded sand cores (warm box). The decored sands exhibit gray colour and fine sand with obvious agglomerates.

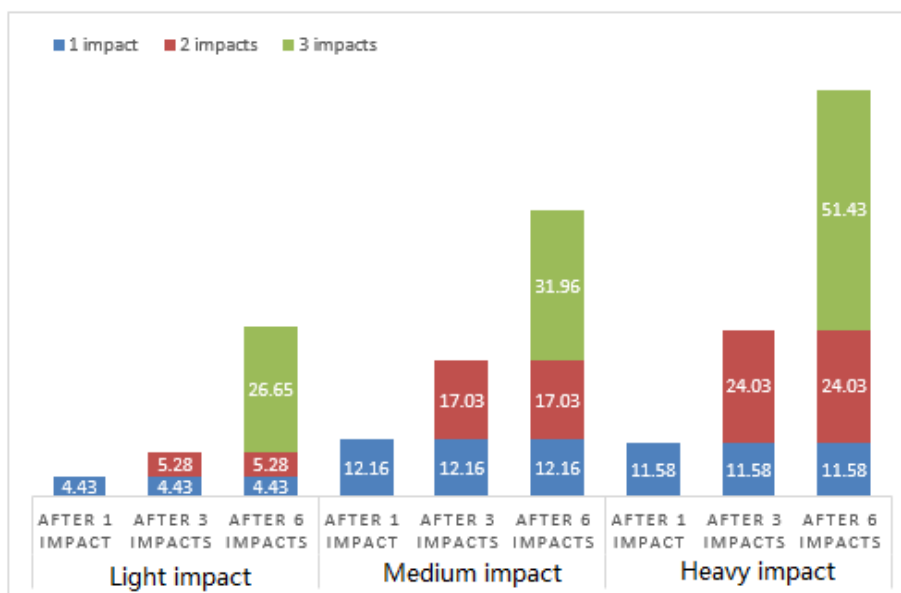


Figure 4-50: Decored sands samples from inorganically bonded sand core of modified silicate binder mixture and promoter (INOTEC™ Promoter EP 4174) in warm box process after impact.

Figure 4-50 shows the amount by weight of decored sand for different impact energies and number of impacts from inorganically bonded sand core of modified silicate binder mixture and promoter (INOTEC™ Promoter EP 4174) (warm box). A maximal value of 51.43 g was obtained by heavy impact for three times, the amount of decored sand was increased by increasing the number of impacts and impact energy. The decored sand obtained by each single impact from inorganically bonded sand core of modified silicate binder mixture and promoter (INOTEC™ Promoter EP 4174) (warm box) was more than for inorganically bonded sand cores with modified silicate binder mixture and promoter (INOTEC™ - Promoter WJ 4000) (warm box).










	1	2	3
Light impact	 9.67 g	 17.54 g	 90.1 g
Medium impact	 14.57 g	 32.49 g	 244.52 g
Heavy impact	 12.39 g	 29.81 g	 38.4 g

Figure 4-51: Decored sands samples from inorganically bonded sand core with water glass 39T® using the warm box process after impact.

In **Figure 4-51**, the decored sand of three inorganic sand cores bonded with water glass 39T® using the warm box process is shown for different impacts and energy. The amount of decored sand from cores increased with more impacts energy similar to organically bonded sand cores (warm box), except for the maximal amount of 244.52 g obtained by a medium energy. The decored sand exhibited a white colour as no decomposition of additives took place. Also the amount of agglomerates increased with the increasing input energy.

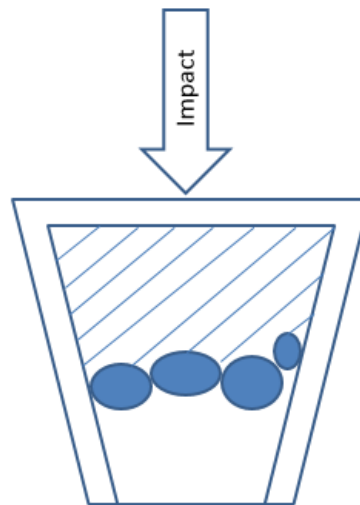


Figure 4-52 : Agglomerates form a bridge structure and hinder fine sand to fall down during decoring.

During impacting, water glass bonded cores formed more agglomerates. These agglomerates gathered and formed a bridge during decoring and blocked up fine sands. With increasing impact energy, the agglomerates disintegrated and fell down together with the fine sand, which led to a sudden increase of the weight of the decored sand.

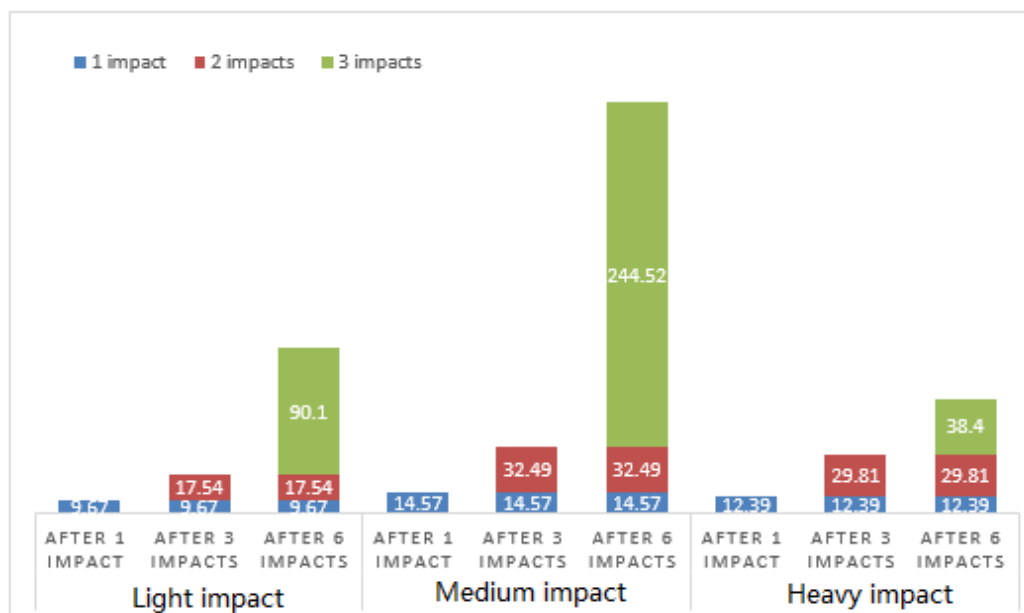


Figure 4-53: Decored sands samples from inorganically bonded sand core with water glass 39T[®] using the warm box process after impact.

Figure 4-53 shows the amount by weight of decored sand for different impact energies and number of impacts from inorganically bonded sand cores with pure water glass – Betol® 39 T using the warm box process. A maximal value of 244.52 g was obtained by medium impact energy repeated for three times. The amount of decored sand from the inorganically bonded pure water glass (Betol® 39 T) hardened with a hot tool were larger than that of inorganically bonded sand cores.

Interestingly, for each impact energy with increasing number of impacts the amount of agglomerates and fine sand increases. However, the highest impact energy does not result in the largest amount of decored sand. Only for the highest energy and three impacts the largest amount is observed.

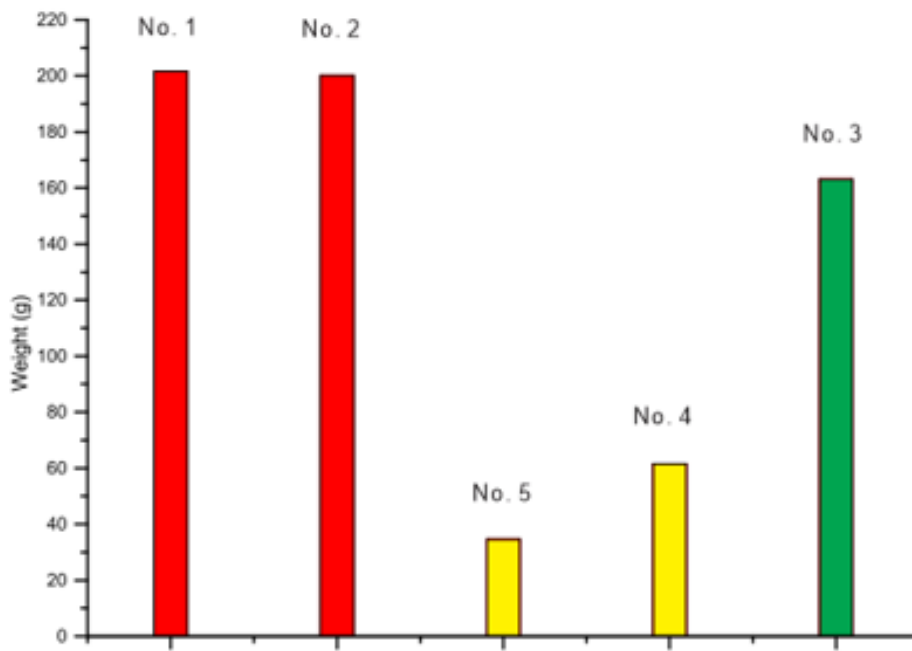


Figure 4-54: Comparison of decoring abilities for five different internal cores, No.1 is the organically bonded sand core with modified urea-furan-phenolic resin (warm box), Nr. 2 is the organically bonded sand core with an aqueous solution of phenol sulfonic acid, aluminum salts, sulfuric acid (warm box), No. 3 is the inorganically bonded sand core with water glass 39T® (warm box), Nr. 4 is the inorganically bonded sand core of modified silicate binder mixture and promoter (INOTEC™ Promoter EP 4174), Nr. 5 is the inorganically bonded sand core with modified silicate binder mixture and promoter (INOTEC™ - Promoter WJ 4000) (warm box).

Figure 4-54 shows that organically bonded sand cores can be easily shaken out after contact with the Al melting and subsequent solidification compared to inorganically bonded cores. However, warm box hardened Betol® 39 T sand core showed a similar decoring

behaviour compared to organically bonded cores. From **Figure 4-54**, it is apparent that organically bonded sand core with modified urea-furan-phenolic resin in warm box process obtained most de-cored sand after impacting, followed by organically bonded sand core with an aqueous solution of phenol sulfonic acid, aluminum salts, sulfuric acid (warm box), inorganically bonded sand core with water glass 39T[®] (warm box), inorganically bonded sand core of modified silicate binder mixture and promoter (INOTEC[™] Promoter EP 4174), and inorganically bonded sand core with modified silicate binder mixture and promoter (INOTEC[™] - Promoter WJ 4000) (warm box) in descending order.

As mentioned before, the organically bonded sand cores were more easily to be de-cored. Therefore, the residual amount of sand in the casting box was less than that for the inorganically bonded sand cores. It was observed that after impact some of organically bonded cores were nearly de-cored. In particular for the inorganically bonded sand core with water glass 39T[®] using the warm box process total decoring was achieved.

4.4 Simulation of dipping trial

The simulated curves are compared to the experimental curves obtained in experiments of dipping trials. The proportional constant Q_{sand} of the thermal conductivity was systematically iterated until the two temperature time curves of experiment and simulation overlapped. If the simulated temperature curves for each testing point overlapped those obtained in experiments, the proportional constant Q_{sand} was chosen and $\lambda_{\text{sand core}}$ can be calculated from the Q_{sand} and thermal conductivity λ ratio of sand used in Magma software (see Chapter 3).

The parameters such as density ρ and specific heat capacity C_p were known for different sands, so that only $\lambda_{\text{sand core}}$ was iterated using the Magma software.

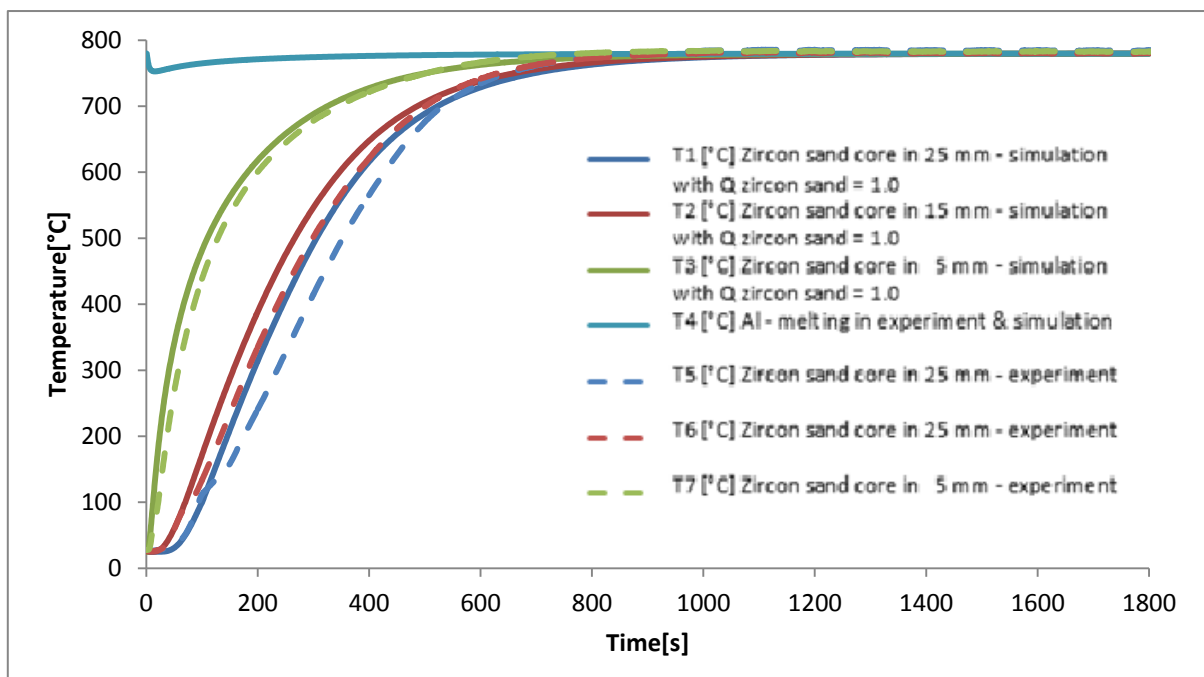


Figure 4-55: Comparison between simulation curve and experiment curve of Zircon sand at the same parameter of 780 °C with the proportional constant $Q_{\text{Quartz Magma}} = 1.0$.

During the iteration of $Q_{\text{zircon sand}}$, $Q_{\text{zircon sand}} = 1.0$ was firstly set into $\lambda_{\text{Zircon sand}} = Q_{\text{Zircon sand}} \times \lambda_{\text{silica sand Magma}}$, in this case, $\lambda_{\text{Zircon sand}} (Q_{\text{zircon sand}} = 1.0) = \lambda_{\text{sand core Magma}}$. Dipping trails (into Al melt) was simulated with the obtained $\lambda_{\text{Zircon sand}}$ at 780 °C, temperature time curves were obtained in three test points with virtual thermal couples. Based on this principle, $\pm 10\%$ tolerances were added to $Q_{\text{zircon sand}} = 1.0$, in these cases, $\lambda_{\text{Zircon sand}} (Q_{\text{zircon sand}} = 1.1) = 1.1 * \lambda_{\text{sand core Magma}}$ and $\lambda_{\text{Zircon sand}} (Q_{\text{zircon sand}} = 0.9) = 0.9 * \lambda_{\text{sand core Magma}}$ were set as parameters to simulate dipping trials, temperature time curves were obtained with $Q_{\text{zircon sand}} = 1.1$ and $Q_{\text{zircon sand}} = 0.9$.

$\lambda_{\text{zircon sand}} = 0.9$. The experimental temperature time curves in three testing points were proposed to compare simulated temperature time curves with $Q_{\text{zircon sand}} = 0.9 / 1.0 / 1.1$. If the temperature time curves of three testing points in experimental and simulated dipping trials were overlapped, $Q_{\text{zircon sand}}$ was confirmed for $\lambda_{\text{Zircon sand}} (Q_{\text{zircon sand}})$.

In **Figure 4-55**, the proportional constant $Q_{\text{zircon sand}}$ was about 1.0 of $\lambda_{\text{sand core Magma}}$ at 780°C. The temperature distributions were close to each other, except the water peak at the centre position and 15mm's position between experiment and simulation, the $Q_{\text{zircon sand}}$ was fixed by comparison.

Therefore, $\lambda_{\text{zircon sand}}$ of Zircon sand core bonded with a specific water glass e.g. Betol® 39 T can be calculated. According to the same principle, other Q_{sand} values were simulated. When the water peak occurred, the temperature time curve was extended to longer time by the amount of time during which the water peak was active.

After iteration simulated curves and experimental curves overlapped except the outside position at which a water peak occurred. These values were obtained by five different base sands bonded by water glass Betol® 39 T at 780°C in dipping trials. Another situation was simulated by the same cores at 700°C for additional confirmation, the simulated $\lambda_{\text{zircon sand core}}$ and known $\rho_{\text{zircon sand core}}$ and $Cp_{\text{zircon sand core}}$ were imported into the simulation, and the obtained curves are shown in **Figure 4-56**.

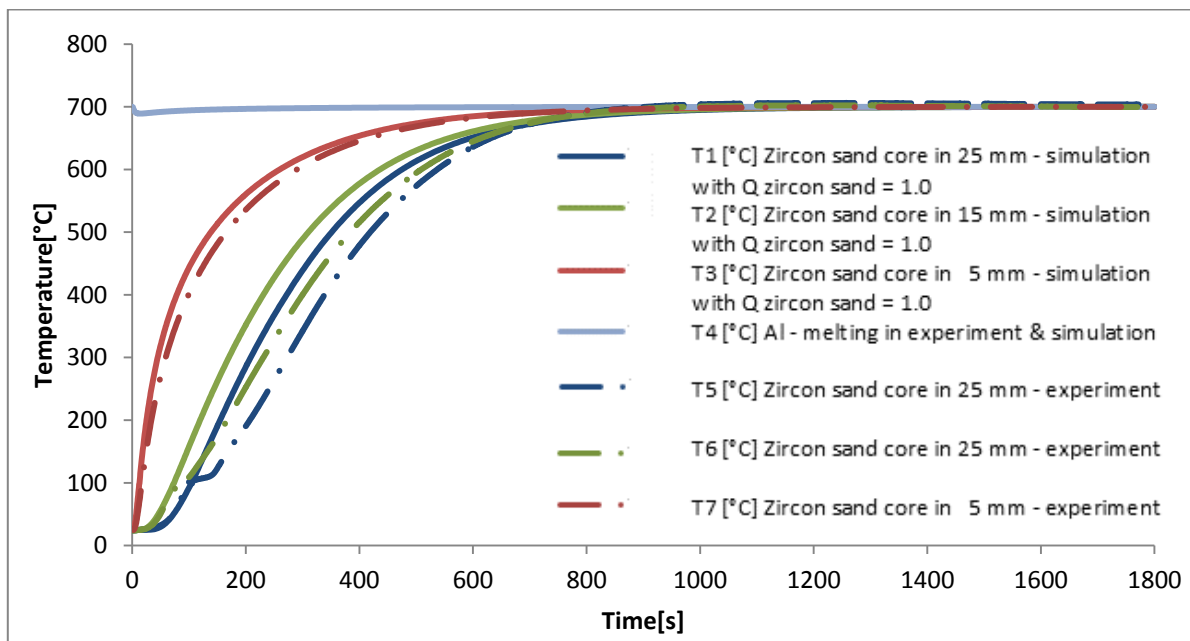


Figure 4-56: Comparison between simulation curves and experiment curves of Zircon sand at the same parameters at 700 °C with the proportional constant $Q_{\text{Magma}}^{\text{Quartz}} = 1.0$.

Figure 4-56 shows the experimental curve of temperature over time in zircon sand cores bonded with water glass Betol® 39 T at 700° C, which overlaps the simulated curves to a high degree once the water peak is taken account of. Except for the water peak at 100°C the curves show good agreement. That means, $\lambda_{\text{zircon sand core}}$ fits for the dipping trials at 780° C and 700° C. The simulated results are listed in **Table 4-3**.

Table 4-3: Simulated different $Q_{\text{sand core}}$ of sand cores.

Sand type	$Q_{\text{sand core}}$
MIN Sand	0.9
Kerphalite sand	0.8
Cerabeads Sand	0.8
Zircon Sand	1.0
H32 Silica sand	0.9

Figure 4-57 shows the calculated $\lambda_{\text{sand cores}}$ values over time from 0° C to 800° C. The curves of $\lambda_{\text{H32 silica sand core}}$ ($Q_{\text{H32 silica sand}} = 0.9$) of H32 silica sand core bonded with water glass (Betol® 39 T) (warm box) and $\lambda_{\text{MIN sand core}}$ ($Q_{\text{MIN sand}} = 0.9$) of MIN sand core bonded with water glass using warm box process overlap. The curves of $\lambda_{\text{Kerphalite sand core}}$ ($Q_{\text{Kerphalite sand}} = 0.8$) of Kerphalite sand core bonded with water glass (Betol® 39 T) (warm box) and $\lambda_{\text{Cerabeads sand core}}$ ($Q_{\text{Cerabeads sand}} = 0.8$) of Cerabeads sand core bonded with water glass (Betol® 39 T) using the warm box process overlap too. Because of $Q_{\text{zircon sand}} = 1.0$, so that the $\lambda_{\text{Zircon sand}}$ ($Q_{\text{zircon sand}} = 1.0$) of zircon sand core bonded with water glass (Betol® 39 T) using the warm box process and $\lambda_{\text{Magma}}^{\text{sand core}}$ also overlap.

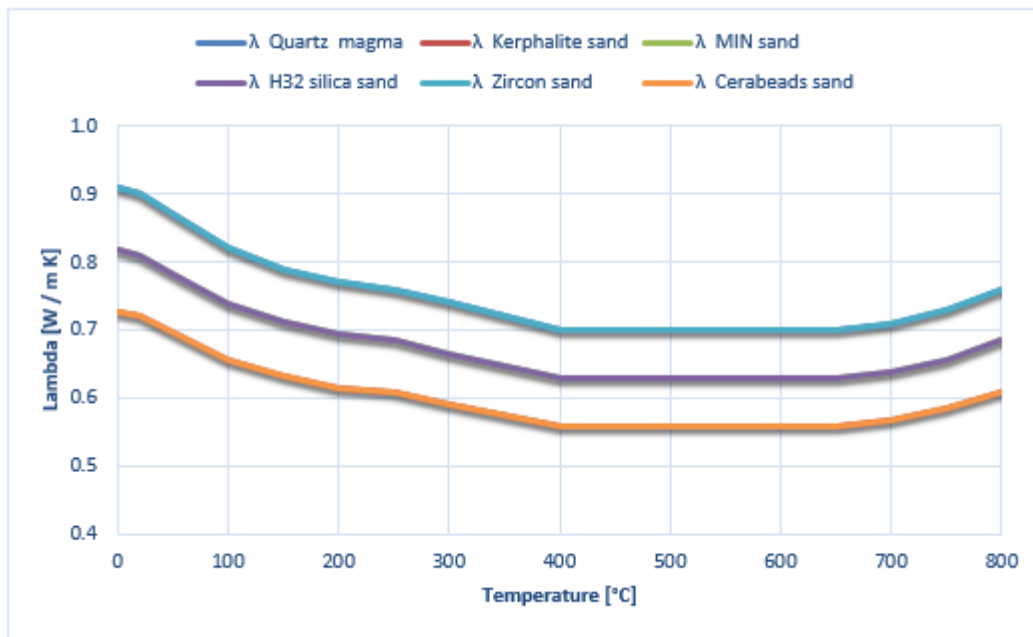


Figure 4-57: Five λ s values over time in different sand cores, λ H32 silica sand and λ MIN sand are overlapped, λ Kerphalite sand and λ Cerabeads sand are overlapped.

5 Conclusion

Five raw sand properties were investigated for their grain size distribution, shape factor, by optical microscopy and scanning electronic microscopy and granulometry. The results of dipping trials and ring mould test allowed to estimate the thermal properties of sand cores relative to Quartz sand. The deforming behaviour (mechanical properties) was investigated by shake out trials.

Raw sand properties

Raw sand properties were investigated by granulometry to analyze grain size distribution, grain morphology 2D – shape factor, optical microscopy, scanning electron microscopy.

Cerabeads sand grains exhibit yellow colour. Their size distribution gives an average grain size of 210 μm and an AFS number of 67.8. Relatively regular spheroidal particles and fine roughness surface were observed. The 2 – D shape factor of Cerabeads sand grains is 1.0, indicating a round shape.

H32 silica sand grains are irregular and transparent. Their size distribution gives an average grain size of 220 μm and an AFS number of 62.0. H32 silica sand exhibits rough surface and fractures. The 2 – D shape factor of H32 silica sand grains is 0.9, indicating an angular shape.

Kerphalite sand grains exhibit gray colour. An average grain size of 150 μm and the largest AFS number of 93.3 were obtained. Kerphalite grains exhibit a sharp morphology with irregular edges and corners, some particles were observed as cubic. The 2 – D shape factor of Kerphalite sand grains is 0.75, indicating a subangular shape.

MIN sand grains are black spheroidal. Their size distribution gives an average grain size of 210 μm and an AFS number of 66.6. MIN sand grains exhibit rough surface with observed dendrite structure resulting from Al_2O_3 growth. The 2 – D shape factor of MIN sand grains is 1.0, indicating a round shape.

Zircon sand particles have smoother surfaces with rounded edges. Their size distribution gives an average grain size of 195 μm and an AFS number of 71.4, Zircon sand grains exhibit per – fractures and groove on the smooth surface. The 2 – D shape factor of Zircon sand grains is 0.9, indicating an angular shape.

Sand cores

The binder bridges in organically bonded sand cores and inorganically bonded sand cores were observed by SEM.

After thermal exposure, the broken bonds were observed. Organically bonded binder bridges had obvious different morphology from inorganically bonded binder bridges. Organically bonded binder bridges exhibited a fully or partly covered cross - section, while inorganically bonded binder bridges with additives exhibited a river path or rain structure, without additives a ring structure was observed.

Thermal physical properties

Thermal physical properties were estimated by dipping trials and ring mould test. The temperature gradient in investigated sand cores during Al melt solidification were obtained. Thermal conductivities of investigated sand cores were simulated by Magma 5 and interactively compared.

In investigated five sand cores, temperature gradients arrange in descending order as:

$$\frac{dT}{dt}(\text{silica sand}) > \frac{dT}{dt}(\text{zircon sand}) > \frac{dT}{dt}(\text{Cerabeads sand}) > \frac{dT}{dt}(\text{Kerphalite sand}) > \frac{dT}{dt}(\text{MIN sand}).$$

Temperature gradient in the cores influences Al melt solidification. The mechanical properties of the casting parts are also influenced by the cooling rate, which effects the secondary dendrite arms.

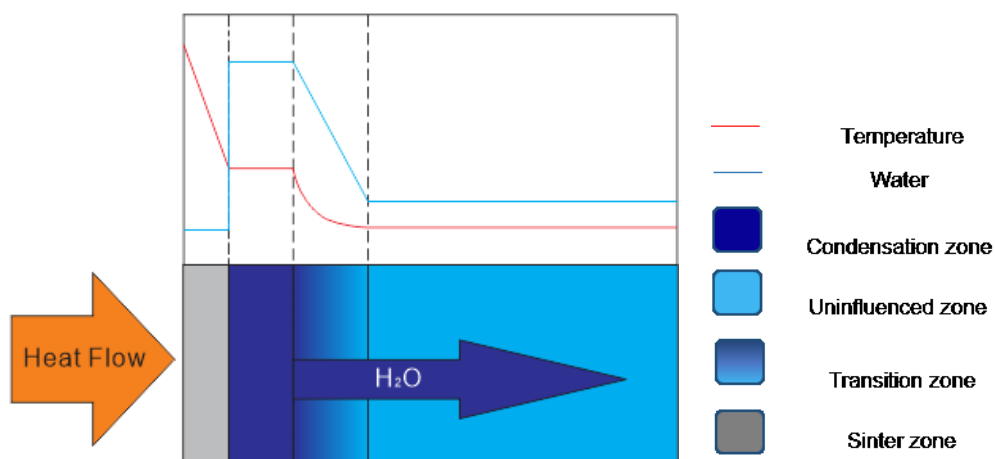


Figure 5-1: Heat flow effects temperature and moisture in sand cores.

In dipping, heat flow drives the moisture from edge into center in the sand cores, as shown in **Figure 5-1**. In the sinter zone, water keeps lower value, and temperature reduce

gradually to the constant value. In condensation zone, water content hold the constant value at 100°C, and temperature value is constant. In the transition zone, locating between condensation zone and uninfluenced zone, the water content reduce rapidly to a constant value, and temperature slowly goes down till a constant value. In the situation of a core the condensation zone moves from the outside to the centre so that the transition zone will impinge to form a condensation zone in the centre.

Decorating behaviour

Decorating behaviour was investigated controlled impacts, which can distinguish the behaviours between organically bonded sand cores and inorganically bonded sand core.

Organically bonded sand core with modified urea-furan-phenolic resin using the warm box process obtained most decorated sand after impacting, followed by organically bonded sand core with an aqueous solution of phenol sulfonic acid, aluminum salts, sulfuric acid using the warm box process, inorganically bonded sand core with water glass 39T[®] using the warm box process, inorganically bonded sand core of modified silicate binder mixture and promoter (INOTEC[™] - Promoter EP 4174), and inorganically bonded sand core with modified silicate binder mixture and promoter (INOTEC[™] - Promoter WJ 4000) using the warm box process in descending order.

References

- [1] Rao P.N., Manufacturing Technology: Foundry, Forming & Welding, 2nd Edition, Tata McGraw-Hill Education, (2001), 97.
- [2] Bawa H.S., Manufacturing Processes-II, Tata McGraw-Hill Education, (2004), 26.
- [3] Yu K. O., Modeling for Casting and Solidification Processing, CRC Press, (2001), 313.
- [4] Solenicki G., Budic I., Ciglar D., Determination of thermal conductivity in foundry mould mixtures, Metalurgija 49 (1), (2010), 3.
- [5] J.P. Klaushish, Manufacturing processes, PHI Learning Private Limited, Second edition, (2013), 194.
- [6] Peter Beeley, Foundry technology, First published 1972, reprinted 1979, 1980, 1982, second edition, (2001), 206.
- [7] Elanchezhian C., Vijaya Ramnath B., Manufacturing Technology I, 2nd Edition, (2006), 37.
- [8] Stehpan D.Chastain, Metall castiny: A Sand Casting Mannual for the Small Foundry Vol.1 America (2004) 126.
- [9] Chastain S., Metal Casting: A Sand Casting Manual for the Small Foundry, Band 1, USA, (2004), 137.
- [10] Brown J., Ferrous Foundryman's handbook, Foseco International Ltd, (2000), 150.
- [11] Flemming E., Tilch W., Formstoffe und Formverfahren, Deutscher Verlag für Grundstoffindustrie, Leipzig-Stuttgart Germany. (1993), 41.
- [12] Zircon sand properties, <http://www.aomevents.com/conferences/afi/papers/Dahlman.pdf>; 24-03-2014.
- [13] Sheidi Haruna Maihankuri, Investigation on properties of local zircon sand for sand casting, Research Journal in Engineering and Applied Sciences 1(6), (2012), 404.
- [14] Resin Coated Special Minerals and their Application in Foundries, <http://www.aomevents.com/conferences/afi/papers/Dahlman.pdf>; 24-03-2014.
- [15] Cerebeads sand properties, <http://www.aomevents.com/conferences/afi/papers/Dahlman.pdf>; 24-03-2014.

-
- [16] Minsand properties, <http://www.lkabminerals.com/en/Products/MinSand/>, 04-04-2014.
- [17] Wang L. K., Hung Y. T., Shamas N. K., Handbook of Advanced Industrial and Hazardous Wastes Treatment, (2009), 157.
- [18] West G., Fookes P. G., Lay J., Sims I., Smith M. R., Collis L., Aggregates: Sand, Gravel and Crushed Rock Aggregates for Construction Purposes(Geological Society Engineering Geology Special Pub.No.17), Hardcover, (2001), 205.
- [19] Aluminum Oxide Nanopowder / Nanoparticles, <http://www.us-nano.com/inc/sdetail/690>.
- [20] Jain P. L., Principles of foundry technology-fourth edition, Tata McGraw-Hill publishing company Limited, India, (2003) 56.
- [21] Brown J. R., Ferrous Foundryman's handbook, Foseco International Ltd, ISBN: 978-0-7506-4284-2, (2000), 16.
- [22] Mishellany A., Delalande G., Descantes Y., Use of the VDG 40 videograder as a grading control device for French highway construction, USA, 2000.
- [23] The standards in germen and international form, <http://www.diedrahtweber.de/de/anwendungen-produkte/drahtgewebe-allgemein/deutsche-u-internationale-normen.html>, 09 -11 – 2014.
- [24] Huang A.B., Mayne P.W., Geotechnical and Geophysical Site Characterization 4, (2013), 1288.
- [25] Prowell B. D., Zhang J. N., Brown E. R., Aggregate properties and the performance of superpave-designed hot mix asphalt, Transportation Research Board - Report 539, USA (2005), 38.
- [26] International standard ISO 3310, Test sieves – technical requirements and testing – part 1: test sieves of metal wire cloth, fourth edition, (2000).
- [27] Altan T, Sand, sand additives, sand properties, and sand reclamation, Marmara University Turkey, http://mimoza.marmara.edu.tr/~altan.turkeli/files/cpt-2-sand_sand.pdf, 03-11-2014.
- [28] Steel castings handbook, sixth edition Steel founders' of society of America, (1995) 27-6
- [29] Spezialsande - Formgrundstoffe für die moderne Kern- und Formherstellung, <http://www.google.de/url?sa=t&rct=j&q=&esrc=s&source=web&cd=2&ved=0CCYQFjAB&url=>

[http%3A%2F%2Fwww.huettenes-albertus.com%2Fno_cache%2Fdownloads%2Findex.html%3Fcid%3D300%26did%3D556%26sechash%3D7d104cac&ei=JHOBVP7dNJCp7AbZ-4DwAQ&usq=AFQjCNFazoyNSnXShlvB5rpsSrY-xyYYMg&bvm=bv.81177339,bs.1,d.bGQ](http://www.huettenes-albertus.com/no_cache/downloads/index.html?cid=3D300%26did=3D556%26sechash=3D7d104cac&ei=JHOBVP7dNJCp7AbZ-4DwAQ&usq=AFQjCNFazoyNSnXShlvB5rpsSrY-xyYYMg&bvm=bv.81177339,bs.1,d.bGQ).

[30] Stauder B., Thermophysikalische Daten Zusammenfassung der Messergebnisse, Nemak, Austria, (2005).

[31] Bradley R. Schrottenboer, Alan F. Arbogast, Locating alternative sand sources for Michigan's foundry industry:A geographical approach, Applied Geography 30, (2010), 697.

[32] Polzin, H., Anorganische Binder zur Form- und Kernherstellung in der Gießerei, Media-Print Informationstechnologie GmbH, Paderborn, (2012), 160.

[33] Elam J. W., Londergan A., Gendt S. D. Bent S. F., Straten O., Roozeboom F., Delabie A., Atomic layer deposition applications 6, vol.33, No.2, USA, (2010), 48.

[34] Totten G.E., MacKenzie D.S., Handbook of Aluminum: Vol.1: Physical Metallurgy and Processes. CRC Press, (2003), 615.

[35] Prass, I., Moulding Sand Casting College Core Manufacturing, Nemak, Austria, (2009).

[36] Saruhan B., Oxide-Based Fiber-Reinforced Ceramic-Matrix Composites: Principles and Materials; Kluwer academic publishers, USA, (2003), 28.

[37] Temperature-Dependent Phase Transitions of ZrO₂, Material design application note (2009), 1

[38] Hagen R., Lamy C., Myhre B. and Peng H., Mullite formation, high – temperature properties of Andalusit – alumina based LCC and ULCC, Presented at UNITECR'09 in Salvador de Bahia, Brazil, (2009), 13

[39]The introduction of Mullite as a refractory material, http://www.kyanite.com/assets/Mullite_SpecSheet.pdf, 15-11-2014.

[40] Sharma B. K., Industry chemistry including chemical engineering, chapter 32 – refractory, GOEL Publishing House, (1997), 641.

[41] The introduction of MINsand as a refractory material, <http://www.lkabminerals.com/en/News/News/Small-beads-big-impact/>, 15-11-2014.

-
- [42] Brümmer G., Döpp R., Trocken statt Begasen mit CO₂ beim Wasserglassverfahren- neue Ansätze bei alten Bindermitteln, Giesserei 84, (1997), Nr.13, 12.
- [43] Sáenz A., Velasco A., Talamantes J., Colás R., Development of inorganic binders for the manufacture of sand cores used in the automotive casting Industry. (2012).
- [44] Brümmer G., Döpp R., Trocken statt Begasen mit CO₂ beim Wasserglassverfahren- neue Ansätze bei alten Bindermitteln, Giesserei 84, (1997), Nr.13, 13.
- [45] Prass I., Comparison of organic core production processes, Nemak Linz GmbH (2012).
- [46] Gardziella A., Pilato L. A., Knop A., Phenolic Resins: Chemistry, Applications, Standardization, Safety and Ecology Springer; Auflage: 2nd completely rev. ed. 2000 (15. Oktober 1999), 303.
- [47] Brown R. J., Foseco Ferrous Foundrymans Handbook 11 th Edition, Butterworth Heinemann, (2000), 189.
- [48] Peter Beeley, Foundry technology, first published 1972, reprinted 1979, 1980, 1982, second edition (2001), 198.
- [49] Brown R. J., Foseco foundryman's handbook, Butterworth-Heinemann; 10 th Edition, Butterworth Heinemann, (1994), 71.
- [50] Jain P. L., Principles of foundry technology-fourth edition, Tata McGraw-Hill publishing company Limited, India, (2003) 91.
- [51] Flemming E., Tilch W., Formstoffe und Formverfahren, Deutscher Verlag für Grundstoffindustrie, Leipzig-Stuttgart Germany. (1993), 78.
- [52] Döpp R., Deike R., Gettwert G., Beitrag zum Wasserglass-CO₂-verfahren, Giesserei 72, (1985), Nr. 22, 628.
- [53] T.V. Ramana Rao, Metal Casting Principles and practice, new age international (p) Ltd., New Delhi, (2010), 24.
- [54] Kleinheyer U., Jahreübersicht Formstoffe (23.Folge) Teil 2: Formverfahren mit nicht tongebundenen Formstoffen; Zusatzstoffe; Überzugstoffe, Giesserei 73, (1986), Nr. 22, 657.
- [55] Osterberg L., Anderson W., Stoberiet 62, 1985, Nr.6, S, 8-16 and Giesserei 73, 1986 Nr. 22, S. 657.

- [56] Polzin H., Untersuchungen zur Mikrowellenverfahren von wasserglasgebundenen Gießereiformstoffen, Technische Universität Bergakademie Freiberg. Freiberg, (2000), 11.
- [57] Kaschnitz E., The influence of the quality of thermal conductivity and thermal expansion data on the numerical simulation in metal part production, Thermal Conductivity 30: Thermal Expansion 18: Joint Conferences: August 29-September 2, 2009, Pittsburgh, Pennsylvania, USA, (2010), 133.
- [58] Voss D., Charakterisierung eines neuen entgasungsarmen und verbrennbaren Formstoffes für Gießereianwendungen Kohlenstoff AeroSande, (2004).
- [59] Eman J. Abed, The influence of different casting method on solidification time and mechanical properties of AL- Sn castings, International Journal of Engineering & Technology IJET-IJENS Vol: 11 No: 06, (2011).
- [60] The Metal Casting and Heat Treating Industry: Guide to Pollution Prevention, Dlnae publishing company, (1996), 60.
- [61] Rajput R. K., A textbook of manufacturing technology: Manufacturing process, Firewall Media, (2007), 108.
- [62] Sharma P. C., A Textbook of Production Technology: Manufacturing Processes, India (2007), 177.
- [63] Sieve analysis, http://en.wikipedia.org/wiki/Sieve_analysis, 23 – 03 – 2014.
- [64] Pavement Interactive. Gradation Test. (2007).
- [65] Pati S., Drelich J., Jha A., Neelameggham N.R., Prentice L., Wang C., Energy Technology 2013: Carbon Dioxide Management and Other Technologies, (2013), 40.

FIGURE CAPTIONS

FIGURE 1-1: COMPLEX CASTING PARTS.	10
FIGURE 2-1: THERMAL EXPANSION OF SILICA AND SILICA SAND, 1. SILICA SAND, 2. SILICA ^[11]	13
FIGURE 2-2: TYPES OF SAND GRAINS ^[20]	15
FIGURE 2-3: THERMAL EXPANSION OF DIFFERENT SANDS BONDED WITH SODIUM SILICATE (WARM BOX HARDENED AND MICROWAVE DRIED) WITH INCREASING TEMPERATURES ^[30]	19
FIGURE 2-4: SILICA STRUCTURE PHASE TRANSFORMATION AT 573 °C ^[32] , (A) A-QUARTZ (TRIGONAL) P = 2. 65 G / CM ³ , (B) B-QUARTZ (HEXAGONAL) P= 2. 30 G / CM ³ WITH A CHANGE POINT AT 573 °C.	19
FIGURE 2-5: PH VALUES OF DIFFERENT BASE SANDS ^{[40] [41]}	21
FIGURE 2-6: PHENOLRESIN AND ISOCYANATE WITH AMIN GAS TO FORM A COLD BOX BINDER BRIDGE ^[45]	23
FIGURE 2-7: HOT BOX PROCESS FOR MAKING CORES ^[46]	23
FIGURE 2-8: UREA AND FORMALDEHYDE WITH PHENOL/FURAN RESIN AND AMMONIUM ISOLATE AS A LATENT CORING AGENT UNDER HEATING TO FORM A HOT BOX BINDER BRIDGE ^[45]	24
FIGURE 2-9: FORMATION OF AN INORGANIC-BINDER BRIDGE ^[45]	27
FIGURE 2-10: TEMPERATURE ALONG A LINE PERPENDICULAR TO THE MOULD-METAL INTERFACE ^[59]	29
FIGURE 3-1: SIEVE SHAKER USED FOR GRANULOMETRY AND SCALE.	32
FIGURE 3-2: BINARY SHAPE OF ZIRCON SAND PARTICELS.	33
FIGURE 3-3: (A) OPTICAL MICROSCOPY EQUIPMENT (ZEISS DISCOVERY 2.0), (B) SEM / EDX EQUIPMENT.	34
FIGURE 3-4: (A) CORE SHOOTING MACHINE WITH THE PREHEATED MOULD (B). INSTALLED CYLINDRICAL SHAPE MOULD (C) INSTALLED TRAPEZOIDAL SHAPE MOULD.	35
FIGURE 3-5: WOODEN MOULD FOR MAKING OUTER CORES (A).THE ENTIRETY WOODEN MOULD (B) THE WOODEN FOUNDATION.....	36
FIGURE 3-6: SKETCH OF POSITIONS OF THERMAL COUPLES.	38
FIGURE 3-7: DEVICE AND PROCESS OF DIPPING TRAILS (A)THE BRACKET FOR FIXING THE SAND CORE AND THERMAL COUPLES; (B) THE PROCESS OF DIPPING INTO THE MELTING AL ALLOY OVEN; (C) DATA ACQUISITION TO MEASURE THE TEMPERATURE (UNIVERSALMAßGERÄTE DEWE – 2000; 1000894); (D) THE MEASUREMENT PROCESS OF DIPPING TRIALS.....	39
FIGURE 3 - 8: SKETCH OF THE RING MOULD TEST WITH THERMAL COUPLES. (A) THREE THERMAL COUPLES FIXED INTO SAND CORE AND LINKED ONE THERMAL COUPLES BETWEEN STEEL RING MOULD AND SAND CORE.....	40
FIGURE 3-9: (A) INTERNAL CORE, OUTER CORE AND STEEL PLATE (B) CASTING BOX BEFORE POURING AL-MELT.	41
FIGURE 3-10: (A) THE STKECH OF PURING AL – MELT INTO FIXED INNER CORE AND SAND MOULD (B) AL – MELT SOLIDIFIED IN A SAND MOULD.....	41
FIGURE 3-11: (A) MOTIFIED SHAKE OUT DEVICE (B) SPECIMEN AFTER SHAKE OUT OPERATION.....	42

FIGURE CAPTIONS

FIGURE 3-12: THE SCHEMATIC SHAKE OUT OPERATION WITH IMPACT DEVICE.	42
FIGURE 3-13: (A) 25 THERMAL TEST POINTS IN THE SAND CORE. (B) GEOMETRY OF SIMULATED SAND CORE WITH 25 THERMAL COUPLES IN SAND CORE	43
FIGURE 3-14: $\Lambda_{\text{SILICA SAND}}$ VALUE WITH TEMPERATURE.....	44
FIGURE 4-1: GRAIN SIZE DISTRIBUTION OF FIVE DIFFERENT BASE SANDS.	45
FIGURE 4-2: GRAIN SIZE DISTRIBUTION BY WEIGHT IN FIVE INVESTIGATED RAW SANDS. (A) H32 SILICA SAND GRAIN SIZE DISTRIBUTION (B) CERABEADS SAND GRAIN SIZE DISTRIBUTION (C) KERPHALITE SAND GRAIN SIZE DISTRIBUTION (D) MIN SAND GRAIN SIZE DISTRIBUTION (E) ZIRCON SAND GRAIN SIZE DISTRIBUTION.	46
FIGURE 4-3: AFS NUMBER OF FIVE DIFFERENT BASE SANDS.	47
FIGURE 4-4: THE RELATIONSHIPS BETWEEN AFS GRAIN FINENESS NUMBER AND AVERAGE GRAIN SIZE IN FIVE SANDS.....	48
FIGURE 4-5: TESTED SAND PARTICLES IN EACH BASE SAND TO MEASURE SHAPE FACTOR (A) CERABEADS SAND (B) H32 SILICA NEW SAND (C) KERPHALITE SAND (D) MIN SAND (E) ZIRCON SAND.	49
FIGURE 4-6: SHAPE FACTOR DISTRIBUTION OF FIVE DIFFERENT BASE SANDS (A) SHAPE FACTOR DISTRIBUTION OF CERABEADS SAND (B) SHAPE FACTOR DISTRIBUTION OF SILICA SAND (C) SHAPE FACTOR DISTRIBUTION OF KERPHALITE SAND (D) SHAPE FACTOR DISTRIBUTION OF MIN SAND (D) SHAPE FACTOR DISTRIBUTION OF ZIRCON SAND.	50
FIGURE 4-7: THE SHAPE FACTORS OF DIFFERENT RAW SANDS.	51
FIGURE 4-8: MICROSCOPY IMAGES OF RAW SANDS (A) CERABEADS 650 RAW SAND (B) SILICA SAND H32 (C) KERPHALITE OR ANDALUSIT RAW SAND (D) MIN SAND (E) ZIRCON RAW SAND.	52
FIGURE 4-9: DIFFERENT SAND PARTICLES OF CERABEADS RAW SAND (A) DIFFERENT SIZE OF ROUNDED SAND PARTICLES (B) SINGLE PARTICLES AND BONDED PARTICLES (C) MORPHOLOGY OF SAND PARTICLE (D) SURFACE OF CERABEADS SAND PARTICLE.	53
FIGURE 4-10: VIEW OF CERABEADS SAND AND THEIR CHEMICAL COMPOSITIONS.	54
FIGURE 4-11: DIFFERENT SAND PARTICLES OF H32 RAW SAND (A) SHAPES OF H32 SILICA SANDS (B) ROUGH SURFACE AND FRACTURE (C) THE PARTICLE WITH DISTINCT FACES (D) SMOOTH ROUND SURFACE.	55
FIGURE 4-12: THE FRACTURED SURFACE AND GROOVE ON SILICA SAND PARTICLE AND ITS CHEMICAL COMPOSITIONS.	56
FIGURE 4-13: DIFFERENT SAND PARTICLES OF KERPHALITE RAW SAND. (A) DIFFERENT SIZE SAND PARTICLES WITH SHARP EDGES AND CORNERS (B) AN OBVIOUS CUBIC SHAPE PARTICLE (C) MORPHOLOGY OF AN IRREGULAR AND SHARPLY POINTED PARTICLES SAND PARTICLE (D) SURFACE OF KERPHALITE SAND PARTICLE.	57
FIGURE 4-14: VIEW OF KERPHALITE SAND AND THEIR CHEMICAL COMPOSITIONS.	58
FIGURE 4-15: DIFFERENT SAND PARTICLES OF MIN RAW SAND. (A) DIFFERENT SIZE SAND PARTICLES WITH ROUND PARTICLES (B) SOME SPHEROIDAL PARTICLES (C) AGGLOMERATION OF TWO PARTICLES (D) SURFACE OF MIN SAND PARTICLE.....	59

FIGURE CAPTIONS

FIGURE 4-16: VIEW OF MIN SAND AND THEIR CHEMICAL COMPOSITIONS.	60
FIGURE 4-17: DIFFERENT SAND PARTICLES OF ZIRCON RAW SAND (A) ROUNDED EDGES IRREGULAR PARTICLES (B) PRE-FRACTURES AND GROOVES ON THE SURFACES (C) FRACTURES ON THE SURFACE (D) SMOOTH SURFACE.	61
FIGURE 4-18: THE MICRO VIEW OF ZIRCON SAND AND CHEMICAL COMPOSITIONS.	62
FIGURE 4-19: (A) AND (B) ORGANICALLY BONDED SAND CORE WITH MODIFIED UREA-FURAN-PHENOLIC RESIN USING THE WARM BOX PROCESS BEFORE CASTING, (C) A CRACK IN THE BINDER BRIDGE BETWEEN TWO SAND PARTICLES AFTER AL CASTING (D) BROKEN BINDER BRIDGES WITH FULLY COVERED INTERSECTION AND PARTLY COVERED INTERSECTION.	63
FIGURE 4-20: (A) AND (B) ORGANICALLY BONDED SAND CORE WITH AN AQUEOUS SOLUTION OF PHENOL SULFONIC ACID, ALUMINUM SALTS, SULFURIC ACID IN WARM BOX PROCESS BEFORE CASTING, (C) AND (D) ORGANICALLY BONDED SAND CORES AFTER CASTING.	64
FIGURE 4-21: (A) AND (B) INORGANICALLY BONDED SAND CORE WITH MODIFIED SILICATE BINDER MIXTURE AND PROMOTER (INOTEC™ - PROMOTER WJ 4000) USING THE WARM BOX PROCESS BEFORE CASTING.	65
FIGURE 4-22: (A) AND (B) INORGANICALLY BONDED SAND CORE WITH MODIFIED SILICATE BINDER MIXTURE WITH PROMOTER (INOTEC™ - PROMOTER WJ 4000) USING THE WARM BOX PROCESS) AFTER CASTING.	66
FIGURE 4-23: (A) AND (B) INORGANICALLY BONDED SAND CORE OF MODIFIED SILICATE BINDER MIXTURE AND PROMOTER (INOTEC PROMOTER EP 4174) USING WARM BOX PROCESS BEFORE CASTING.	66
FIGURE 4-24: (A) AND (B) INORGANICALLY BONDED SAND CORE OF MODIFIED SILICATE BINDER MIXTURE AND PROMOTER (INOTEC PROMOTER EP 4174) USING WARM BOX PROCESS AFTER CASTING SHOWING AN UNBROKEN BINDER BRIDGE AND A TYPICAL INORGANIC FRACTURE SURFACE INDICATING A BRITTLE BEHAVIOUR.	67
FIGURE 4-25: (A) AND (B) INORGANICALLY BONDED SAND CORE WITH WATER GLASS 39T® USING THE WARM BOX PROCESS BEFORE CASTING.	67
FIGURE 4-26: (A) AND (B) INORGANICALLY BONDED SAND CORE WITH WATER GLASS 39T® USING THE WARM BOX PROCESS AFTER CASTING.	68
FIGURE 4-27: TEMPERATURE OVER TIME CURVES OF MIN SAND SPECIMEN DIPPING TRIAL IN 780 °C AL- MELTS.	69
FIGURE 4-28: TEMPERATURE DISTRIBUTION IN DIFFERENT SANDS AT THE 25 MM TESTING POINT DURING DIPPING TRIAL IN 780 °C AL - MELT.....	70
FIGURE 4-29: TEMPERATURE TIME CURVES IN DIFFERENT SANDS AT 15 MM TESTING POINT DURING DIPPING TRIAL IN 780 °C AL- MELT.....	71
FIGURE 4-30: TEMPERATURE TIME CURVES IN DIFFERENT SANDS AT 5 MM TESTING POINT IN DIPPING TRIAL IN 780 °C AL - MELT ALLOYS.....	72
FIGURE 4-31: THE WATER PEAK IN H32 SILICA SAND CORES WITH DIFFERENT DRYING TIMES BY MICROWAVE (0 MINS / 5 MINS / 10 MINS), THE SAND SPECIMENS DIPPING INTO AL – MELT AT 780 °C.	73
FIGURE 4-32: THE SIGNIFICANT POINTS IN THE CURVES IN THE RING MOULD TEST.	74

FIGURE CAPTIONS

FIGURE 4-33: TEMPERATURE TIME CURVE AT THE CENTRE POSITION FOR RING MOULD TESTS WITH DIFFERENT CORE SAND TYPES WITH WATER WATER GLASS BETOL [®] 39 T.....	75
FIGURE 4-34: TEMPERATURE TIME CURVE AT THE POSITION OF 15 MM FOR RING MOULD TESTS WITH DIFFERENT CORE SAND TYPES WITH WATER WATER GLASS BETOL [®] 39 T.	76
FIGURE 4-35: TEMPERATURE TIME CURVE AT THE POSITION OF 5 MM FOR RING MOULD TESTS WITH DIFFERENT CORE SAND TYPES BONDED WITH WATER WATER GLASS BETOL [®] 39 T.	76
FIGURE 4-36: COMPARISON OF DT / DT _(0-250°C) IN DIFFERENT SANDS AND DIFFERENT POSITION.....	77
FIGURE 4-37: RING MOULD TEST OF WITH WATER GLASS 39T BONDED H32 SILICA SAND WITH AN INITIAL TEMPERATURE OVER 100 °C WITH MICRO WAVE OVEN TREATMENT.	78
FIGURE 4-38: RING MOULD TEST OF WITH WATER GLASS 39T BONDED H32 SILICA SAND WITH AN INITIAL TEMPERATURE OVER 100 °C WITHOUT MICRO WAVE OVEN TREATMENT.	79
FIGURE 4-39: RING MOULD TEST OF WITH WATER GLASS 39T BONDED H32 SILICA SAND WITH AN INITIAL TEMPERATURE BELOW 100 °C WITHOUT MICRO WAVE OVEN TREATMENT.	79
FIGURE 4-40: RING MOULD TEST OF WITH WATER GLASS 39T BONDED H32 SILICA SAND WITH AN INITIAL TEMPERATURE BELOW 100 °C WITH MICRO WAVE OVEN TREATMENT.	80
FIGURE 4-41: (A) AND (B) FEATURES OF THREE DIFFERENT IMPACT ENERGIES AND TIMES BY IMPACT DEVICE IN ORGANICALLY BONDED INTERNAL CORE.	81
FIGURE 4-42: SCHEMATIC CROSS SECTION OF SPECIMENS AFTER THE DECORED SAND REMOVED AL CASTING (A) ONE IMPACT (B) TWO IMPACTS (C) THREE IMPACTS.....	81
FIGURE 4-43: DECORED SANDS SAMPLES FROM ORGANICALLY BONDED SAND CORE WITH MODIFIED UREA-FURAN-PHENOLIC RESIN IN WARM BOX PROCESS AFTER IMPACTING.....	82
FIGURE 4-44: DECORED SANDS SAMPLES FROM ORGANICALLY BONDED SAND CORE WITH MODIFIED UREA-FURAN-PHENOLIC RESIN IN WARM BOX PROCESS AFTER IMPACTS.....	82
FIGURE 4-45: DECORED SANDS SAMPLES FROM ORGANICALLY BONDED SAND CORE WITH AN AQUEOUS SOLUTION OF PHENOL SULFONIC ACID, ALUMINUM SALTS, SULFURIC ACID (WARM BOX) AFTER IMPACT.	83
FIGURE 4-46: DECORED SANDS SAMPLES FROM ORGANICALLY BONDED SAND CORE WITH AN AQUEOUS SOLUTION OF PHENOL SULFONIC ACID, ALUMINUM SALTS, SULFURIC ACID IN WARM BOX PROCESS AFTER IMPACT.....	84
FIGURE 4-47: DECORED SANDS SAMPLES FROM INORGANICALLY BONDED SAND CORE WITH MODIFIED SILICATE BINDER MIXTURE AND PROMOTER (INOTEC [™] - PROMOTER WJ 4000) IN WARM BOX PROCESS AFTER IMPACT.....	84
FIGURE 4-48: DECORED SANDS SAMPLES FROM INORGANICALLY BONDED SAND CORE WITH MODIFIED SILICATE BINDER MIXTURE AND PROMOTER (INOTEC [™] - PROMOTER WJ 4000) IN WARM BOX PROCESS AFTER IMPACT.....	85

FIGURE CAPTIONS

FIGURE 4-49: DECORED SANDS SAMPLES FROM INORGANICALLY BONDED SAND CORE OF MODIFIED SILICATE BINDER MIXTURE AND PROMOTER (INOTEC™ PROMOTER EP 4174) IN WARM BOX PROCESS AFTER IMPACT.....	86
FIGURE 4-50: DECORED SANDS SAMPLES FROM INORGANICALLY BONDED SAND CORE OF MODIFIED SILICATE BINDER MIXTURE AND PROMOTER (INOTEC™ PROMOTER EP 4174) IN WARM BOX PROCESS AFTER IMPACT.....	86
FIGURE 4-51: DECORED SANDS SAMPLES FROM INORGANICALLY BONDED SAND CORE WITH WATER GLASS 39T® USING THE WARM BOX PROCESS AFTER IMPACT.....	87
FIGURE 4-52 : AGGLOMERATES FORM A BRIDGE STRUCTURE AND HINDER FINE SAND TO FALL DOWN DURING DECORING.	88
FIGURE 4-53: DECORED SANDS SAMPLES FROM INORGANICALLY BONDED SAND CORE WITH WATER GLASS 39T® USING THE WARM BOX PROCESS AFTER IMPACT.....	88
FIGURE 4-54: COMPARISON OF DECORING ABILITIES FOR FIVE DIFFERENT INTERNAL CORES, NO.1 IS THE ORGANICALLY BONDED SAND CORE WITH MODIFIED UREA-FURAN-PHENOLIC RESIN (WARM BOX), NR. 2 IS THE ORGANICALLY BONDED SAND CORE WITH AN AQUEOUS SOLUTION OF PHENOL SULFONIC ACID, ALUMINUM SALTS, SULFURIC ACID (WARM BOX), NO. 3 IS THE INORGANICALLY BONDED SAND CORE WITH WATER GLASS 39T® (WARM BOX), NR. 4 IS THE INORGANICALLY BONDED SAND CORE OF MODIFIED SILICATE BINDER MIXTURE AND PROMOTER (INOTEC™ PROMOTER EP 4174), NR. 5 IS THE INORGANICALLY BONDED SAND CORE WITH MODIFIED SILICATE BINDER MIXTURE AND PROMOTER (INOTEC™ - PROMOTER WJ 4000) (WARM BOX).....	89
FIGURE 4-55: COMPARISON BETWEEN SIMULATION CURVE AND EXPERIMENT CURVE OF ZIRCON SAND AT THE SAME PARAMETER OF 780 °C WITH THE PROPORTIONAL CONSTANT $Q_{MAGMA}^{QUARTZ} = 1.0$	91
FIGURE 4-56: COMPARISON BETWEEN SIMULATION CURVES AND EXPERIMENT CURVES OF ZIRCON SAND AT THE SAME PARAMETERS AT 700 °C WITH THE PROPORTIONAL CONSTANT $Q_{MAGMA}^{QUARTZ} = 1.0$	92
FIGURE 4-57: FIVE Λ VALUES OVER TIME IN DIFFERENT SAND CORES, $\Lambda_{H32\ SILICA\ SAND}$ AND $\Lambda_{MIN\ SAND}$ ARE OVERLAPPED, $\Lambda_{KERPHALITE\ SAND}$ AND $\Lambda_{CERABEADS\ SAND}$ ARE OVERLAPPED.	94
FIGURE 5-1: HEAT FLOW EFFECTS TEMPERATURE AND MOISTURE IN SAND CORES.	96

TABLE CAPTIONS

TABLE 2-1. COMPARISON OF PHYSIC PROPERTIES OF RAW SANDS ^[19]	15
TABLE 2-2. THE RELATIVE VALUES BETWEEN AVERAGE GRAIN SIZE AND AFS GRAIN FINENESS NUMBER ^[21]	16
TABLE 2-3 . LINEAR EXPANSION COEFFICIENT OF THE MOULD BASE MATERIALS ^[29]	18
TABLE 2-4: PROPERTIES OF WATER GLASS MODULE IN THE SAND CORE ^[52]	26
TABLE 3-1 : IMPORTANT PARAMETERS IN THE SIEVE ANALYSIS ^[65]	32
TABLE 3-2: THE PARAMETERS OF PRODUCING FIVE INVESTIGATED INTERNAL CORES	37
TABLE 4-1: COMPARISON OF DT / DT IN DIFFERENT BASE SANDS.	72
TABLE 4-2: THE PROCESS PARAMETERS DURING THE RING MOULD TEST.	74
TABLE 4-3: SIMULATED DIFFERENT Q _{SAND CORE} OF SAND CORES.	93

Appendixes

TABLE A- 1: GRAIN SIZE SIEVE ANALYSIS H32 SILICA SAND.....	1
TABLE A- 2: GRAIN SIZE SIEVE ANALYSIS CERABEADS SAND.....	2
TABLE A- 3: GRAIN SIZE SIEVE ANALYSIS KERPHALITE SAND	3
TABLE A- 4: GRAIN SIZE SIEVE ANALYSIS MIN SAND	4
TABLE A- 5: GRAIN SIZE SIEVE ANALYSIS ZIRCON SAND.....	5
TABLE A- 6: THE KEY PARAMETERS IN THE RING MOULD TEST IN ZIRCON SAND CORE 1 #.....	6
TABLE A- 7: THE KEY PARAMETERS IN THE RING MOULD TEST IN ZIRCON SAND CORE SAMPLE 2 #.....	7
TABLE A- 8: THE KEY PARAMETERS IN THE RING MOULD TEST IN MIN SAND CORE 1 #	8
TABLE A- 9: THE KEY PARAMETERS IN THE RING MOULD TEST IN MIN SAND CORE 2 #	9
TABLE A- 10: THE KEY PARAMETERS IN THE RING MOULD TEST IN KERPHALITE SAND CORE-1	10
TABLE A- 11: THE KEY PARAMETERS IN THE RING MOULD TEST IN KERPHALITE SAND CORE 2 #.....	11
TABLE A- 12: THE KEY PARAMETERS IN THE RING MOULD TEST IN H32 SAND CORE 1 #.....	12
TABLE A- 13: THE KEY PARAMETERS IN THE RING MOULD TEST IN H32 SAND CORE 2 #.....	13
TABLE A- 14: THE KEY PARAMETERS IN THE RING MOULD TEST IN CERABEADS SAND CORE 1 #.....	14
TABLE A- 15: THE KEY PARAMETERS IN THE RING MOULD TEST IN CERABEADS SAND CORE 2 #.....	15
TABLE A- 16 : SPECIAL HEAT CAPACITY OF H32 SILICA SAND OVER TEMPERATURE.....	16
TABLE A- 17 : SPECIAL HEAT CAPACITY OF KERPHALITE SAND OVER TEMPERATURE	17
TABLE A- 18 : SPECIAL HEAT CAPACITY OF CERABEADS SAND OVER TEMPERATURE.....	18
TABLE A- 19 : SPECIAL HEAT CAPACITY OF MIN SAND OVER TEMPERATURE.....	19
TABLE A- 20 : SPECIAL HEAT CAPACITY OF ZIRCON SAND OVER TEMPERATURE	20
TABLE A- 21 : THE DENSITY OVER TEMPERATURE OF FIVE BASE SAND	21
FIGURE A- 1: THE ILLUSTRATION OF THE CASTING BOX MOULD BOTTOM PLATE	22
FIGURE A- 2: THE ILLUSTRATION OF THE CASTING BOX MOULD INSIDE CORE	23
FIGURE A- 3: THE ILLUSTRATION OF THE CASTING BOX MOULD OUTSIDE CORE.....	24

Table A- 1: Grain size sieve analysis H32 silica sand

Nemak Linz GmbH			
Firma	: Nemak Linz GmbH	Datum	: 24.10.2013
Bearbeiter	: Xin	lfd. Nr.	: 4497
Analyse	: 24.10.2013 H32	Datei	: I:\QSL\75Grain\Konfig\Laborprojekte2013.sip
Material	: H32		
Probenvorbereitung :			
Probeentnahme 24.10.2013 8:30Uhr			
Siebmaschine	: AS200 digit	Amplitude [mm]	: 1.500
Intervall (j/n)	: nein	Siebintervall [s]	: ----
Siebbewegung	: dreidimensional	Naßsiebung	: nein
Durchmesser[mm]	: 200.0	Siebhöhe [mm]	: 50.0
Normhauptnummer	: DIN ISO 3310 Teil 1		
Einwaage	: 100.04	Siebzeit [min]	: 10.000
Siebhilfe	:		

Kornklasse [µm]	Massenanteil		Häufigkeit q3[1/µm]	kumulativ	
	[g]	[%]		Q3[%]	1-Q3[%]
< 63	0.95	0.9	0.0002	0.9	99.1
63 - 90	0.88	0.9	0.0003	1.8	98.2
90 - 125	0.56	0.6	0.0002	2.4	97.6
125 - 180	17.94	17.9	0.0033	20.3	79.7
180 - 250	45.42	45.4	0.0065	65.7	34.3
250 - 355	26.61	26.6	0.0025	92.3	7.7
355 - 500	6.74	6.7	0.0005	99.0	1.0
500 - 710	0.81	0.8	0.0000	99.8	0.2
710 - 1000	0.09	0.1	0.0000	99.9	0.1
1000 - 1400	0.03	0.0	0.0000	100.0	0.0
> 1400	0.04	0.0		100.0	0.0

Table A- 2: Grain size sieve analysis Cerabeads sand

Nemak Linz GmbH			
Firma	: Nemak Linz GmbH	Datum	: 24.10.2013
Bearbeiter	: Xin	lfd. Nr.	: 4498
Analyse	: 24.10.2013 C650	Datei	: I:\QSL\75Grain\Konfig\Laborprojekte2013.sip
Material	: C650		
Probenvorbereitung :			
Probeentnahme 24.10.2013 8:30Uhr			
Siebmaschine	: AS200 digit	Amplitude [mm]	: 1.500
Intervall (j/n)	: nein	Siebintervall [s]	: ----
Siebbewegung	: dreidimensional	Naßsiebung	: nein
Durchmesser [mm]	: 200.0	Siebhöhe [mm]	: 50.0
Normhauptnummer	: DIN ISO 3310 Teil 1		
Einwaage	: 100.03	Siebzeit [min]	: 10.000
Siebhilfe	:		

Kornklasse [µm]	Massenanteil		Häufigkeit q3 [1/µm]	kumulativ	
	[g]	[%]		Q3 [%]	1-Q3 [%]
< 63	0.11	0.1	0.0000	0.1	99.9
63 - 90	0.47	0.5	0.0002	0.6	99.4
90 - 125	3.43	3.4	0.0010	4.0	96.0
125 - 180	33.41	33.3	0.0061	37.3	62.7
180 - 250	43.94	43.8	0.0063	81.2	18.8
250 - 355	18.64	18.6	0.0018	99.8	0.2
355 - 500	0.08	0.1	0.0000	99.8	0.2
500 - 710	0.07	0.1	0.0000	99.9	0.1
710 - 1000	0.03	0.0	0.0000	99.9	0.1
1000 - 1400	0.02	0.0	0.0000	100.0	0.0
> 1400	0.04	0.0		100.0	0.0

Table A- 3: Grain size sieve analysis Kerphalite sand

Nemak Linz GmbH			
Firma	: Nemak Linz GmbH	Datum	: 24.10.2013
Bearbeiter	: Xin	lfd. Nr.	: 4499
Analyse	: 24.10.2013 KF	Datei	: I:\QSL\75Grain\Konfig\Laborprojekte2013.slp
Material	: KF		
Probenvorbereitung :			
Probeentnahme 24.10.2013 8:30Uhr			
Siebmaschine	: AS200 digit	Amplitude [mm]	: 1.500
Intervall (j/n)	: nein	Siebintervall [s]	: ----
Siebbewegung	: dreidimensional	Naßsiebung	: nein
Durchmesser[mm]	: 200.0	Siebhöhe[mm]	: 50.0
Normhauptnummer	: DIN ISO 3310 Teil 1		
Einwaage	: 100.01	Siebzeit [min]	: 10.000
Siebhilfe	:		

Kornklasse [µm]	Massenanteil		Häufigkeit q3[1/µm]	kumulativ	
	[g]	[%]		Q3[%]	1-Q3[%]
< 63	7.45	7.4	0.0012	7.4	92.6
63 - 90	2.67	2.7	0.0010	10.1	89.9
90 - 125	2.43	2.4	0.0007	12.5	87.5
125 - 180	33.89	33.9	0.0062	46.4	53.6
180 - 250	27.04	27.0	0.0039	73.4	26.6
250 - 355	20.36	20.3	0.0019	93.7	6.3
355 - 500	5.90	5.9	0.0004	99.6	0.4
500 - 710	0.30	0.3	0.0000	99.9	0.1
710 - 1000	0.04	0.0	0.0000	100.0	0.0
1000 - 1400	0.01	0.0	0.0000	100.0	0.0
> 1400	0.02	0.0		100.0	0.0

Table A- 4: Grain size sieve analysis MIN Sand

Nemak Linz GmbH			
Firma	: Nemak Linz GmbH		
Bearbeiter	: Xin	Datum	: 24.10.2013
Analyse	: 24.10.2013 MIN-Sand	lfd. Nr.	: 4495
Datei	: I:\QSL\75Grain\Konfig\Laborprojekte2013.slp		
Material	: Min-Sand		
Probenvorbereitung :			
Probeentnahme 24.10.2013 8:30Uhr			
Siebmaschine	: AS200 digit	Amplitude [mm]	: 1.500
Intervall (j/n)	: nein	Siebintervall [s]	: ----
Siebbewegung	: dreidimensional	Naßsiegung	: nein
Durchmesser [mm]	: 200.0	Siebhöhe [mm]	: 50.0
Normhauptnummer	: DIN ISO 3310 Teil 1		
Einwaage	: 100.04	Siebzeit [min]	: 10.000
Siebhilfe	:		

Kornklasse [µm]	Massenanteil		Häufigkeit q3[1/µm]	kumulativ	
	[g]	[%]		Q3[%]	1-Q3[%]
< 63	0.34	0.3	0.0001	0.3	99.7
63 - 90	3.55	3.5	0.0013	3.9	96.1
90 - 125	1.20	1.2	0.0003	5.1	94.9
125 - 180	29.85	29.8	0.0054	34.8	65.2
180 - 250	30.40	30.3	0.0043	65.2	34.8
250 - 355	31.23	31.1	0.0030	96.3	3.7
355 - 500	3.59	3.6	0.0002	99.9	0.1
500 - 710	0.09	0.1	0.0000	100.0	0.0
710 - 1000	0.02	0.0	0.0000	100.0	0.0
1000 - 1400	0.01	0.0	0.0000	100.0	0.0
> 1400	0.01	0.0		100.0	0.0

Table A- 5: Grain size sieve analysis Zircon Sand

Nemak Linz GmbH			
Firma	: Nemak Linz GmbH	Datum	: 29.10.2013
Bearbeiter	: Pawlik	lfd. Nr.	: 4510
Analyse	: 29.10.2013 ZK	Datei	: I:\QSL\75Grain\Konfig\Laborprojekte2013.sip
Material	: Zirkon-Sand		
Probenvorbereitung :			
Probeentnahme 29.10.2013 6:00Uhr			
Siebmaschine	: AS200 digit	Amplitude [mm]	: 1.500
Intervall (j/n)	: nein	Siebintervall [s]	: ----
Siebbewegung	: dreidimensional	Naßsiebung	: nein
Durchmesser [mm]	: 200.0	Siebhöhe [mm]	: 50.0
Normhauptnummer	: DIN ISO 3310 Teil 1		
Einwaage	: 100.04	Siebzeit [min]	: 10.000
Siebhilfe	:		

Kornklasse [µm]	Massenanteil		Häufigkeit q3 [1/µm]	kumulativ	
	[g]	[%]		Q3 [%]	1-Q3 [%]
< 63	0.10	0.1	0.0000	0.1	99.9
63 - 90	1.44	1.4	0.0005	1.5	98.5
90 - 125	3.31	3.3	0.0009	4.8	95.2
125 - 180	36.82	36.8	0.0067	41.6	58.4
180 - 250	49.39	49.3	0.0070	91.0	9.0
250 - 355	8.90	8.9	0.0008	99.8	0.2
355 - 500	0.05	0.0	0.0000	99.9	0.1
500 - 710	0.06	0.1	0.0000	100.0	0.0
710 - 1000	0.02	0.0	0.0000	100.0	0.0
1000 - 1400	0.00	0.0	0.0000	100.0	0.0
> 1400	0.03	0.0		100.0	0.0

Table A- 6: The key parameters in the ring mould test in Zircon sand core 1 #

	Ring mold	T air in mold	Core center	Core side 15mm	Core side 5mm
Pouring time Temp.	200	160	113	116	134
Gradient at 200°C(dT / dt)	-	-	0.37	0.55	2.27
Time at 200°C(s)	-	6,0-6,5	233,0	154	29,0
Max. Temperature	397,07	638	320	323	366
Time at Max Temp.(s)	125,0	3,0	674,0	582,0	236,0
Casting melting	739°C		Core size	H: 50mm	D: 50mm

Table A- 7: The key parameters in the ring mould test in Zircon sand core sample 2 #

	Ring mold	T air in mold	Core center	Core side 15mm	Core side 5mm
Pouring time Temp.	200,36	105,74	31,38	35,58	42,47
Gradient at 200°C(dT / dt)	-	-	0.54	0.69	1.75
Time at 200°C(s)	-	0,5-1,0	311,0	237,0	90,0
Max. Temperature	408,28	638	301	306	320
Time at Max Temp.(s)	85,5	2,0	754,5	696,0	488,5
Casting melting	730°C		Core size	H: 50mm	D: 50mm

Table A- 8: The key parameters in the ring mould test in MIN sand core 1 #

	Ring mold	T air in mold	Core center	Core side 15mm	Core side 5mm
Pouring time Temp.	200	160	59	64	79
Gradient at 200°C(dT / dt)	-	-	0.42	0.52	2.14
Time at 200°C(s)	-	0,5-1,0	334,0	261	56.5
Max. Temperature	396	638	293	291	332
Time at Max Temp.(s)	103,5	2,0	777,5	684,0	336,5
Casting melting	736°C		Core size	H: 50mm	D: 50mm

Table A- 9: The key parameters in the ring mould test in MIN sand core 2 #

	Ring mold	T air in mold	Core center	Core side 15mm	Core side 5mm
Pouring time Temp.	200°C	131°C	137°C	146°C	147°C
Gradient at 200°C(dT / dt)	-	-	0.24	0.40	1.05
Time at 200°C(s)	-	1,0-1,5	263,0	135,0	50,5
Max. Temperature	406°C	626°C	312°C	321°C	345°C
Time at Max Temp.(s)	113,5	4,5	764,0	612,5	368,0
Casting melting	725°C		Core size	H: 50mm	D: 50mm

Table A- 10: The key parameters in the ring mould test in Kerphalite sand core-1

KF SAND _1					
	Ring mold	T air in mold	Core center	Core side 15mm	Core side 5mm
Pouring time Temp.	200°C	104°C	28°C	33°C	44°C
Gradient at 200°C(dT / dt)	-	-	0.51	0.67	2.44
Time at 200°C(s)	-	2,0-2,5	335,0	239,5	64,0
Max. Temperature	398	610°C	289°C	298°C	315°C
Time at Max Temp.(s)	99,0	8,0	795,0	720,5	420,0
Casting melting	719°C		Core size	H: 50mm	D: 50mm

Table A- 11: The key parameters in the ring mould test in Kerphalite sand core 2 #

	Ring mold	T air in mold	Core center	Core side 15mm	Core side 5mm
Pouring time Temp.	200°C	119°C	28°C	31°C	38°C
Gradient at 200°C(dT / dt)	-	-	0.55	0-63	1.54
Time at 200°C(s)	-	1,0-1,5	312,0	266,5	105,5
Max. Temperature	412°C	640°C	312°C	304°C	333°C
Time at Max Temp.(s)	96,0	5,5	769,5	711,0	501,0
Casting melting	748°C		Core size	H: 50mm	D: 50mm

Table A- 12: The key parameters in the ring mould test in H32 sand core 1 #

	Ring mold	T air in mold	Core center	Core side 15mm	Core side 5mm
Pouring time Temp.	200°C	129°C	149°C	161°C	161°C
Gradient at 200°C(dT / dt)	-	-	0.30	0.34	1.16
Time at 200°C(s)	-		172,0	116,0	33,5
Max. Temperature	412°C		324°C	337°C	358°C
Time at Max Temp.(s)	95,5	635°C	586,0	554	315,5
Casting melting	741°C	4,0	Core size	H: 50mm	D: 50mm

Table A- 13: The key parameters in the ring mould test in H32 sand core 2 #

	Ring mold	T air in mold	Core center	Core side 15mm	Core side 5mm
Pouring time Temp.	200°C	111°C	36°C	39°C	53°C
Gradient at 200°C(dT / dt)	-	-	0.57	0.71	3.27
Time at 200°C(s)	-		285,5	226,0	45,0
Max. Temperature	408°C	628°C	296°C	306°C	342°C
Time at Max Temp.(s)	105,0	3,5	718,0	643,5	325,5
Casting melting	733°C		Core size	H: 50mm	D: 50mm

Table A- 14: The key parameters in the ring mould test in Cerabeads sand core 1 #

	Ring mold	T air in mold	Core center	Core side 15mm	Core side 5mm
Pouring time Temp.	200°C	114°C	33°C	38°C	52°C
Gradient at 200°C(dT / dt)	-	-	0.53	0.79	2.29
Time at 200°C(s)	-		315,0	205,5	64,5
Max. Temperature	385°C	619°C	292°C	300°C	330°C
Time at Max Temp.(s)	102,0	2,0	744,5	637,5	386,5
Casting melting	720°C		Core size	H: 50mm	D: 50mm

Table A- 15: The key parameters in the ring mould test in Cerabeads sand core 2 #

	Ring mold	T air in mold	Core center	Core side 15mm	Core side 5mm
Pouring time Temp.	200°C	102°C	41°C	46°C	64°C
Gradient at 200°C(dT / dt)	-	-	0.52	0.70	2.00
Time at 200°C(s)	-		307,0	221,0	68,0
Max. Temperature	403°C	616°C	303°C	310°C	333°C
Time at Max Temp.(s)	117,0	7,5	756,0	665,5	415,0
Casting melting	730°C		Core size	H: 50mm	D: 50mm

Table A- 16 : Special heat capacity of H32 silica sand over temperature

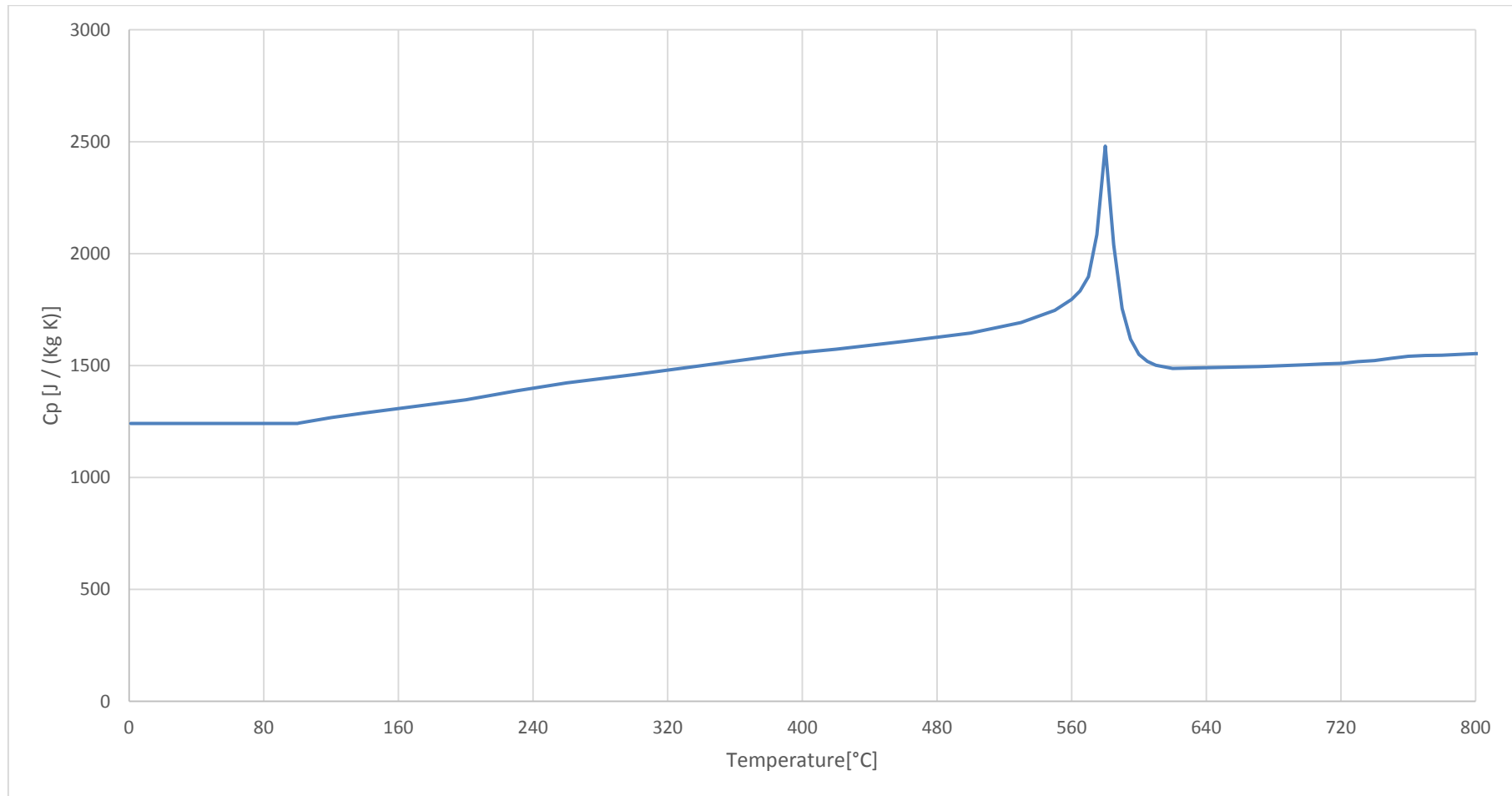


Table A- 17 : Special heat capacity of Kerphalite sand over temperature

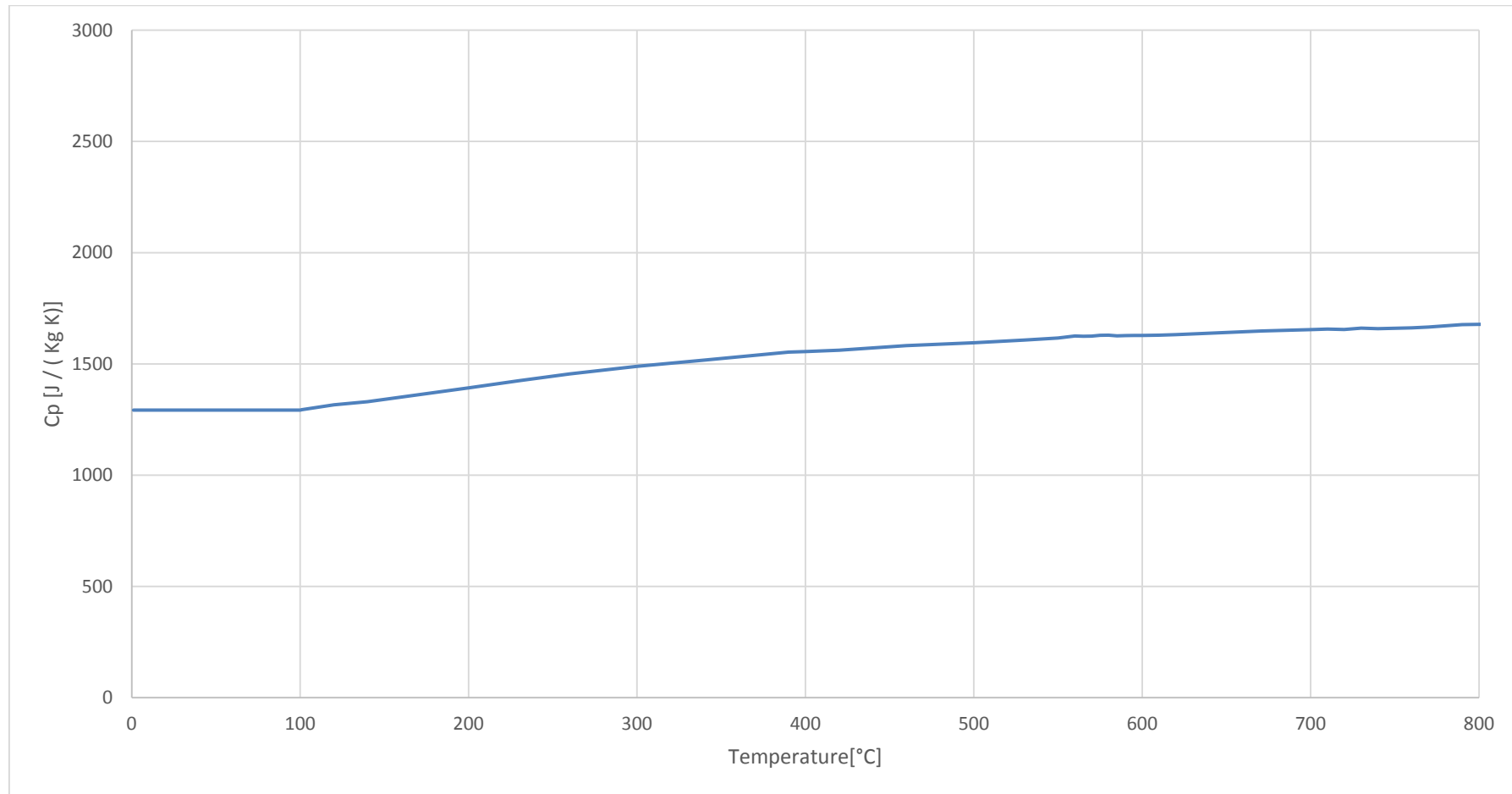


Table A- 18 : Special heat capacity of Cerabeads sand over temperature

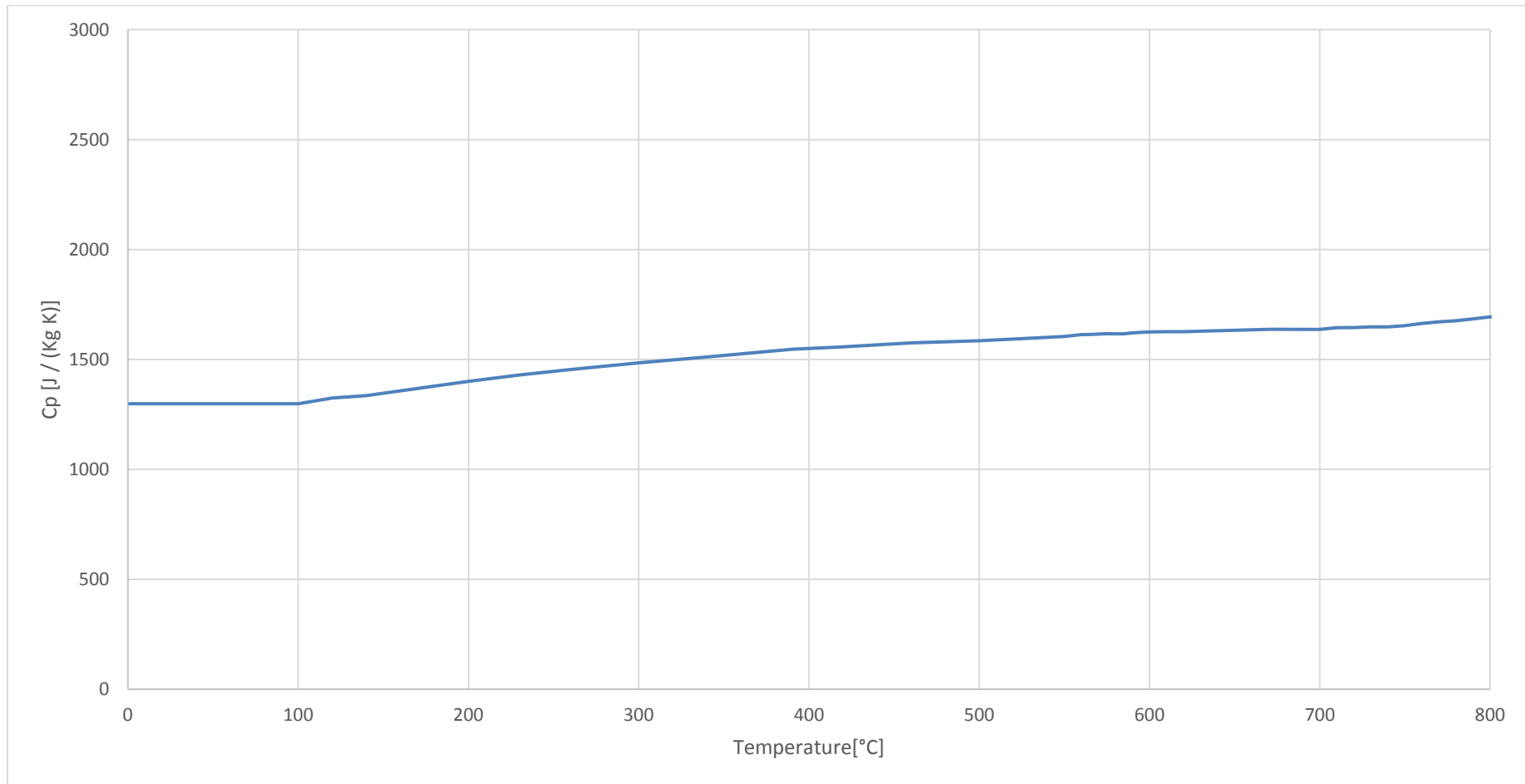


Table A- 19 : Special heat capacity of MIN sand over temperature

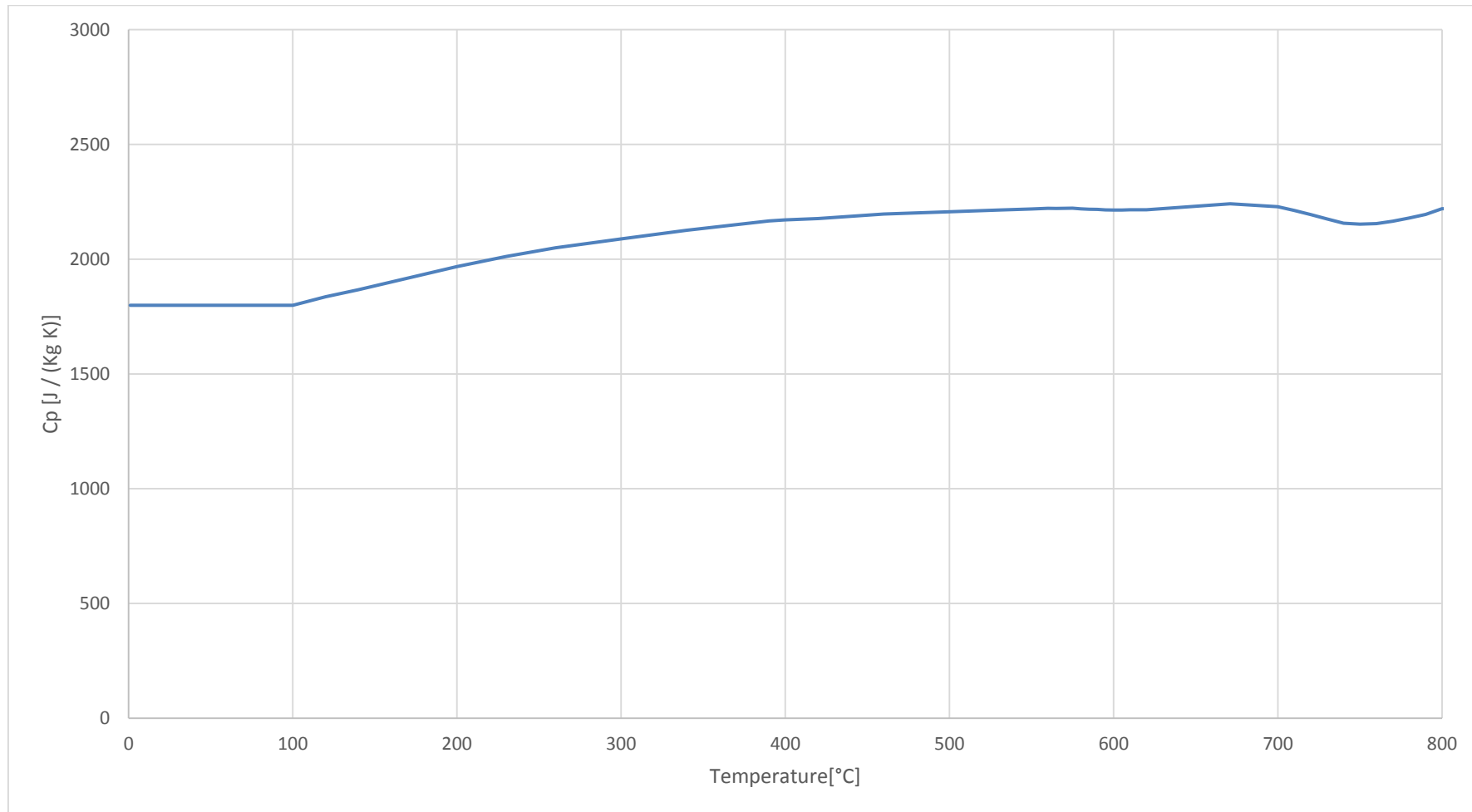


Table A- 20 : Special heat capacity of Zircon sand over temperature

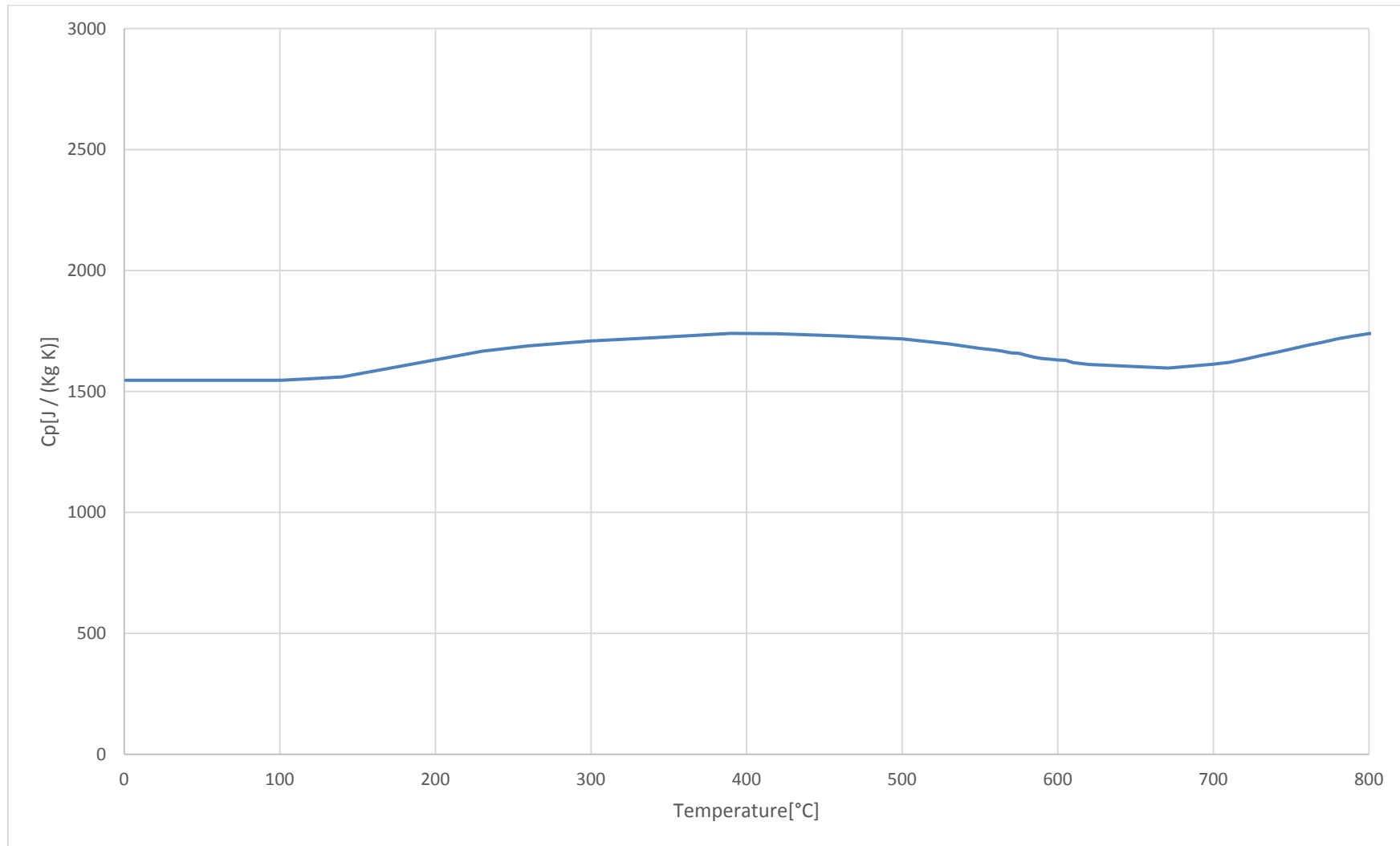


Table A- 21 : The density over temperature of five base sand

Temperature[°C]	Silica sand [Kg/m ³]	Kerphalite sand[Kg/m ³]	Cerabeads sand[Kg/m ³]	Minsand [Kg/m ³]	Zircon sand [Kg/m ³]
1	1430	1450	1470	2030	2410
100	1427	1448	1470	2027	2410
200	1421	1446	1469	2024	2407
300	1414	1443	1467	2020	2405
400	1405	1439	1465	2016	2402
500	1394	1434	1462	2011	2399
600	1368	1428	1459	2008	2391
780	1342	1422	1456	2005	2383
2000	1316	1416	1453	2002	2375

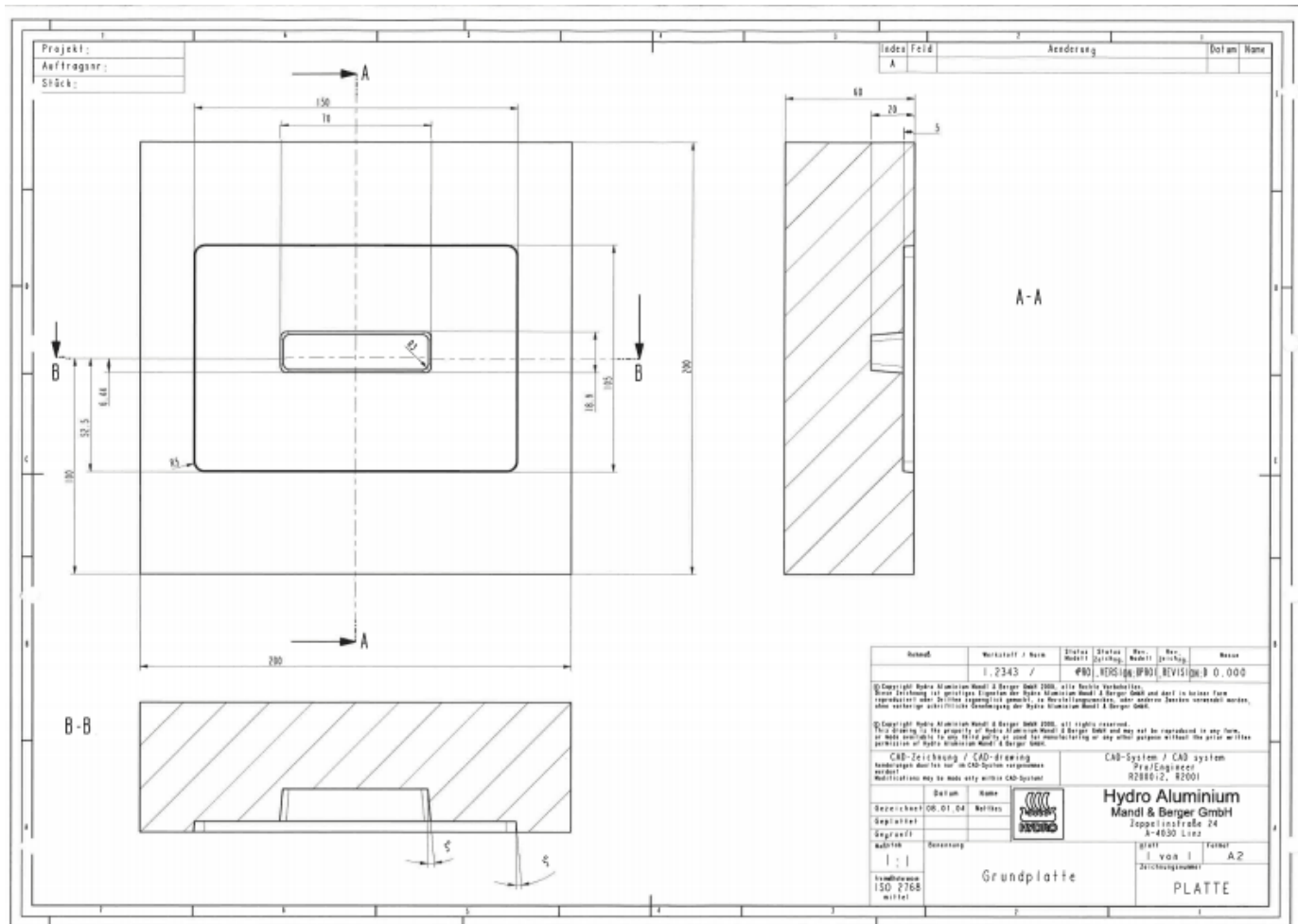


Figure A- 1: The illustration of the Casting Box mould bottom plate

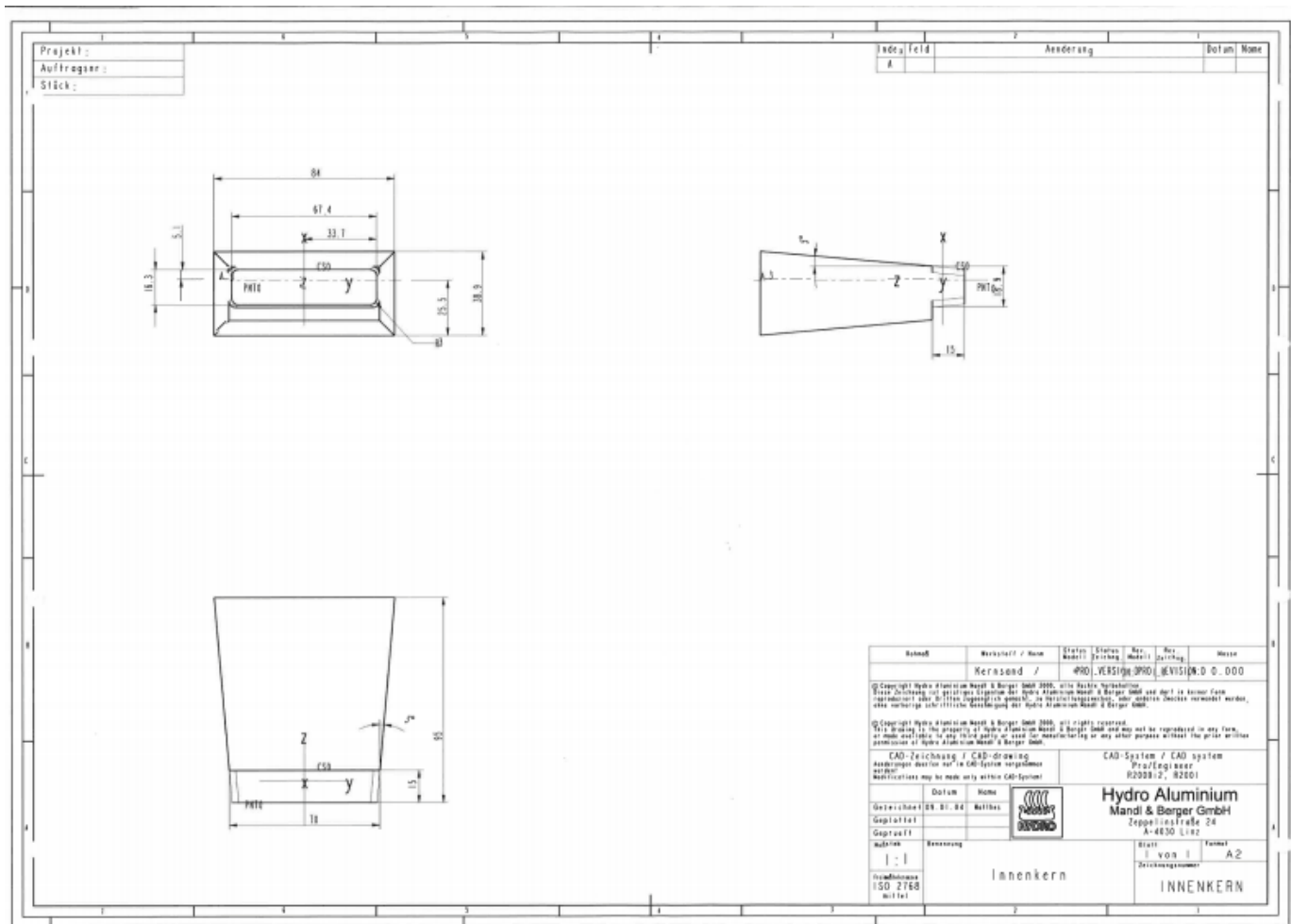


Figure A- 2: The illustration of the Casting Box mould inside core

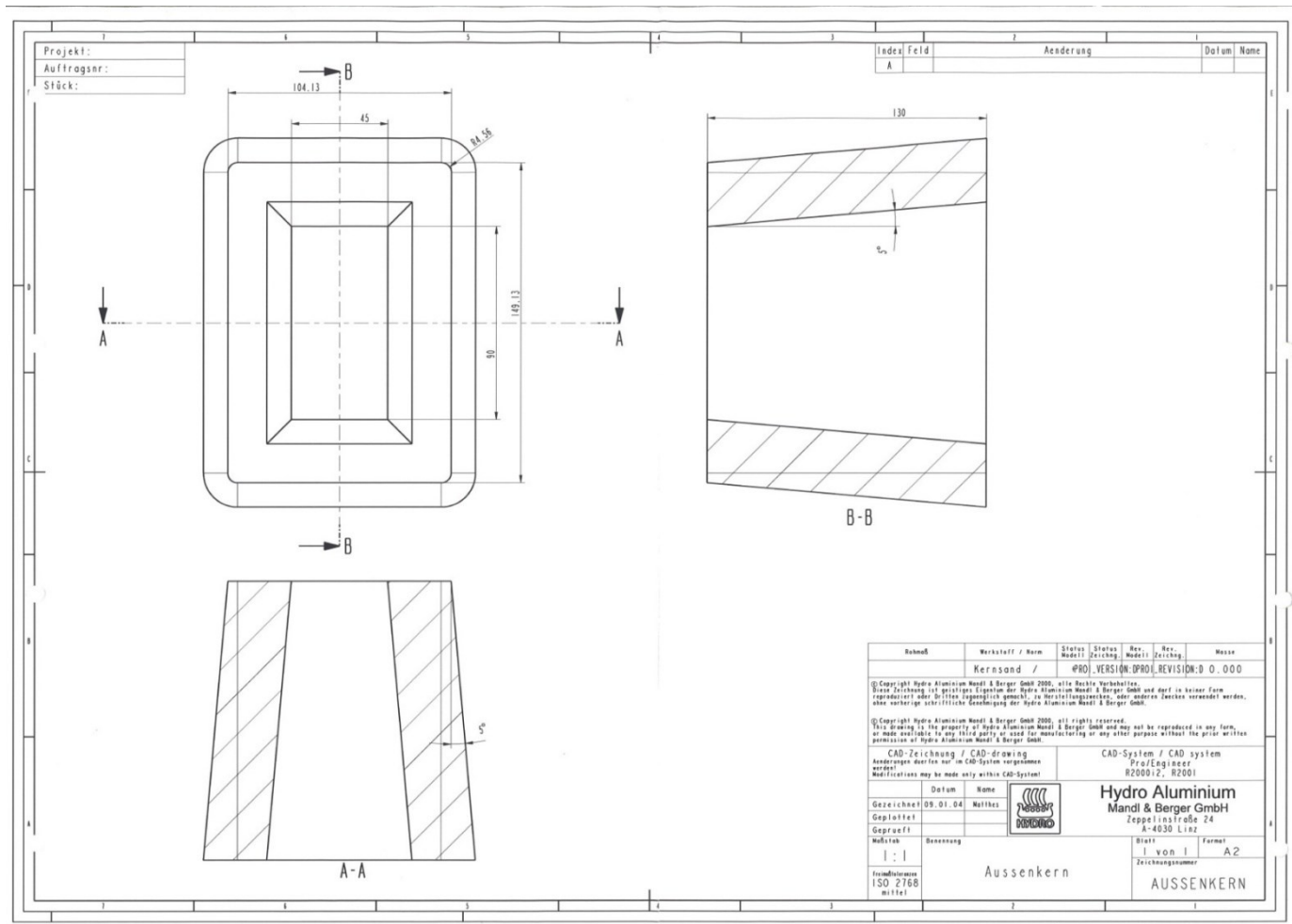


Figure A- 3: The illustration of the Casting Box mould outside core

